INFORMATION TO USERS

This manuscript has been reproduced from the microfilm master. UMI films the text directly from the original or copy submitted. Thus, some thesis and dissertation copies are in typewriter face, while others may be from any type of computer printer.

The quality of this reproduction is dependent upon the quality of the copy submitted. Broken or indistinct print, colored or poor quality illustrations and photographs, print bleedthrough, substandard margins, and improper alignment can adversely affect reproduction.

In the unlikely event that the author did not send UMI a complete manuscript and there are missing pages, these will be noted. Also, if unauthorized copyright material had to be removed, a note will indicate the deletion.

Oversize materials (e.g., maps, drawings, charts) are reproduced by sectioning the original, beginning at the upper left-hand comer and continuing from left to right in equal sections with small overlaps.

UMI®

GEOMETRIC METHODS FOR MULTI-ROBOT

PLANNING AND CONTROL

Calin Belta

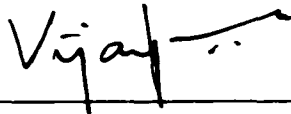### A DISSERTATION

in

Mechanical Engineering and Applied Mechanics

Presented to the Faculties of the University of Pennsylvania in Partial

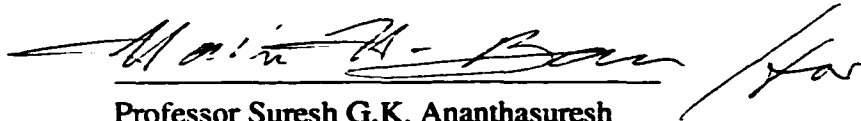Fulfillment of the Requirements for the Degree of Doctor of Philosophy.

2003

Professor Vijay Kumar

Supervisor of Dissertation

Professor Suresh G.K. Ananthasuresh

Graduate Group Chairperson

UMI Number: 3095859

Copyright 2003 by
Belta, Calin Andrei

All rights reserved.

UMI®

COPYRIGHT

Calin Belta

2003

In memoria Tatalui meu.

Acknowledgements

I would like first of all to express my admiration and gratitude to my advisor and mentor, Professor Vijay Kumar. Without his support, guidance, and encouragement, this work would have never been completed. And without his friendship and sense of humor, my stay in the GRASP Lab would not have been such a pleasant experience.

I also want to thank the remainder of my dissertation committee, Professors Naomi Leonard, George Pappas, and Jim Ostrovski for their comments and suggestions. I especially want to express my appreciation to George Pappas for his advice and useful discussions on topics which go beyond the scope of this work.

During the past four years, GRASP lab was my second home and the graspees were my family. Many thanks to John Spletzer, Paulo Tabuada, Aveek Das, Peng Song, and Volkan Isler for their unconditional frienship and for being such fun companions. It is difficult to enumerate all the others who contributed to the genuinely friendly and supportive atmosphere in the lab: Joel, Sorangi, Ani, Bert, Lorenzo, Joao, Xenofon, Selcuk, Luiz, Guilherme. I also want to show my gratitude to the Starbucks people downstairs for making all the above possible.

Finally, I want to thank my family back home in Romania: my mother, my sister, and my brother-in-law. I could not have started and finished this journey without their love, support, and advice.

My last thought goes to Ruxandra. She gave me reason and hope all these years. Multumesc fomoase TIST.

iv

ABSTRACT

GEOMETRIC METHODS FOR MULTI-ROBOT PLANNING AND CONTROL

Calin Belta

Vijay Kumar

Motion planning for a multi-robotic system refers to finding trajectories for each robot in a team so that a certain task is performed. In general, this problem is under-determined because of two main reasons. First, the tasks are usually specified in terms of reaching a final position starting from a given initial one. Mathematically, this translates to generating interpolating curves with given boundary conditions in a certain configuration space, problem which usually admits several solutions. One of the main ideas of this dissertation is that a natural way to solve this indeterminacy is to find a solution which is optimal with respect to a performance criterion, *e.g.*, energy consumption. Second, especially in the case when the team is composed of large numbers of robots, the task might be specified in high level terms of the type "the robots should gather in a certain region of the space". Explicitly generating individual trajectories, though feasible, is highly under-determined and computationally unattractive. The second main idea of the dissertation is that, in this case, the motion generation and control problems should be solved in a lower dimensional space which captures the behavior of the group and the nature of the cooperative task.

First, we consider the problem of generating minimum kinetic energy motion for a rigid body in a 3D environment. We develop a computationally efficient method for interpolation on SE(3) that produces nearly optimal trajectories, which are also invariant

v

to changes in the reference frame. Second, we study the rigidity condition and develop a method of optimal motion planning for groups of robots required to maintain a rigid formation. In the third part of this work, we propose a method to control a large number of agents based on an abstraction of the configuration space of the robots to a lower dimensional manifold, which has a product structure of a Lie group, which captures the dependence of the ensemble on the world frame, and a shape manifold, which is an intrinsic description of the team. Illustrative experimental results are included.

Contents

viii

x

List of Figures

xii

Chapter 1

Introduction

There has been a lot of interest in cooperative robotics in the last few years, triggered mainly by the technological advances in control techniques for single vehicles and the explosion in computation and communication capabilities. The research in the field of control and coordination for multiple robots is currently progressing in areas like automated highway systems [83, 79, 88], formation flight control [55, 2], unmanned underwater vehicles [73], satellite clustering [54], exploration [23], surveillance [34], search and rescue [48], mapping of unknown or partially known environments [44], distributed manipulation [53, 70] and transportation of large objects [75, 76].

There are roughly three approaches to multi-vehicle coordination reported in literature: leader-following, behavioral methods, and virtual structure techniques. In leader following, some robots are designated as leaders, while others are followers [28]. In behavior-based control [1, 24], several desired behaviors are prescribed for each agent,

1

the final control being derived by weighting the relative importance of each behavior. In the virtual structure approach, the entire formation is treated as a rigid body [61, 62, 60], [31, 32], [89], [50]. Desired motion is assigned to the virtual structure which traces out trajectories for each member of the formation to follow. Virtual structures have been proposed in [81] and used for motion planning [39], coordination and control of space-crafts, etc. Maybe the most interesting application is in laser interferometry, which requires that several instruments, spaced up to a kilometer apart, maintain a fixed geometry within one centimeter.

Since energy consumption is an important issue, especially for deep space formations, motion planning for virtual structures is often accomplished by posing the problem as an *optimization problem*. For example, satellite formation reconfiguration demands a fuel-optimal trajectory to preserve mission life and is constrained by the limited thrust available. Virtual structures, as rigid bodies, evolve on the Lie group of all translations and orientations in 3D, $SE(3)$. With this in mind, the first part of this thesis is concerned with *optimally interpolating trajectories on $SE(3)$*. The second part investigates the *rigidity constraint* and shows how individual motion plans can be constructed so that the overall energy of the formation is minimized. The methodology and results in these first two parts are organized around two main issues: *optimality* and *invariance of the generated trajectories*. The price one has to pay to achieve these is, of course, a large amount of computation. We expect the methods developed in the second part to only find applications in areas where the number of agents is small and fuel consumption is critical,

2

as satellite reconfiguration.

When a large number of agents is required to be coordinated and controlled, some level of abstraction is necessary, dependent on the imposed task. The virtual structure approach, which can be seen as an abstraction, is not appropriate in many applications, including tunnel passing and obstacle avoidance. The third part of the thesis proposes a method for *abstraction and control for large groups of agents*. The derived control architecture can be used to coordinate hundreds of small, inexpensive robots.

As suggested above, the contributions of the thesis are in three areas. In the following sections, we motivate these three topics and review the relevant literature.

1.1   Interpolation on $SE(3)$

The problem of finding a smooth interpolating curve is well understood in Euclidean spaces [33, 43, 35], but it is not clear how these techniques can be generalized to curved spaces. There are two main issues that need to be addressed, particularly on non-Euclidean spaces. First, it is desired that the computational scheme be independent of the description of the space and invariant with respect to the choice of the coordinate systems used to describe the motion. Second, the smoothness properties and the optimality of the trajectories need to be considered.

Shoemake [71] proposed a scheme for interpolating rotations with Bezier curves based on the spherical analog of the de Casteljau algorithm. This idea was extended by Ge and Ravani [38] and Park and Ravani [65] to spatial motions. The focus in these articles is

3

on the generalization of the notion of interpolation from the Euclidean space to a curved space.

Another class of methods is based on the representation of Bezier curves with Bernstein polynomials. Ge and Ravani [37] used the dual unit quaternion representation of $SE(3)$ and subsequently applied Euclidean methods to interpolate in this space. Jütler [46] formulated a more general version of the polynomial interpolation by using dual (instead of dual unit) quaternions to parameterize $SE(3)$. In such a parameterization, an element of $SE(3)$ corresponds to a whole equivalence class of dual quaternions. Srinivasan [74] and Jütler [49] propose the use of spatial rational B-splines for interpolation. Park and Kang [64] derived a rational interpolating scheme for the group of rotations $SO(3)$ by representing the group with Cayley parameters and using Euclidean methods in this parameter space. Marthinsen [52] suggests the use of Hermite interpolation and the use of truncated inverse of the differential of the exponential mapping and the truncated Baker-Campbell-Hausdorff formula to simplify the construction of interpolation polynomials. The advantage of these methods is that they produce rational curves.

It is worth noting that all these works (with the exception of [65]) use a particular parameterization of the group and do not discuss the invariance of their methods. In contrast, Noakes *et al.* [57] derived the necessary conditions for cubic splines on general manifolds without using a coordinate chart. These results are extended in [27] to the dynamic interpolation problem. Necessary conditions for higher-order splines are derived in Camarinha *et al.* [25]. A coordinate free formulation of the variational approach

4

was used to generate shortest paths and minimum acceleration and jerk trajectories on $SO(3)$ and $SE(3)$ in [91]. However, analytical solutions are available only in the simplest of cases, and the procedure for solving optimal motions, in general, is computationally intensive. If optimality is sacrificed, it is possible to generate bi-invariant trajectories for interpolation and approximation using the exponential map on the Lie algebra [90]. While the solutions are of closed-form, the resulting trajectories have no optimality properties.

1.2 Motion planning and control for rigid formations

The literature on motion planning, stabilization and control of virtual structures is rather extensive. This section discusses some recent papers closely related to the approach in this thesis. Most of these works model formations using *formation graphs*, which are graphs whose nodes capture the individual agent kinematics or dynamics, and whose edges represent inter-agent constraints that must be satisfied.

Desai *et.al.* [28] propose that formations be modeled as a triple (g, r, H), where g ∈ $SE(3)$ represents the gross position and orientation of the team (for example, the pose of the leader), r is a set of shape variables that describes the relative positions of the robots in the team, and H is a control graph which describes the control strategy used by each robot.

The notions of *graph rigidity* and *minimally rigid graphs* are used by Olfati-Saber and Murray in [61, 62, 60]. In all these works, a graph is a triple $\mathcal{G} = (\mathcal{V}, \mathcal{E}, \mathcal{W})$, where $\mathcal{V}$ is a set of vertices, $\mathcal{E}$ is a set of edges and $\mathcal{W}$ is a set of weights, indexed by $\mathcal{E}$. Each

5

vertex is an agent, whose position vector in some inertial frame evolves according to a dynamically fully-controlled system. Each weight gives the desired distance between a pair of robots connected in the graph. In [61], the *shape* variables are defined pairwise for connected agents, as being the error between the desired and the actual distance. Using, the dynamics of the agents, the shape dynamics are straightforward to derive using the chain rule. Stabilization of the shape at zero is called *structural stabilization*. The authors approach the problem of a two agent system and, using a simple change of coordinates, show that shape dynamics can be controlled separately from translational and rotational dynamics. Then, they introduce a procedure called *dynamic node augmentation* that allows construction of a larger formation of more agents that can be rendered structurally stable in a distributed manner from some initial formation that is structurally stable. Closely related to [61] is the work of the same authors [62]. The main contribution of this paper is introducing new properties of minimally rigid graphs that allow composition of smaller rigid subgraphs that construct a larger rigid graph. The authors construct an *algebra over graphs* that allows performing some basic operations on graphs including rejoining two graphs, node augmentation to a graph and splitting of a graph. The same formation graphs are used by the authors in [60] to design centralized and distributed control laws to achieve structural stability. An *equilibrium formation* is defined as a zero of a (positive definite) *structural potential function*. Two types of structural potential functions are constructed in this paper, one giving rise to a centralized, and one to a decentralized controller, based on vertex neighbor definition. The desired controllers

6

achieving structural stabilization are guaranteed to work properly if the agents are in so-called c - *neighborhoods* of the formation graph induced by the potential function and if the initial velocities are small enough.

Very related to the approach described in the above paragraph is the work of Eren and Morse [31, 32]. The aim of these papers is mainly to draw attention to some results in the rigidity literature, as the ones described in [86, 69], and to develop some specific new results along the same lines. Minimally rigid graphs are now called *isostatic* graphs and very similar problems are approached. The closing rank problem, which is the problem of designing rearrangements of maintenance links among vehicles in case of vehicle removals, so that remaining vehicles maintain a rigid formation, is approached in [31]. The 2D and 3D cases are considered separately. The removal of a node with two, three, four and higher maintenance links is solved for each case by determining the additional links to be added after removal so that isostasy of the graph is maintained. A *rigidity condition*, very similar to the one derived in a more geometrical framework in Chapter 5 of this thesis, is presented in [32]. Also, two inductive methods for construction of rigid formations are included. The first generates an isostatic graph and is based on a Hennenberg construction. While this method creates rigid formations, it does not consider the lengths of maintenance links and the angles between them, and, therefore, it is not of much practical use. A way around this limitations is developed by the authors by use of a new construction method based on Delaunay triangulation.

An alternative to constructing natural structural potential functions from the formation

7

graphs and a relaxation to the rigidity requirement as described in [61, 62, 60] is to use *artificial potential functions*, as Leonard and Fiorelli suggest in [50]. The use of artificial potentials in their work is based on the following elements inspired from biology: (1) attraction to distant neighbors up to a maximum distance, (2) repulsion from neighbors too close, and (3) alignment with neighbors. Besides the actual fully actuated vehicles, the formation is augmented with *virtual leaders*, used to introduce the mission: direct and manipulate the vehicle group bahaviour. The control law for each agent is derived as the sum of the gradients of two types of potential functions: inter-vehicle potential fields and potential fields associated with virtual leaders. A dissipative term is added to achieve asymptotic stability. The procedure provides the construction of a Lyapunov function to prove closed loop local asymptotic stabilitity using the system kinetic energy and the artificial potential energy. The global minimum is, in general, not unique. Since there is no ordering of the vehicles, any permutation in a given configuration that corresponds to a global minimum will also be a global minimum. Further, because the potentials only depend upon relative distance, the solution exhibits $SE(l)$, $l = 1, 2, 3$ symmetry and also expansion/contraction symmetries. These symmetries are further exploited by the authors in [59] to decouple the mission control problem into a formation keeping subproblem and a maneuver subproblem. The designed trajectories of the virtual leaders play a key role in both subproblems: the path is designed to satisfy the group mission while the speed along the path is limited to ensure convergence and stability of the formation. The latter is guaranteed by regulating the virtual leader speed according to a feedback measurement

8

of a formation error function.

Virtual leaders and robots are also used for coordination and control in [58], [30]. The robots are modeled as affine control systems with outputs given by the position in plane or space. The formation constraint is modeled as the zero of a differentiable, positive definite and strictly convex *formation function* of the outputs. Desired trajectories for the robots are constructed along the steepest descent direction of the formation function. The novelty of this work is that the time is re-parameterized along these trajectories so that, while moving towards the desired configuration (zero of the formation function), the robots "wait" for each other if necessary

Along different lines, a geometric formulation of formation graphs is given in [80]. Centralized formations are modeled as undirected graphs and decentralized formations as directed graphs. Differential geometric conditions that guarantee formation feasibility given the individual agent kinematics are derived.

1.3 Abstraction and control for large groups of robots

When a large number of agents is required to be coordinated and controlled, some level of abstraction is necessary, dependent on the imposed task. The virtual structure approach, which can be seen as an abstraction, is not appropriate in many applications, including passing through narrow tunnels and obstacle avoidance.

It is believed that motion planning and control of large numbers of inexpensive robots can benefit from the understanding of behaviors and communication structures observed

9

in fish, termites, ants, or bees. Mathematical biologists have been working on modeling of swarming behavior for a long time. The general understanding now is that the swarming behavior is a result of an interplay between a long range attraction and a short range repulsion between the individuals. For example, in [21] the authors propose a simple model consisting of a constant attraction term and a repulsion term proportional to the square of the distance between two members, whereas in [85] a whole family of attraction - repulsion functions is studied.

In parallel with the biologists, physicists have done interesting work on swarming behavior. Their general approach is to model each individual as a particle and study the collective behavior due to their interactions. In [84], Vicsek et. al. propose a simple discrete-time model of n autonomous agents producing interesting flocking and schooling behaviors. In [84], all agents are moving in the plane with the same speed but with different headings. Each agent's heading is updated using a local rule based on the average of its own heading plus the headings of the *neighbors*. Agent i's neighbors at time t are those agents for which are in a circle of a specified radius centered at agent's i current position. The authors call this the *nearest neighbor rule*. A more sophisticated, almost similar model was developed by Reynolds [68] for simulating visually satisfying flocking and schooling-like behaviors for the animation industry. In both [84] and [68], it is proved by simulation that the nearest neighbor rule can cause all agents to eventually move in the same direction despite the absence of centralized coordination. A theoretical explanation for this observed interesting behavior is given by Jadbabaie et. al. in [47]. The neighbor

10

relationships are modeled on undirected graphs: the nodes are agents and an edge between two agents means that the agents are in each other's neighborhood. The proof of convergence is based on the Wolfowitz Theorem on *row stochastic* matrices.

A more practical approach can be found in [67], where the authors consider a distributed control scheme for groups of robots, called social potential fields method, which is based on artificial force laws between individual robots and robot groups. The force laws are inverse power (inspired from molecular interactions) or spring force laws, incorporating both attraction and repulsion. Interesting simulation results are included, but there are no rigorous proofs of convergence.

A continuous time model for swarm aggregation is presented in [36]. This work is based on the pairwise definition of a simple scalar function of relative positions of the robots which is attractive for large distances and repulsive for small distances. Each individual is applied a vector field which the sum of the attraction and repulsion of all the other members on this member. The authors show that, under this particular vector field, the agents will form a cohesive swarm and eventually come to rest. An explicit bound on the swarm size, which only depends on the parameters of the swarm model, is also given.

Partial differential equations are also used to model swarming behavior. In [82], the population density is shown to satisfy an advection equation and numerical simulation show that the population density is roughly constant in the region occupied by the swarm, results similar to the ones observed in nature. A finite difference approximation to the solution of the PDEs that arise from a gradient flow energy minimization are used for

11

mobile robot path planning in [51].

The geometric pattern formation in swarms is approached in discrete time as well. In [77], the authors propose a simple distributed heuristic algorithm for convergence to a circle, while in [78], algorithms for converging to a single point are presented.

1.4 Organization of the dissertation

The remainder of this thesis is organized as follows. Chapter 2 is a short overview of the differential geometry tools that are used in this thesis. After introducing some useful Lie groups, invariance of both metrics and vector fields are reviewed. Geodesics and higher order optimal curves for a given metric are characterized and the parameterizations used in this thesis are defined.

One of the problems treated in this thesis is finding a trajectory of a rigid body between given starting and ending positions and orientations that minimizes a given cost function. Because the set of all positions and orientations ($SE(3)$) is not Euclidean, there is no obvious choice of a metric on this set. Chapter 3 is a detailed discussion on the existence of useful metrics, with emphasis on invariance.

Chapter 4 describes a method for generating smooth trajectories for a moving rigid body with specified boundary conditions. The method is based on first constructing optimal trajectories in a larger manifold and then project them on the Lie group of rigid body displacements. The overall procedure is invariant to the choice of the inertial frame and computationally less expensive than traditional methods.

12

Smooth trajectories for a set of mobile robots satisfying constraints on relative positions are generated in Chapter 5. It is shown that, given two end configurations of the set of robots, by tuning one parameter, the user can choose an interpolating trajectory from a continuum of curves varying from the trajectory corresponding to maintaining a rigid formation to trajectories that allow the formation to change and the robots to reconfigure while moving.

Chapter 6 approaches the problem of controlling a large number of agents required to accomplish a task. The specific task suggest a corresponding abstraction of the formation. The method proposed in this chapter involves the definition of a low-cardinality set of *group variables* and design a control system on the corresponding *group manifold*. The designed control vector field on the group manifold will determine a specific control law for each agent, dependent only on the group variables and its own state.

In Chapter 7, we show how the ideas developed in Chapter 6 can be easily extended to control teams of car-like robots. Illustrative experimental results are included, together with a succinct description of out experimental platform.

The thesis concludes with final remarks and directions of future work in Chapter 8.

Chapter 2

The geometry of rigid body motion

This chapter is a short review of the differential geometry tools necessary to understand our approach to the study of rigid body motion. It is not intended to provide complete definitions and characterizations, but merely to introduce notation. The reader is assumed to be familiar with the notions of differentiable manifolds, coordinate charts, and Lie groups. A nice review is given in the Appendix of [56]. Detailed definitions can be found in [29].

Section 2.1 introduces the Lie groups which are relevant for this work: $GL(n)$, $GL^+(n)$, $SO(n)$, $GA(n)$, $GA^+(n)$, and $SE(n)$. Left invariant vector fields and metrics are defined in Sections 2.2 and 2.3, respectively. The geodesics and higher order optimal curves for a given metric can be characterized as in Section 2.4. Exponential coordinates and quaternions, the two types of parameterizations of $SO(3)$ that are used in this thesis are defined in Sections 2.5 and 2.6.

14

2.1 Matrix Lie groups

Let $GL^+(n)$ denote the set of all $n \times n$ real matrices with positive determinant:

$$GL^+(n) = \{M \mid M \in \mathbf{R}^{n \times n}, \det M > 0\} \tag{2.1}$$

$SO(n)$ is a subset of GL^+, defined as

$$SO(n) = \{R \mid R \in GL^+(n), RR^T = I\} \tag{2.2}$$

Let

$$GA^+(n) = \left\{ B \mid B = \begin{bmatrix} M & d \\ 0 & 1 \end{bmatrix}, \ M \in GL^+(n), d \in \mathbf{R}^n \right\}, \tag{2.3}$$

and

$$SE(n) = \left\{ A \mid A = \begin{bmatrix} R & d \\ 0 & 1 \end{bmatrix}, \ R \in SO(n), d \in \mathbf{R}^n \right\}. \tag{2.4}$$

$GL^+(n)$, $SO(n)$, $GA^+(n)$, and $SE(n)$ have the structure of a group under matrix multiplication. Moreover, matrix multiplication and inversion are both smooth operations, which make all $GL^+(n)$, $SO(n)$, $GA^+(n)$, and $SE(n)$ Lie groups [29].

$GL^+(n)$ and $GA^+(n)$ are subgroups of the general linear group $GL(n)$ (the set of all nonsingular $n \times n$ matrices) and of the affine group $GA(n) = GL(n) \times \mathbf{R}^n$, respectively. $SO(n)$ is referred to as the special orthogonal group or the rotation group on $\mathbf{R}^n$. $SE(n)$ is the special Euclidean group, and is the set of all rigid displacements in $\mathbf{R}^n$.

Special consideration will be given to $SO(3)$ and $SE(3)$. Consider a rigid body moving in free space. Assume any inertial reference frame $\{F\}$ fixed in space and a frame

15

$\{M\}$ fixed to the body at point O' as shown in Figure 2.1. At each instance, the config-uration (position and orientation) of the rigid body can be described by a homogeneous transformation matrix, $A \in SE(3)$, corresponding to the displacement from frame $\{F\}$ to frame $\{M\}$.
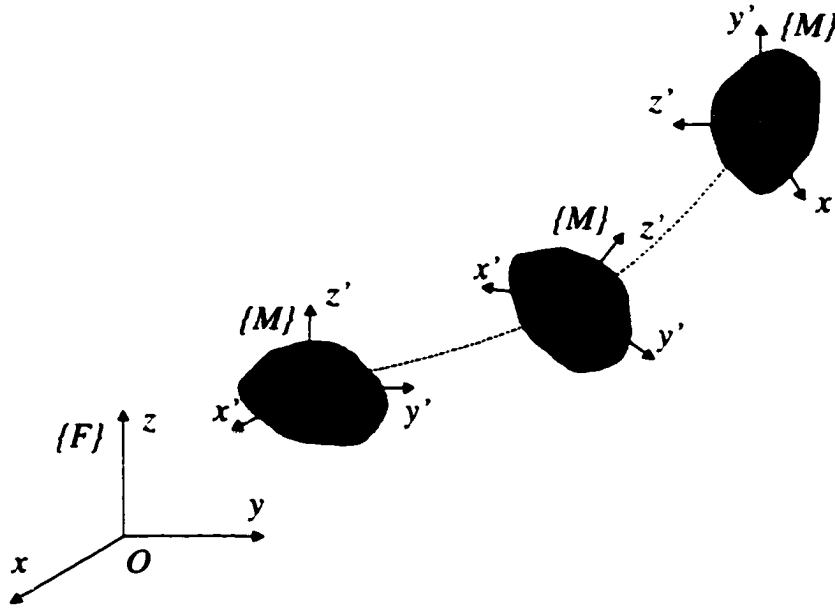
Figure 2.1: The inertial (fixed) frame and the moving frame attached to the rigid body

On any Lie group the tangent space at the group identity has the structure of a Lie algebra. The Lie algebras of $SO(3)$ and $SE(3)$, denoted by $so(3)$ and $se(3)$ respectively, are given by:

$$so(3) = \left\{ \hat{\omega} \mid \hat{\omega} \in \mathbf{R}^{3\times3}, \hat{\omega}^T = -\hat{\omega} \right\}, \tag{2.5}$$

$$se(3) = \left\{ S = \begin{bmatrix} \hat{\omega} & v \\ 0 & 0 \end{bmatrix} \mid \hat{\omega} \in so(3), v \in \mathbf{R}^3 \right\}, \tag{2.6}$$

where $(\hat{\ })$ is the skew-symmetric operator.

16

Given a curve

$$A(t) : [-a, a] \to SE(3), \quad A(t) = \begin{bmatrix} R(t) & d(t) \\ 0 & 1 \end{bmatrix}$$

an element $S(t)$ of the Lie algebra $se(3)$ can be identified with the tangent vector $\dot{A}(t)$ at an arbitrary point t by:

$$S(t) = A^{-1}(t)\dot{A}(t) = \begin{bmatrix} \tilde{\omega}(t) & R^T \dot{d} \\ 0 & 0 \end{bmatrix}. \tag{2.7}$$

where $\tilde{\omega}(t) = R(t)^T \dot{R}(t)$ is the corresponding element from $so(3)$.

A curve on $SE(3)$ physically represents a motion of the rigid body. If $\{\omega(t), v(t)\}$ is the vector pair corresponding to $S(t)$, then ω physically corresponds to the angular velocity of the rigid body while v is the linear velocity of the origin O' of the frame $\{M\}$, both expressed in the frame $\{M\}$. In kinematics, elements of this form are called twists and $se(3)$ thus corresponds to the space of twists. The twist $S(t)$ computed from Equation (2.7) does not depend on the choice of the inertial frame $\{F\}$. The proof is given in the next chapter. For this reason, $S(t)$ is called the left invariant representation of the tangent vector $\dot{A}$.

The standard basis for the vector space $so(3)$ is:

$$L_1^o = \tilde{e}_1 \quad L_2^o = \tilde{e}_2 \quad L_3^o = \tilde{e}_3 \tag{2.8}$$

where

$$e_1 = \begin{bmatrix} 1 & 0 & 0 \end{bmatrix}^T, \; e_2 = \begin{bmatrix} 0 & 1 & 0 \end{bmatrix}^T, \; e_3 = \begin{bmatrix} 0 & 0 & 1 \end{bmatrix}^T$$

17

L_1^o, L_2^o and L_3^o represent instantaneous rotations about the Cartesian axes x, y and z, respectively. The components of a $\hat{\omega} \in so(3)$ in this basis are given precisely by the angular velocity vector ω.

The standard basis for $se(3)$ is:

$$L_1 = \begin{bmatrix} L_1^o & 0 \\ & \\ 0 & 0 \end{bmatrix} \quad L_2 = \begin{bmatrix} L_2^o & 0 \\ & \\ 0 & 0 \end{bmatrix} \quad L_3 = \begin{bmatrix} L_3^o & 0 \\ & \\ 0 & 0 \end{bmatrix}$$

$$L_4 = \begin{bmatrix} 0 & e_1 \\ & \\ 0 & 0 \end{bmatrix} \quad L_5 = \begin{bmatrix} 0 & e_2 \\ & \\ 0 & 0 \end{bmatrix} \quad L_6 = \begin{bmatrix} 0 & e_3 \\ & \\ 0 & 0 \end{bmatrix} \tag{2.9}$$

The twists L_4, L_5 and L_6 represent instantaneous translations along the Cartesian axes x, y and z, respectively. The components of a twist $S \in se(3)$ in this basis are given precisely by the velocity vector pair, $s := \{\omega, v\} \in \mathbf{R}^6$.

2.2 Left invariant vector fields

A *differentiable vector field* is a smooth assignment of a tangent vector to each element of the manifold. An example of a differentiable vector field, X, on $SE(3)$ is obtained by left translation of an element $S \in se(3)$. The value of the vector field X at an arbitrary point $A \in SE(3)$ is given by:

$$X(A) = \bar{S}(A) = AS. \tag{2.10}$$

A vector field generated by Equation (2.10) is called a left invariant vector field and the notation $\bar{S}$ is used to indicate that the vector field was obtained by left translating the Lie

18

algebra element S.

Since the vectors $L_1, L_2, \ldots, L_6$ are a basis for the Lie algebra $se(3)$, the vectors $\bar{L}_1(A), \ldots, \bar{L}_6(A)$ form a basis of the tangent space at any point $A \in SE(3)$. Therefore, any vector field X can be expressed as

$$X = \sum_{i=1}^{6} X^i \bar{L}_i, \qquad (2.11)$$

where the coefficients X^i vary over the manifold. If the coefficients are constants, then X is left invariant. By defining:

$$\omega = [X^1, X^2, X^3]^T, \qquad v = [X^4, X^5, X^6]^T,$$

we can associate a vector pair of functions $\{\omega, v\}$ to an arbitrary vector field X. If a curve $A(t)$ describes a motion of the rigid body and $V = dA/dt$ is the vector field tangent to $A(t)$, the vector pair $\{\omega, v\}$ associated with V corresponds to the instantaneous twist (screw axis) for the motion. In general, the twist $\{\omega, v\}$ changes with time.

2.3 Riemannian metrics on Lie groups

If a smoothly varying, positive definite, bilinear, symmetric form $< ., . >$ is defined on the tangent space at each point on the manifold, such a form is called a Riemannian metric and the manifold is Riemannian [29]. On a n dimensional manifold, the metric is locally characterized by a $n \times n$ matrix of C^∞ functions $g_{ij} = < X_i, X_j >$ where X_i are basis vector fields. If the basis vector fields can be defined globally, then the matrix $[g_{ij}]$ completely defines the metric.

19

On $SE(3)$ (on any Lie group), an inner product on the Lie algebra can be extended to a Riemannian metric over the manifold using left (or right) translation. To see this, consider the inner product of two elements $S_1, S_2 \in se(3)$ defined by

$$< S_1, S_2 >_I = s_1^T G s_2,$$ (2.12)

where s_1 and s_2 are the 6×1 vectors of components of S_1 and S_2 with respect to some basis and G is a positive definite matrix. If V_1 and V_2 are tangent vectors at an arbitrary group element $A \in SE(3)$, the inner product $< V_1, V_2 >_A$ in the tangent space $T_A SE(3)$ can be defined by:

$$< V_1, V_2 >_A = < A^{-1}V_1, A^{-1}V_2 >_I .$$ (2.13)

The metric obtained in such a way is said to be left invariant [29]. A detailed description and characterization of invariant metrics on $SE(3)$ is given in Chapter 3.

2.4 Affine connection, covariant derivative, geodesics and minimum acceleration curves

Any motion of a rigid body is described by a smooth curve $A(t) \in SE(3)$. The velocity is the tangent vector to the curve $V(t) = \frac{dA}{dt}(t)$.

An *affine connection* on $SE(3)$ is a map that assigns to each pair of C^∞ vector fields X and Y on $SE(3)$ another C^∞ vector field $\nabla_X Y$ which is R-bilinear in X and Y and, for any smooth real function f on $SE(3)$ satisfies $\nabla_{fX} Y = f \nabla_X Y$ and $\nabla_X fY = f \nabla_X Y + X(f)Y$.

20

The *Christoffel symbols* Γ^i_{jk} of the connection at a point $A \in SE(3)$ are defined by $\nabla_{\bar{L}_j} \bar{L}_k = \Gamma^i_{jk} \bar{L}_i$, where $\bar{L}_1, \ldots, \bar{L}_6$ is the basis in $T_A SE(3)$ and the summation is understood.

If $A(t)$ is a curve and X is a vector field, the *covariant derivative* of X along A is defined by

$$\frac{DX}{dt} = \nabla_{\dot{A}(t)} X$$

X is said to be *auto-parallel* along A if $DX/dt = 0$. A curve A is a *geodesic* if $\dot{A}$ is auto-parallel along A. An equivalent characterization of a geodesic is the following set of equations:

$$\ddot{a}^i + \Gamma^i_{jk} \dot{a}^j \dot{a}^k = 0 \tag{2.14}$$

where a_i, $i = 1, \ldots, 6$ is an arbitrary set of local coordinates on $SE(3)$. Geodesics are also minimum length curves. The length of a curve $A(t)$ between the points $A(a)$ and $A(b)$ is defined to be:

$$L(A) = \int_a^b < V, V >^{\frac{1}{2}} dt \tag{2.15}$$

where $V = \frac{dA(t)}{dt}$. It can be shown [29], that if there exists a curve that minimizes the functional L, this curve also minimizes the so called *energy functional*:

$$E(A) = \int_a^b < V, V > dt \tag{2.16}$$

For a manifold with a Riemannian (or pseudo-Riemannian) metric, there exists a

21

unique symmetric connection which is compatible with the metric [29]. Given a connection, the acceleration and higher derivatives of the velocity can be defined. The acceleration, $\mathcal{A}(t)$, is the covariant derivative of the velocity along the curve:

$$A = \frac{D}{dt}\left(\frac{dA}{dt}\right) = \nabla_V V \tag{2.17}$$

Minimum acceleration curves are defined as curves minimizing the square of the L^2 norm of the acceleration:

$$L_a = \int_a^b < \nabla_V V, \nabla_V V > dt, \tag{2.18}$$

where $V(t) = \frac{dA(t)}{dt}$, $A(t)$ is a curve on the manifold, and ∇ is the unique symmetric connection compatible with the given metric. The initial and final point as well as the initial and final velocity for the motion are prescribed.

2.5 Exponential map and local parameterization of $SE(3)$

If M is a manifold with a connection ∇, the *exponential map* at an arbitrary $q \in M$ is defined as follows. Let $\gamma_V(t)$ be the unique geodesic passing through q at $t = 0$ with velocity V, i.e. $\gamma_V(0) = q$ and $\dot{\gamma}_V(0) = V$. Then, by definition, $\exp_q$ maps $V \in T_q M$ to the point $\gamma_V(1) \in M$. Using homogeneity of geodesics, it is easy to prove [29] that $\gamma_{tV}(s) = \gamma_V(ts)$ which gives $\exp_q(tV) = \gamma_V(t)$. Also, $\exp_q$ is a diffeomorphism of a neighborhood of $0 \in T_q M$ to a neighborhood of $q \in M$. This gives a local chart for M called *normal coordinates*. These coordinates are convenient for computations (as in this work) because rays through 0 are geodesics.

22

The exponential map on $SO(3)$ with metric $G = \alpha I$ is given special consideration in this thesis. For $R \in SO(3)$ and $V \in T_R SO(3)$, one can define $\exp_R(V) = Re^{R^T V}$. If $v = [v_1\ v_2\ v_3]$ is the expansion of V in the local basis of $T_R SO(3)$ (i.e. $V = v_1 \bar{L}_1^o + v_2 \bar{L}_2^o + v_3 \bar{L}_3^o$), it is easy to see that $\exp_R(V) = Re^{\hat{v}}$. As a special case, for $S \in so(3)$, $\exp_I(S) = e^{\hat{\sigma}}$, where $\sigma = [\sigma_1\ \sigma_2\ \sigma_3]$ is the expansion of S in the basis L_1^o, L_2^o, L_3^o. This gives a local parameterization of $SO(3)$ around identity known as *exponential coordinates*.

A parameterization of $SE(3)$ induced by the product structure $SO(3) \times \mathbf{R}^3$ can be chosen. In other words, a set of coordinates $\sigma_1, \sigma_2, \sigma_3, d_1, d_2, d_3$ for an arbitrary element $A = (R, d) \in SE(3)$ is defined so that d_1, d_2, d_3 are the coordinates of d in $\mathbf{R}^3$ and $R = e^{\hat{\sigma}}$, $\sigma \in \mathbf{R}^3$. Exponential coordinates are valid for $R \in SO(3)$ sufficiently close to the identity (*i.e.*, excluding the points $Tr(R) = -1$ ($Tr(A) = 0$), or, equivalently, rotations through angles $0 < \theta < \pi$).

The time derivative of σ can be expressed in terms of the body velocity as [22]:

$$\dot{\sigma} = \left(I + \frac{1}{2}\hat{\sigma} + (1 - \alpha(\|\sigma\|)) \frac{\hat{\sigma}^2}{\|\sigma\|^2} \right) \omega \qquad (2.19)$$

where $\alpha(y) = (y/2)cot(y/2)$.

2.6 Quaternions as parameterization of $SO(3)$

Consider the Euclidean $\mathbf{R}^4$ with coordinates (x_1, x_2, x_3, x_4). Following the usual notation, the basis vectors in the tangent space $T_x \mathbf{R}^4$ at an arbitrary point $x \in \mathbf{R}^4$ are denoted by

23

$\frac{\partial}{\partial x_i}$, $i = 1, \ldots, 4$. For $x \neq 0$, define a linear mapping

$$Q(x) : T_x\mathbb{R}^4 \to T_x\mathbb{R}^4, \quad Q(x) = \begin{bmatrix} x_4 & -x_3 & x_2 & -x_1 \\ x_3 & x_4 & -x_1 & -x_2 \\ -x_2 & x_1 & x_4 & -x_3 \\ -x_1 & -x_2 & -x_3 & -x_4 \end{bmatrix} \tag{2.20}$$

It is easy to see that $Q(x)$ is orthonormal ($QQ^T = Q^TQ = I_4$) when restricted to the unit

sphere S^3. Using Q, we define a change of basis at each $T_x\mathbb{R}^4$. The new basis vectors

$Y_j^{\cdot}(x)$ are defined by:

$$\frac{1}{2}Q^T(x)Y_j^{\cdot}(x) = \frac{\partial}{\partial x_j}, \quad j = 1, \ldots, 4 \tag{2.21}$$

The coordinates of the vectors $Y_j^{\cdot}$ in the basis $\frac{\partial}{\partial x_j}$ $j = 1, \ldots, 4$ are given by the columns

of Q multiplied by 2, respectively. Therefore, $Y_j^{\cdot}$, $j = 1, \ldots, 4$ are orthogonal. Moreover,

$Y_1^{\cdot}, Y_2^{\cdot}, Y_3^{\cdot}$ form a orthogonal basis of T_xS^3. Indeed, for $x \in S^3$, it is easy to see that, in

coordinates, $\bar{x}^TY_j^{\cdot} = 0$, $j = 1, 2, 3$ and $\bar{x}^TY_4^{\cdot} = -2$, where $\bar{x}$ is the vector drawn from the

origin to $x \in S^3$. The vector field

$$\dot{x} = \frac{1}{2}Q(x) \begin{bmatrix} \omega_1 \\ \omega_2 \\ \omega_3 \\ 0 \end{bmatrix} \tag{2.22}$$

evolves on a sphere in R^4. In the particular case when the initial $x(0)$ is at distance 1

from the origin, the system evolves on the unit sphere S^3. The coordinates (x_1, x_2, x_3, x_4)

restricted to S^3 are called unit quaternions. They can be used to parameterize any rotation

24

matrix $R \in SO(3)$:

$$R = \begin{bmatrix} x_1^2 - x_2^2 - x_3^2 + x_4^2 & 2(x_1 x_2 - x_3 x_4) & 2(x_1 x_3 + x_2 x_4) \\ 2(x_1 x_2 + x_3 x_4) & -x_1^2 + x_2^2 - x_3^2 + x_4^2 & 2(x_2 x_3 - x_1 x_4) \\ 2(x_1 x_3 - x_2 x_4) & 2(x_1 x_4 + x_2 x_3) & -x_1^2 - x_2^2 + x_3^2 + x_4^2 \end{bmatrix}$$

with the advantage that this parameterization does not have singularities. ω_i, $i = 1, 2, 3$ from (2.22) are exactly the components of the angular body velocity $\omega = (\omega_1, \omega_2, \omega_3)$ as defined in Section 2.1. Finally, the connection with the exponential coordinates σ defined in Section 2.5 can be easily seen if σ is written in the form $\sigma = \theta u$, where $u \in \mathbb{R}^3$ is a unit vector giving the axis of rotation and θ is the amount of rotation around u:

$$x = \begin{bmatrix} u \sin \frac{\theta}{2} \\ \cos \frac{\theta}{2} \end{bmatrix}$$

25

Chapter 3

Metric properties of $SE(3)$

One of the problems treated in this thesis is finding a trajectory of a rigid body between given starting and ending positions and orientations that minimizes a given cost function. Because the set of all positions and orientations ($SE(3)$) is not Euclidean, there is no obvious choice of a metric on this set. This chapter is a detailed discussion on the existence of useful metrics, with emphasis on invariance. Most of the results in this chapter can be found, in a slightly different form, in [56]. The adjoint action of $SE(3)$ on its Lie algebra $se(3)$, the basic tool for transforming twists for one frame to the other, together with the corresponding transformation rules, are given in Section 3.1. The notion of invariance of metrics on $SE(3)$ and $SO(3)$ is described and characterized in Section 3.2. The kinetic energy metric together with some corresponding optimal curves is analyzed in Section 3.3. The last section of this chapter is a discussion on screw motions, mostly to clarify the distinction between geodesics and one parameter subgroups.

26

3.1 Adjoint action of $SE(3)$ on $se(3)$ and frame transformation rules

Definition 1. *Let M be a smooth manifold and G a Lie group. A left action of G on M is a smooth map $\Phi_g : M \to M$, $g \in G$ such that*

- $\Phi_e(x) = x$, *for any $x \in M$;*

- *For every g, $h \in G$ and $x \in M$, $\Phi_g(\Phi_h(x)) = \Phi_{gh}(x)$.*

Definition 2. *Let G be a Lie group. The map $I_g : G \to G$, $g \in G$ given by $I_g(h) = ghg^{-1}$ is called the conjugation map.*

It is easy to see that the map I_g defines a left action of G on itself.

Definition 3. *The tangent map of I_g at identity e, $Ad_g = T_e I_g$ is called the adjoint action of G on $\mathbf{g}$, its Lie algebra.*

If G is a subgroup of $GL(n, \mathbf{R})$ (like $SO(3)$ and $SE(3)$), then $Ad_g S = gSg^{-1}$ where $S \in \mathbf{g}$ is written in matrix form [56]. In this work, we are interested in the actions of the groups $SO(3)$ and $SE(3)$ on their Lie algebras $so(3)$ and $se(3)$, respectively. The adjoint action of $A = \begin{bmatrix} R & d \\ 0 & 1 \end{bmatrix} \in SE(3)$ on $S \in se(3)$ is given by:

$$S = \begin{bmatrix} \hat{\omega} & v \\ 0 & 0 \end{bmatrix} \in se(3), \quad Ad_A S = ASA^{-1} = \begin{bmatrix} \widehat{R\omega} & Rv - \widehat{R\omega}d \\ 0 & 0 \end{bmatrix} \in se(3) \quad (3.1)$$

27

If the twist is written in vector form, the adjoint action Ad_A can be represented by a 6×6 matrix $[Ad_A]$:

$$s = \begin{bmatrix} \omega \\ v \end{bmatrix} \in se(3), \quad Ad_A s = [Ad_A]s \in se(3), \quad [Ad_A] = \begin{bmatrix} R & 0 \\ \dot{d}R & R \end{bmatrix} \tag{3.2}$$

The adjoint action of $SE(3)$ on $se(3)$ can be used to write transformation rules for trajectories and twists when the inertial or the body frame are displaced.

Assume we have a rigid body moving in 3D space. Let $\{F\}$ be an inertial (fixed) frame and $\{M\}$ be a frame fixed to the body (body frame). The motion of the body in the inertial frame can be uniquely described by a curve $A(t) = g_{FM}(t) \in SE(3)$ giving the rotation of $\{M\}$ in $\{F\}$ and the position of the center of $\{M\}$ in $\{F\}$. For each curve $A(t)$ from $SE(3)$, consider the twist $S(t) = A^{-1}(t)\dot{A}(t) \in se(3)$.

Proposition 1 gives the transformation rule for displacements of body frames.

Proposition 1. *Assume the body frame is displaced by (a constant) $g_{MM'}$ to $\{M'\}$ (see Figure 3.1). Let $A'(t) = g_{FM'}(t) \in SE(3)$ describe the motion of $\{M'\}$ in $\{F\}$ and $S'(t)$ be the corresponding twist. Then, the following are true:*

- $A'(t) = A(t)g_{MM'}$

- $S'(t) = Ad_{g_{M'M}}S(t)$

Proof. The first part follows immediately from composition rule for elements in $SE(3)$. For the second part from the composition rule $g_{FM'} = g_{FM}g_{MM'}$, the definition of adjoint map and the definition of twists we have

$$S'(t) = A'^{-1}(t)\dot{A}'(t) = g_{FM'}^{-1}\dot{g}_{FM'} = g_{MM'}^{-1}g_{FM}^{-1}\dot{g}_{FM}g_{MM'} = Ad_{g_{MM'}^{-1}}S(t) = Ad_{g_{M'M}}S(t)$$

28

or, if the twists are written in vector form,

$$s'(t) = [Ad_{g_{M'M}}]s(t)$$

where the 6×6 matrix form of the adjoint action is given by (3.2). □
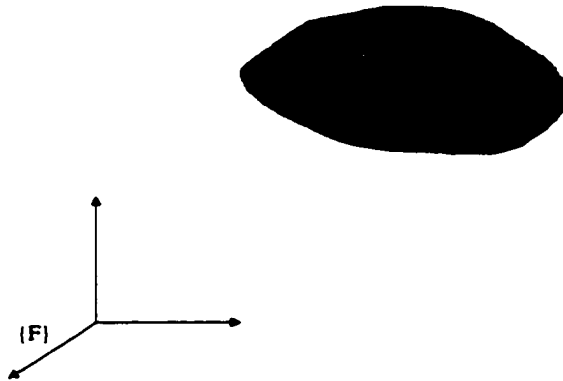
Figure 3.1: Displacement of body frame

Proposition 2 describes the transformation rules for changes in the inertial frame.

Proposition 2. *Assume that the inertial frame* $\{F\}$ *is displaced by a constant* $g_{FF'}$ *to a new* $\{F'\}$ *as the body fixed frame* $\{M\}$ *is left unchanged (see Figure 3.2). Let* $A'(t) = g_{F'M} \in SE(3)$ *denote the motion of* $\{M\}$ *as seen from* $\{F'\}$. *The following describe the relation between curves and twists when the inertial frame is displaced:*

- $A'(t) = g_{F'F}A(t)$;

- $S'(t) = S(t)$.

29

Proof. For the first part, $A'(t) = g_{F'M}(t) = g_{FF'}^{-1}g_{FM}(t) = g_{F'F}A(t)$. For the second part, we can write:

$$S'(t) = A'^{-1}(t)\dot{A}'(t) = g_{F'M}^{-1}\dot{g}_{F'M} = g_{FM}^{-1}g_{F'F}^{-1}g_{FF'}\dot{g}_{FM} = g_{FM}^{-1}\dot{g}_{FM} = S(t)$$

$\square$
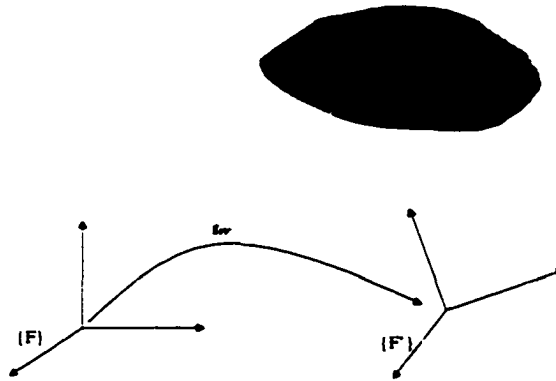
Figure 3.2: Displacement of inertial frame

Corollary 1. *The twist* $S(t) = A^{-1}(t)\dot{A}(t)$ *is invariant to changes in the pose of the inertial frame. The adjoint of the transformation of body frame relates the twists when the body frame is displaced.*

3.2 Invariant metrics on $SE(3)$

Assume that the inner product of two elements $S_1, S_2 \in se(3)$ is defined by

$$< S_1, S_2 >_I = s_1^T W s_2, \quad W = [w_{ij}], \quad w_{ij} = < L_i, L_j >_I \tag{3.3}$$

30

where L_i, $i = 1, \ldots, 6$ is the basis of $se(3)$ as defined in (2.9) and W is a positive definite symmetric matrix. If V_1 and V_2 are tangent vectors at an arbitrary group element $A \in SE(3)$, the inner product $< V_1, V_2 >_A$ in the tangent space $T_A SE(3)$ can be defined by extending the metric at identity through left invariance:

$$< V_1, V_2 >_A = < A^{-1} V_1, A^{-1} V_2 >_I .$$

(3.4)

If the basis L_1, L_2, ..., L_6 is extended through left invariance throughout the manifold to $\bar{L}_1$, $\bar{L}_2$, ..., $\bar{L}_6$, then we can write

$$V_1 = \sum_i V_1^i \bar{L}_i = A \sum_i V_1^i L_i, \quad V_2 = \sum_i V_2^i \bar{L}_i = A \sum_i V_2^i L_i$$

and the metric at $A \in SE(3)$ becomes:

$$< V_1, V_2 >_A = < A^{-1} V_1, A^{-1} V_2 >_I = \sum_{i,j} V_1^i V_2^j < L_i, L_j >_I = \sum_{i,j} V_1^i V_2^j w_{ij}$$

So a left invariant inner product of two vectors at an arbitrary point on $SE(3)$ can be written using the local coordinates of the vectors and the matrix of the metric defined at identity.

Proposition 3. *A left invariant metric is independent of the choice of the inertial frame.*

Proof. Let any $A \in SE(3)$ and any V_1, $V_2 \in T_A SE(3)$. We can always find two curves $A_1(t), A_2(t) \in SE(3)$ so that $A_1(0) = A_2(0) = A$ and $V_1 = \frac{dA_1}{dt}(0)$, $V_2 = \frac{dA_2}{dt}(0)$. Then,

$$< V_1, V_2 >_A = < \frac{dA_1}{dt}(0), \frac{dA_2}{dt}(0) >_A = < A_1^{-1}(0) \frac{dA_1}{dt}(0), A_2^{-1}(0) \frac{dA_2}{dt}(0) >_I$$

where left invariance of the metric has been used. But the twists inside $<, >_I$ are invariant to change of inertial frame by Proposition 2, and the proposition is proved. $\square$

31

The following Lemma gives a description of bi-invariant quadratic forms in terms of adjoint actions.

Lemma 1. *Let $<,>$ be a quadratic form (bilinear and symmetric) defined at identity of $SE(3)$ and extended through left invariance throughout the manifold. Then, $<,>$ is bi-invariant if and only if*

$$< S_1, S_2 >_I = < Ad_A S_1, Ad_A S_2 >_I, \quad \forall A \in SE(3), \quad \forall S_1, S_2 \in se(3) \qquad (3.5)$$

Proof. To prove necessity, because $< . >$ is both left and right invariant, for any $S_1, S_2 \in se(3)$ and any $A \in SE(3)$, we have:

$$< S_1, S_2 >_I = < AS_1, AS_2 >_A = < AS_1 A^{-1}, AS_2 A^{-1} >_{AA^{-1}} = < AS_1 A^{-1}, AS_2 A^{-1} >_I$$

For sufficiency, we only need to prove that the quadratic form is right invariant. Let $V_1(B)$ and $V_2(B)$ be two vectors from $T_B SE(3)$ where B is an arbitrary element of $SE(3)$. Then, for any $A \in SE(3)$, we have

$$< V_1(B)A, V_2(B)A >_{BA} = < (BA)^{-1} V_1(B)A, (BA)^{-1} V_2(B)A >_{(BA)^{-1}BA} =$$

$$< A^{-1}B^{-1} V_1(B)A, A^{-1}B^{-1} V_2(B)A >_I =$$

$$< AA^{-1}B^{-1} V_1(B)AA^{-1}, AA^{-1}B^{-1} V_2(B)AA^{-1} >_I =$$

$$< B^{-1} V_1(B), B^{-1} V_2(B) >_I = < V_1(B), V_2(B) >_B$$

which proves right invariance. Left invariance has been used twice and equation (3.5) once. ☐

32

It is interesting to note that Lemma 1 is not only valid for SE(3), but also for a generic Lie group G and its Lie algebra g.

Theorem 1. *Let W be the matrix representation of a quadratic form $<,>$ defined at identity of $SE(3)$ and extended through left invariance throughout the manifold. Then the quadratic is bi-invariant if and only if W has the form:*

$$W = \begin{bmatrix} \alpha I & \beta I \\ \beta I & 0 \end{bmatrix} \tag{3.6}$$

Proof. By Lemma 1, $<,>$ is bi-invariant if and only if (3.5) is valid for all S_1, $S_2 \in se(3)$ and $A \in SE(3)$. Let

$$W = \begin{bmatrix} M & N \\ N^T & P \end{bmatrix}$$

where M, N, $P \in \mathbf{R}^{3 \times 3}$ and M, P are symmetric. If we write (3.5) with the twists in vector form (and consequently the adjoint map Ad_A in matrix form) we get:

$$s_1^T W s_2 = s_1^T [Ad_A]^T W [Ad_A] s_2, \quad \forall A \in SE(3), \forall s_1, s_2 \in \mathbf{R}^6$$

which is true if and only if

$$W = [Ad_A]^T W [Ad_A], \quad \forall A \in SE(3)$$

Let a generic element $A \in SE(3)$. Then, by (3.1),

$$A = \begin{bmatrix} R & d \\ 0 & 1 \end{bmatrix} \Rightarrow [Ad_A] = \begin{bmatrix} R & 0 \\ \hat{d}R & R \end{bmatrix}$$

33

Then the condition for bi-invariance becomes:

$$\begin{bmatrix} M & N \\ N^T & P \end{bmatrix} = \begin{bmatrix} R^T & -R^T\hat{d} \\ 0 & R^T \end{bmatrix} \begin{bmatrix} M & N \\ N^T & P \end{bmatrix} \begin{bmatrix} R & 0 \\ \hat{d}R & R \end{bmatrix}$$

which is equivalent to:

$$M = R^T M R - R^T \hat{d} N^T R + R^T N \hat{d} R - R^T \hat{d} P \hat{d} R$$

$$N = R^T N R - R^T \hat{d} P R \tag{3.7}$$

$$P = R^T P R$$

The third equation from (3.7) is equivalent to finding a symmetric $P \in \mathbf{R}^{3 \times 3}$ which

commutes with all $R \in SO(3)$. Let v be an eigenvector of P corresponding to eigenvalue

γ. Then $Pv = \gamma v$ and $RPv = PRv$, from which $P(Rv) = \gamma(Rv)$, $\forall R \in SO(3)$.

Therefore, $Pw = \gamma w$, $\forall w$ on the unit sphere in $\mathbf{R}^3$. By taking w as the standard Euclidean

basis in $\mathbf{R}^3$ it follows that

$$P = \gamma I$$

Now let $d = 0$ in the first and second equations from (3.7). By the same argument earlier,

$$N = \beta I, \quad M = \alpha I$$

If P, N and M are replaced in the first equation of (3.7), it follows that $\gamma(\hat{d})^2 = 0$, $\forall d \in$

$\mathbf{R}^3$ from which $\gamma = 0$. $\qquad \square$

Note that the matrix in (3.6) is not definite. Indeed, it has two distinct eigenvalues

$$\lambda_1 = \frac{1}{2}(\alpha + \sqrt{\alpha^2 + 4\beta^2}) \quad \lambda_2 = \frac{1}{2}(\alpha - \sqrt{\alpha^2 + 4\beta^2}),$$

34

both of multiplicity 3. Their product is $\lambda_1\lambda_2 = -\beta^2$. If $\beta = 0$, then $\lambda_2 = 0$. If $\beta \neq 0$ then $\lambda_2 < 0$. In both cases, the matrix cannot be positive definite. Hence we have the following:

Corollary 2. *There does not exist a bi-invariant metric on SE(3).*

Now it is easy to restrict all the discussion above to the Lie group $SO(3)$ of rotations in $\mathbf{R}^3$. For a curve $R(t) \in SO(3)$, the corresponding time-dependent element from $so(3)$ can be written in matrix form $\hat{\omega} = R^T(t)\dot{R}(t)$ or in vector form $\omega \in \mathbf{R}^3$. Because $SO(3)$ is a subgroup of the general linear group $GL(3, \mathbf{R})$, the action of the adjoint map on an element from $so(3)$ written in matrix form can be written as

$$Ad_R(\omega) = R\hat{\omega}R^T$$

By the general fact that

$$\widehat{R\omega} = R\hat{\omega}R^T, \quad \forall \omega \in \mathbf{R}^3 \ \forall R \in SO(3)$$

we conclude that the action of the adjoint on an element from $so(3)$ written in vector form is simply multiplication with R from the right. A similar result to Theorem 1 can now be stated and proved for $SO(3)$:

Theorem 2. *Let W be the matrix representation of a quadratic form $<,>$ defined at identity of $SO(3)$ and extended through left invariance throughout the manifold. Then the quadratic is bi-invariant if and only if W has the form:*

$$W = \alpha I \tag{3.8}$$

35

Proof. By Lemma 1, the quadratic is bi-invariant if and only if

$$< \omega_1, \omega_2 >_I = < Ad_R\omega_1, Ad_R\omega_2 >_I, \quad \forall R \in SO(3), \quad \forall \omega_1, \omega_2 \in se(3)$$

or, equivalently,

$$\omega_1^T W \omega_2 = \omega_1^T R^T W R \omega_2, \quad \forall R \in SO(3), \forall \omega_1, \omega_2 \in \mathbf{R}^3$$

which is true if and only if

$$W = R^T W R, \quad \forall R \in SO(3)$$

The proof is complete by the same argument as in Theorem 1. $\qquad\square$

If α from Theorem 2 is positive, the quadratic form becomes a metric and the following is true:

Corollary 3. *Let W be the matrix representation of a metric $<, >$ defined at identity of $SO(3)$ and extended through left invariance throughout the manifold. Then the metric is bi-invariant if and only if W has the form:*

$$W = \alpha I, \ \alpha > 0 \tag{3.9}$$

3.3   The kinetic energy metric

A metric that is attractive for trajectory planning can be obtained by considering the dynamic properties of the rigid body. The kinetic energy of a rigid body is a scalar that does not depend on the choice of the inertial reference frame. It thus defines a left invariant

metric. If the body-fixed reference frame is attached at the centroid and aligned with the principal axis of the body, the matrix W as in Eq. (3.3) is given by

$$W = \frac{1}{2} \begin{bmatrix} H & 0 \\ 0 & mI \end{bmatrix},$$

(3.10)

where m is the mass of the rigid body and H is the diagonal inertia matrix of the body about the body frame $\{M\}$. If $\{\omega, v\} \in se(3)$ is the vector pair associated with some velocity vector V, the norm of the vector V assumes the familiar expression of the kinetic energy:

$$< V, V > = \frac{1}{2}\omega^T H \omega + \frac{1}{2}mv^T v.$$

(3.11)

The kinetic energy metric depends on the choice of the body fixed frame M. The following proposition describes this dependence.

Proposition 4. *Assume the body fixed frame is displaced from* $\{M\}$ *to* $\{M'\}$ *by*

$$g_{M'M} = \begin{bmatrix} R & d \\ 0 & 1 \end{bmatrix}$$

Then the matrix of the kinetic energy metric is changed to

$$W_g = \begin{bmatrix} R^T H R - mR^T(\hat{d})^2 R & -mR^T \hat{d}R \\ mR^T \hat{d}R & mI \end{bmatrix},$$

(3.12)

Proof. Because of the change of body frame, according to Proposition 1, the new twists become:

$$S_1' = Ad_{g_{M'M}}S_1, \quad S_2' = Ad_{g_{M'M}}S_2, \quad [Ad_{g_{M'M}}] = \begin{bmatrix} R & 0 \\ \hat{d}R & R \end{bmatrix}$$

37

Therefore, we can write (all the metrics are written at identity):

$$< S_1', S_2' >_I = < Ad_{g_{M'M}} S_1, Ad_{g_{M'M}} S_2 >_I = s_1^T [Ad_{g_{M'M}}]^T W [Ad_{g_{M'M}}] s_2$$

So, the matrix of the metric becomes

$$W_g = [Ad_{g_{M'M}}]^T W [Ad_{g_{M'M}}] = \begin{bmatrix} R^T & -R^T \hat{d} \\ 0 & R^T \end{bmatrix} \begin{bmatrix} H & 0 \\ 0 & mI \end{bmatrix} \begin{bmatrix} R & 0 \\ \hat{d}R & R \end{bmatrix}$$

which is the same as (3.12).   □

In [91] it has been proved that a geodesic $A(t)$ on $SE(3)$ equipped with metric (3.10)

is described by

$$\frac{d\omega}{dt} = -H^{-1}(\omega \times (H\omega)) \tag{3.13}$$

$$\ddot{d} = 0. \tag{3.14}$$

If $H = \alpha I$, an analytical expression for the geodesic passing through

$$A(0) = \begin{bmatrix} R(0) & d(0) \\ 0 & 1 \end{bmatrix}, \quad A(1) = \begin{bmatrix} R(1) & d(1) \\ 0 & 1 \end{bmatrix} \tag{3.15}$$

at $t = 0$ and $t = 1$ respectively, is given by [91]:

$$A(t) = \begin{bmatrix} R(t) & d(t) \\ 0 & 1 \end{bmatrix} \in SE(3) \tag{3.16}$$

where

$$R(t) = R(0) \exp(\hat{\omega}_0 t) \tag{3.17}$$

$$d(t) = (d(1) - d(0)) \, t + d(0) \tag{3.18}$$

$$\hat{\omega}_0 = \log(R(0)^T R(1)) \tag{3.19}$$

38

In the case when $H \neq \alpha I$, there is no closed form expression for the corresponding geodesic and numerical methods should be employed.

If $H = \alpha I$, the differential equations to be satisfied by a minimum acceleration curve are [91]:

$$\omega^{(3)} + \omega \times \ddot{\omega} = 0 \tag{3.20}$$

$$d^{(4)} = 0, \tag{3.21}$$

As observed in [57], equation (3.20) can be integrated to obtain

$$\omega^{(2)} + \omega \times \dot{\omega} = \text{constant}$$

However, this equation cannot be further integrated analytically for arbitrary boundary conditions. In [91] it is shown that for special choice of the initial and final velocities, minimum acceleration curves are re-parameterized geodesics. If $H \neq \alpha I$ in metric (3.10), the differential equations to be satisfied by the minimum acceleration curves are difficult to derive and not suited for numerical integration.

3.4   Screw motions

One of the fundamental results in rigid body kinematics was proved by Chasles at the beginning of the 19th century: *Any rigid body displacement can be realized by a rotation about an axis combined with a translation parallel to that axis*. Note that a displacement must be understood as an element of $SE(3)$ while a motion is a curve on $SE(3)$. If the

39

rotation from Chasles's theorem is performed at constant angular velocity and the translation at constant translational velocity, the motion leading to the displacement becomes a *screw motion*. Chasles's theorem then says that *any rigid body displacement can be realized by a screw motion*.

A curve $A(t)$ on a Lie group is called a *one-parameter subgroup* if $A(t + s) = A(t)A(s)$. The following are equivalent ways of defining a screw motion $A(t) \in SE(3)$:

- $A^{-1}(t)\dot{A}(t) = $ constant.

- $\{\omega, v\} = $ constant.

- $A(t)$ is a one-parameter subgroup of $SE(3)$.

- The tangent vectors $\dot{A}(t)$ to the curve form a left invariant vector field.

With this mathematical definition, the Chasles's theorem can be restated in the form: *For every element in $SE(3)$ different from identity, there is a unique one-parameter subgroup to which that element belongs*. Note that the definition of a one-parameter subgroup is not dependent on a metric.

Given two end positions on $SE(3)$, one concludes that there always exists an interpolating screw motion. Is this motion physically meaningful and/or optimal from some point of view? To talk about optimality, one first needs to define a metric on the manifold. Optimal interpolating motions with respect to a given metric are geodesics, minimum acceleration curves, minimum jerk curves, and so on.

40

What is the connection between geodesics as defined in Section 2.4 and screw motions (one-parameter subgroups)? The following result is true for any Lie group [29]: for a bi-invariant metric, the geodesics that start from the identity are one-parameter subgroups.

As a particular case, geodesics through the identity on $SO(3)$ with metric $G = \alpha I$ are one-parameter subgroups (ω = constant). Also, for the bi-invariant semi-Riemannian metric on $SE(3)$

$$G = \begin{bmatrix} \alpha I_3 & \beta I_3 \\ \beta I_3 & 0 \end{bmatrix}, \ \alpha, \ \beta > 0 \tag{3.22}$$

geodesics through the identity are screw motions.

The conclusion is that an interpolating screw motion is not the appropriate choice if the metric on $SE(3)$ is different from the bi-invariant metric (3.22), which is the case of the kinetic energy metric.

41

Chapter 4

An SVD-based projection method for interpolation on $SE(3)$

As shown in Section 3.3, closed form solutions for optimal curves on $SE(3)$ with metric (3.10) are known only for geodesics with $H = \alpha I$. The differential equations satisfied by geodesics for metrics with $H \neq \alpha I$ and minimum acceleration curves for Euclidean metrics $H = \alpha I$ can be integrated using numerical methods for boundary value problems such as shooting or relaxation [66]. If $H \neq \alpha I$, the equations to be satisfied by minimum acceleration and higher order curves are not known, mainly because the calculation of the corresponding Riemmanian curvature is too involved.

This chapter describes an alternative method for generating smooth trajectories for a moving rigid body with specified boundary conditions. The method involves two key steps: (1) the generation of optimal trajectories in $GA^+(n)$, a subgroup of the affine

42

group in $\mathbb{R}^n$; (2) the projection of the trajectories onto $SE(3)$, the Lie group of rigid body displacements. The overall procedure is invariant with respect to both the local coordinates on the manifold and the choice of the inertial frame. The benefits of the method are three-fold. First, it is possible to apply any of the variety of well-known, efficient techniques to generate optimal curves on $GA^+(n)$. Second, the method yields approximations to optimal solutions for general choices of Riemannian metrics on $SE(3)$. Third, from a computational point of view, the method we propose is less expensive than traditional methods.

It is first shown (Section 4.1.1) how one can define a metric on $GL^+(n)$, so that it induces an appropriate metric on $SO(n)$. A similar procedure is used in Section 4.1.3 to equip $GA^+(n)$ with a metric that induces a suitable metric in $SE(n)$. Then, in Sections 4.2 and 4.3, a projection operator is defined, which allows one to project points and curves in the ambient space to $SO(n)$ and $SE(n)$, while invariance with respect to changes in reference frames is preserved. The projection method is formalized and studied in Section 4.4. Section 4.5 presents some interesting results giving the closeness of the projected curves to the exact geodesics on $SO(3)$ for the particular case when the metric on $SO(3)$ is Euclidean. A comparison between the projection and the relaxation method for solving boundary value problems, together with simulation results and discussions on complexity and implementation are given in Section 4.6.

43

4.1 Riemannian metrics on $SO(n)$ and $SE(n)$

In this section it is shown that there is a simple way of defining a left or right invariant metric on $SO(n)$ $(SE(n))$ by introducing an appropriate constant metric in $GL^+(n)$ $(GA^+(n))$. Defining a metric (i.e. the kinetic energy) at the Lie algebra $so(n)$ (or $se(n)$) and extending it through left (right) translations will be equivalent to inheriting the appropriate metric at each point from the ambient manifold.

4.1.1 A metric in $GL^+(n)$

Let W be a symmetric positive definite $n \times n$ matrix. For any $M \in GL^+(n)$ and any $X, Y \in T_M GL^+(n)$, define

$$< X, Y >_{GL^+} = Tr(X^T Y W) = Tr(W X^T Y) = Tr(Y W X^T) \tag{4.1}$$

By definition, form (4.1) is the same at all points in $GL^+(n)$. It is clear that it is quadratic in the entries of X and Y. Let $x, y \in \mathbf{R}^{n^2}$ be the column vectors obtained by collecting all the elements of X and Y row by row. Then,

$$< X, Y >_{GL^+} = x^T \bar{W} y,$$

where

$$\bar{W} = \text{diag}(W^T, W^T, \ldots, W^T), \quad \bar{W} \in \mathbf{R}^{n^2 \times n^2}.$$

It is easy to see that $\bar{W}$ is symmetric and positive definite if and only if W is symmetric and positive definite. Therefore, (4.1) is a Riemmanian metric on $GL^+(n)$ when W is symmetric and positive definite. We next prove the following interesting result.

44

Proposition 5. *The metric given by (4.1) defined on $GL^+(n)$ is left invariant when restricted to $SO(n)$. The restriction on $SO(n)$ is bi-invariant if $W = \alpha I$, $\alpha > 0$, I is the $n \times n$ identity matrix.*

Proof. Let any $M \in GL^+(n)$ and any vectors X, Y in the tangent space at an arbitrary point of $GL^+(n)$. Then, we have

$$< X, Y >_{GL^+} = Tr(X^T Y W)$$

and

$$< MX, MY >_{GL^+} = Tr(X^T M^T M Y W)$$

from which we conclude that the metric [1] is invariant under left translations by elements from $SO(n)$. Therefore, when restricted to $SO(n)$, metric (4.1) is left invariant. For right invariance, if $R \in SO(n)$, we have

$$< X, Y >_{GL^+} = Tr(Y W X^T)$$

and

$$< XR, YR >_{GL^+} = Tr(Y R W R^T X^T).$$

So, right invariance is guaranteed only under the condition that $RWR^T = W$, *i.e.* when W commutes with all the elements $R \in SO(n)$, which, by an argument similar to that in the proof of Theorem 1 from Chapter 3 is equivalent to $W = \alpha I$. □

---

[1] We will use the subscript GL^+ whenever we refer to the metric in the ambient space $GL^+(n)$.

Remark 1. *If right invariance on $SO(n)$ is desired (and left invariance is not needed), we can define*

$$<< X, Y >>_{GL^+} = Tr(XY^TW) = Tr(Y^TWX) = Tr(WXY^T)$$

A similar proof shows that the metric $<<,>>_{GL^+}$ will be right invariant on $SO(n)$ for W symmetric and positive definite and bi-invariant if $W = \alpha I$.

Remark 2. *The metric $<.>_{GL^+}$ is constant with respect to the canonical coordinate basis and the corresponding Christoffel symbols are all zero. Therefore, given two arbitrary points M_1 and M_2 in $GL^+(n)$, the interpolating geodesic starting at $t = 0$ and ending at $t = 1$ is simply $M(t) = M_1 + (M_2 - M_1)t$ (see Section 4.4.2 for a proof that this straight line stays in $GL^+(n)$ under reasonable assumptions). Thus, the distance between M_1 and M_2 is given by*

$$d(M_1, M_2)^2 = \|M_2 - M_1\|_{GL^+}^2 = Tr[(M_2 - M_1)^T(M_2 - M_1)W] \tag{4.2}$$

4.1.2 The induced metric on $SO(3)$

Even though the following derivation can be done in the general case of a $n(n-1)/2$ - dimensional manifold $SO(n)$ in the ambient n^2 - dimensional manifold $GL^+(n)$, we will limit our discussion to the $n = 3$ case to avoid new notation. Further, the results are of direct interest in $SO(3)$.

Let R be an arbitrary element in $SO(3)$. Let X, Y be two vectors from $T_RSO(3)$ and

46

$R_x(t)$, $R_y(t)$ the corresponding local flows so that

$$X = \dot{R}_x(t), \quad Y = \dot{R}_y(t), \quad R_x(t) = R_y(t) = R.$$

The metric inherited from $GL^+(3)$ can be written as:

$$< X, Y >_{SO} = < X, Y >_{GL^+} = Tr(\dot{R}_x^T(t)\dot{R}_y(t)W) =$$

$$= Tr(\dot{R}_x^T(t)RR^T\dot{R}_y(t)W) = Tr(\hat{\omega}_x^T\hat{\omega}_y W)$$

where $\hat{\omega}_x = R_x(t)^T\dot{R}_x(t)$ and $\hat{\omega}_y = R_y(t)^T\dot{R}_y(t)$ are the corresponding twists from the Lie algebra $so(3)$. If we write the above relation using the vector form of the twists, some elementary algebra leads to:

$$< X, Y >_{SO} = \omega_x^T G\omega_y \tag{4.3}$$

where

$$G = Tr(W)I_3 - W \tag{4.4}$$

is the matrix of the metric on $SO(3)$ as defined by (2.12). A different but equivalent way of arriving at the expression of G as in (4.4) would be defining the metric in $so(3)$ (*i.e.* at identity of $SO(3)$) as being the one inherited from $T_IGL^+(3)$: $g_{ij} = Tr(L_i^{oT}L_j^oW)$, $i, j = 1, 2, 3$ (L_1^o, L_2^o, L_3^o is the basis in $so(3)$). Left translating this metric throughout the manifold is equivalent to inheriting the metric at each 3-dimensional tangent space of $SO(3)$ from the corresponding 9-dimensional tangent space of $GL^+(3)$.

Proposition 6. *The metric W on $GL^+(3)$ and the induced metric G on $SO(3)$ share the following properties:*

47

- G is symmetric if and only if W is symmetric.

- If W is positive definite, then G is positive definite.

- If G is positive definite, then W is positive definite if and only if the eigenvalues of G satisfy the triangle inequality.

Proof. The first part follows immediately from (4.4). For the second part, we can use (4.4) to prove that the eigenvalues μ_i of G are given in terms of the eigenvalues λ_i of W by:

$$
\begin{aligned}
\mu_1 &= \lambda_2 + \lambda_3, \\
\mu_2 &= \lambda_1 + \lambda_3, \\
\mu_3 &= \lambda_1 + \lambda_2.
\end{aligned}
\tag{4.5}
$$

Because W is positive definite, it follows that $\lambda_i > 0$ which implies $\mu_i > 0$, i.e. G is positive definite. For the third part, from (4.5) we have

$$
\begin{aligned}
\lambda_1 &= \frac{\mu_2 + \mu_3 - \mu_1}{2} \\
\lambda_2 &= \frac{\mu_1 + \mu_3 - \mu_2}{2}. \\
\lambda_3 &= \frac{\mu_1 + \mu_2 - \mu_3}{2}.
\end{aligned}
\tag{4.6}
$$

If μ_i satisfy the triangle inequality, λ_i are positive and the claim is proved. $\square$

Remark 3. *In the particular case when* $W = \alpha I$, $\alpha > 0$, *from (4.4), we have* $G = 2\alpha I$, *which is the standard bi-invariant metric on* $SO(3)$. *This is consistent with the second*

48

assertion in Proposition 5. For $\alpha = 1$, *metric (4.1) induces the well known Frobenius*

matrix norm on $GL^+(3)$. *[40]*

Remark 4. *The quadratic form* $\omega^T G \omega$ *associated with metric (4.3) can be interpreted*

as the (rotational) kinetic energy. Consequently, $2G$ *can be thought of as the inertia*

matrix of a rigid body with respect to a certain choice of the body frame $\{M\}$. *The*

triangle inequality restriction from Proposition 6 therefore simply states that the principal

moments of inertia of a rigid body satisfy the triangle inequality, which, by definition, is

true for any rigid body. Therefore, for an arbitrarily shaped rigid body with inertia matrix

$2G$, *we can formulate a (positive definite) metric (4.1) in the ambient manifold* $GL^+(3)$

with matrix

$$W = \frac{1}{2}Tr(G)I_3 - G \tag{4.7}$$

Thus (4.7) gives us a formula for constructing an ambient metric space that is compatible

with the given metric structure of $SO(3)$.

4.1.3 A metric in $GA^+(n)$

Let

$$\tilde{W} = \begin{bmatrix} W & a \\ a^T & w \end{bmatrix} \tag{4.8}$$

be a symmetric positive definite $(n+1) \times (n+1)$ matrix, where W is the matrix of metric

(4.1), $a \in \mathbf{R}^n$, and $w \in \mathbf{R}$. Let X and Y be two vectors from the tangent space at an

arbitrary point of $GA^+(n)$ (X and Y are $(n+1) \times (n+1)$ matrices with all entries of the

49

last row equal to zero). Similar to Section 4.1.1, a quadratic form

$$< X, Y >_{GA^+} = Tr(X^T Y \tilde{W})$$

(4.9)

is symmetric and positive definite if and only if $\tilde{W}$ is symmetric and positive definite.

Remark 5. *As in the case of* $GL^+(n)$ *(see Remark 2), the distance between two arbitrary points* B_1, $B_2 \in GA^+(n)$ *is given by:*

$$d(B_1, B_2)^2 = \|B_2 - B_1\|^2_{GA^+} = Tr[(B_2 - B_1)^T(B_2 - B_1)\tilde{W}]$$

(4.10)

4.1.4 The induced metric in $SE(3)$

We can get a left invariant metric on $SE(n)$ by letting $SE(n)$ inherit the metric $< . >_{GA^+}$ given by (4.9) from $GA^+(n)$. To derive the induced metric in $SE(3)$ we follow the same procedure as in Section 4.1.2 for the particular case of $n = 3$.

Let A be an arbitrary element from $SE(3)$. Let X, Y be two vectors from $T_A SE(3)$ and $A_x(t), A_y(t)$ the corresponding local flows so that

$$X = \dot{A}_x(t), \quad Y = \dot{A}_y(t), \quad A_x(t) = A_y(t) = A.$$

Let

$$A_i(t) = \begin{bmatrix} R_i(t) & d_i(t) \\ 0 & 1 \end{bmatrix}, \quad i \in \{x, y\}$$

and the corresponding twists at time t:

$$S_i = A_i^{-1}(t)\dot{A}_i(t) = \begin{bmatrix} \hat{\omega}_i & v_i \\ 0 & 0 \end{bmatrix}, \quad i \in \{x, y\}$$

50

The metric inherited from $GA^+(3)$ can be written as:

$$< X, Y >_{SE} = < X, Y >_{GA^+} = Tr(\dot{A}_x^T(t)\dot{A}_y(t)\tilde{W}) =$$

$$= Tr(S_x^T A^T A S_y \tilde{W})$$

Now using the orthogonality of the rotational part of A and the special form of the twist matrices, a straightforward calculation leads to the result:

$$< X, Y >_{SE} = Tr(S_x^T S_y \tilde{W}) =$$

$$= Tr(\hat{\omega}_x^T \hat{\omega}_y W) + Tr(\hat{\omega}_x^T v_y a^T) +$$

$$+ v_x^T \hat{\omega}_y a + v_x^T v_y w$$

Keeping the notation from section 4.1.2, if G is the matrix of the metric in $SO(3)$ induced by $GL^+(3)$, then

$$< X, Y >_{SE} = \begin{bmatrix} \omega_x^T & v_x^T \end{bmatrix} \tilde{G} \begin{bmatrix} \omega_y \\ v_y \end{bmatrix}, \quad \tilde{G} = \begin{bmatrix} G & \hat{a} \\ -\hat{a} & w I_3 \end{bmatrix} \tag{4.11}$$

and G is given by (4.4).

Remark 6. *The metric given by (4.11) is left invariant since the matrix $\tilde{G}$ of this metric in the left invariant basis vector field is constant.*

Remark 7. *If $\tilde{W}$ is symmetric and positive definite, then $\tilde{G}$ given by (4.11) is symmetric and positive definite.*

Remark 8. *The quadratic form $s^T \tilde{G} s$ associated with metric (4.11) can be interpreted as being the kinetic energy of a moving (rotating and translating) rigid body, where w is*

51

twice the mass m *of the rigid body. If the body fixed frame* $\{M\}$ *is placed at the centroid of the body, then* $a = 0$. *Moreover, if* $\{M\}$ *is aligned with the principal axes of the body, then* $G = \frac{1}{2}H$, *where* H *is the diagonal inertia matrix of the body. In the most general case, when the frame* $\{M\}$ *is displaced by some* (R_0, d_0) *from the centroid and the orientation parallel with the principal axes, we have:*

$$G = R_0^T H R_0 - m R_0^T \tilde{d}_0^2 R_0, \quad a = -m R_0 d_0$$

which is in accordance with (3.12).

4.2   Projection on $SO(n)$

We can use the norm induced by metric (4.1) to define the distance between elements in $GL^+(3)$. Using this distance, for a given $M \in GL^+(3)$, we define *the projection* of M on $SO(3)$ as being the closest $R \in SO(3)$ with respect to metric (4.1).

The solution of the projection problem is derived for the general case of $GL^+(n)$ and is based on the following lemma (a related treatment can be found in [41]):

Lemma 2. *Let* $M \in GL^+(n)$ *and* $M = U\Sigma V^T$ *its singular value decomposition. Then* $R = UV^T$ *is the solution to the maximization problem*

$$\max_{R \in SO(n)} Tr(M^T R).$$

Proof. Let $\Sigma = diag\{\sigma_1, \ldots, \sigma_n\}$ and $C = R^T U$, where $R \in SO(3)$. Consider column-wise partitions for V and C

$$V = [v_1, \ldots, v_n], \quad C = [c_1, \ldots, c_n]$$

52

Then, we have:

$$Tr(M^T R) = Tr(V\Sigma U^T R) = Tr(V\Sigma C^T)$$

$$= Tr(\sum_{i=1}^{n} \sigma_i v_i c_i^T) = \sum_{i=1}^{n} \sigma_i Tr(v_i c_i^T) = \sum_{i=1}^{n} \sigma_i v_i^T c_i$$

Now C and V are both orthogonal, and $\|c_i\| = \|v_i\| = 1$. On the other hand, by Cauchy-Schwartz, $(v_i^T c_i)^2 \leq \|v_i\|^2 \|c_i\|^2 = 1$ and the equality holds for $v_i = c_i$, or $V = C$, which implies $R = UV^T$. Therefore, $\sum_{i=1}^{n} \sigma_i$ is an upper bound for $Tr(M^T R)$ which is attained for $R = UV^T$. $\qquad\square$

The following proposition is the main result of this section:

Proposition 7. *Let $M \in GL^+(n)$ and U, Σ, V the singular value decomposition of MW (i.e., $MW = U\Sigma V^T$). Then the projection of M on $SO(n)$ with respect to metric (4.1) is given by $R = UV^T$.*

Proof. The problem to be solved is a minimization problem:

$$\min_{R \in SO(n)} \|M - R\|_{GL^+}^2$$

We have

$$\|M - R\|_{GL^+}^2 = < M - R, M - R >_{GL^+} =$$

$$= Tr[(M - R)^T (M - R)W] =$$

$$= Tr(M^T MW - M^T RW - R^T MW + R^T RW)$$

Note that $Tr(R^T MW) = Tr(WM^T R) = Tr(M^T RW)$ and the quantities $M^T MW$ and $R^T RW = W$ are constant and therefore does not affect the optimization. Therefore, the

53

problem to be solved becomes:

$$\max_{R \in SO(n)} Tr(WM^T R)$$

With $MW = U\Sigma V^T$, according to Lemma 2, the solution to the above problem is $R = UV^T$. $\square$

Remark 9. *Let* S*(n) denote the* $n(n + 1)/2$ *dimensional subset of symmetric matrices of* $GL^+(n)$.

- *For the particular case when* $W = I_n$, S*(n) describes the set of all matrices that project to identity in metric (4.1)- the fiber at identity. Note that the dimensions agree:* $SO(n)$ *is* $n(n - 1)/2)$ *- dimensional, the fiber* S*(n) is* $n(n + 1)/2$ *- dimensional; the sum gives* n^2, *which is the dimension of the ambient* $GL^+(n)$. *Also, in this case, given* $R \in SO(n)$, *the set that projects to* R *(fiber at* R*) is obtained by left translation* RS*(n)*;

- *In the general case, the set of matrices that project to some given* $R \in SO(3)$ *in metric (4.1) is* RS$(n)W^{-1}$.

Remark 10. *It is easy to see that the distance between* M *and* R *in metric (4.1) is given by* $Tr(W^{-1}V\Sigma^2 V^T) + Tr(W) - 2Tr(\Sigma)$. *For the particular case when* $W = I_3$, *the distance becomes* $\sum_{i=1}^n (\sigma_i - 1)^2$, *which is the standard way of describing how "far" a matrix is from being orthogonal.*

The question we might ask is what happens with the solution to the projection problem when the manifold $GL^+(n)$ is acted upon by the group $SO(n)$. The answer is given below.

54

Proposition 8. *The solution to the projection problem on $SO(n)$ is left invariant under actions of elements from $SO(n)$. If $W = \alpha I_3$, the solution is bi-invariant.*

Proof. Let $M \in GL^+(n)$, $MW = U\Sigma V^T$ and the corresponding projection $R \in SO(n)$, $R = UV^T$. Consider the action of any $L \in SO(n)$ on M: $\bar{M} = LM$. Then an SVD for $\bar{M}W$ yields $\bar{M}W = (LU)\Sigma V^T$. Then, by Proposition 7, the projection of $\bar{M}$ on $SO(3)$ is $\bar{R} = LUV^T = LR$, which proves left invariance. However, right translation of M by $L \in SO(3)$ gives $\bar{M} = ML$ and $\bar{M}W = U\Sigma V^T W^{-1} LW$. The translated projection is $UV^T L$. Right invariance is therefore guaranteed if $W^{-1}LW = L$, *i.e.*, W commutes with arbitrary elements from $SO(n)$. This is true only if $W = \alpha I$. $\square$

Remark 11. *For the case $W = I$, it is worthwhile to note that other projection methods do not exhibit bi-invariance. For instance, it is customary to find the projection $R \in SO(n)$ by applying a Gram-Schmidt procedure (QR decomposition). In this case it is easy to see that the solution is left invariant, but in general it is not right invariant.*

4.3 Projection on $SE(n)$

Similar to the previous section, if a metric of the form (4.9) is defined on $GA^+(n)$ with the matrix of the metric given by (4.8), we can find the corresponding projection on $SE(n)$. We consider the case $a = 0$, which corresponds to a body frame $\{M\}$ fixed at the centroid of the body.

Proposition 9. *Let $B \in GA^+(n)$ with the following block partition*

$$B = \begin{bmatrix} B_1 & B_2 \\ 0 & 1 \end{bmatrix}, \quad B_1 \in GL^+(n), \quad B_2 \in \mathbf{R}^n$$

and U, Σ, V be the singular value decomposition of $B_1 W$. Then the projection of B on $SE(n)$ is given by

$$A = \begin{bmatrix} UV^T & B_2 \\ 0 & 1 \end{bmatrix} \in SE(n).$$

Proof. Let

$$A = \begin{bmatrix} R & d \\ 0 & 1 \end{bmatrix}, \quad R \in SO(n), \quad d \in \mathbf{R}^n$$

The problem to be solved can be formulated as follows:

$$\min_{A \in SE(n)} \| B - A \|^2_{GA^+}$$

We have:

$$\| B - A \|^2_{GA^+} = Tr[(B - A)^T (B - A)\tilde{W}]$$

$$= Tr(B^T B \tilde{W}) - 2Tr(B^T A \tilde{W}) + Tr(A^T A \tilde{W})$$

The quantity $B^T B \tilde{W}$ is not involved in the optimization. Therefore, the problem becomes

$$\min_{A \in SE(n)} [-2Tr(B^T A \tilde{W}) + Tr(A^T A \tilde{W})]$$

Since

$$Tr(A^T A \tilde{W}) = Tr(W) + (d^T d + 1)w,$$

56

and

$$Tr(B^T A \tilde{W}) = Tr(B_1^T RW) + (B_2^T d + 1)w$$

we can separate the initial problem into two subproblems:

(a) $\max_{R \in SO(n)} Tr(B_1^T RW) = \max_{R \in SO(n)} Tr(W B_1^T R)$

and

(b) $\min_{d \in \mathbb{R}^n} \left[-2B_2^T d + d^T d \right]$

From Lemma 2, the solution to subproblem (a) is $R = UV^T$. For the second subproblem, note that $d = B_2$ is the only critical point of the scalar function $-2B_2^T d + d^T d$. It is easy to verify that the Hessian at this point is $2I$, which is positive definite. Therefore, the solution is $d = B_2$ which concludes the proof. $\quad\square$

Similar to the $SO(n)$ case, the projection on $SE(n)$ exhibits several interesting invariance properties.

Proposition 10. *The solution to the projection problem on $SE(n)$ is left invariant under actions of elements from $SE(n)$. In the special case when $W = \alpha I$, the projection is bi-invariant under rotations.*

Proof. Let

$$B = \begin{bmatrix} B_1 & B_2 \\ 0 & 1 \end{bmatrix} \in GA^+(n)$$

and define A, U, Σ, V such that

$$B_1 W = U \Sigma V^T, \quad A = \begin{bmatrix} UV^T & B_2 \\ 0 & 1 \end{bmatrix} \in SE(n)$$

57

Let

$$Q = \begin{bmatrix} R & d \\ 0 & 1 \end{bmatrix}$$

be an arbitrary element from $SE(n)$. Under left actions of Q, the solution pair becomes

$$QB = \begin{bmatrix} RB_1 & RB_2 + d \\ 0 & 1 \end{bmatrix},$$

$$QA = \begin{bmatrix} RUV^T & RB_2 + d \\ 0 & 1 \end{bmatrix}$$

which proves left invariance of the projection. For the second part, note that the right translated solution pair is

$$BQ = \begin{bmatrix} B_1 R & B_1 d + B_2 \\ 0 & 1 \end{bmatrix},$$

$$AQ = \begin{bmatrix} UV^T R & UV^T d + B_2 \\ 0 & 1 \end{bmatrix}$$

It is easy to see that $B_1 RW = U\Sigma V^T W^{-1} RW$. With $W = \alpha I$, we have $B_1 RW = U\Sigma V^T R$. If only rotations ($d = 0$) are taken into consideration, right invariance is proved.

□

58

4.4 The projection method

Based on the results we proved so far, we can outline a method to generate an interpolating curve $A(t) \in SE(3)$, $t \in [0, 1]$ while satisfying the boundary conditions:

$$A(0), \ A(1), \ \dot{A}(0), \ \dot{A}(1), \ldots \ldots A^{(m)}(0), \ A^{(m)}(1)$$

where the superscript $(\cdot)^{(m)}$ denotes the m-th derivative. The projection procedure consists of two steps:

- **Step 1:** Generating the optimal curve $B(t)$ in the ambient manifold $GA^+(3)$, which satisfies the boundary conditions and

- **Step 2:** Projecting $B(t)$ from Step 1 onto $A(t) \in SE(3)$.

Due to the fact that the metric we defined on $GA^+(3)$ is the same at all points, the corresponding Christoffel symbols are all zero. Consequently, the optimal curves in the ambient manifold assume simple analytical forms. For example, geodesics are straight lines, minimum acceleration curves are cubic polynomial curves, and minimum jerk curves are fifth order polynomial curves in $GA^+(3)$, all parameterized by time. Therefore, in Step 1, the following curve is constructed in $GA^+(3)$:

$$B(t) = B_0 + B_1 t + \ldots + B_{2m-1} t^{2m-1}$$

where the coefficients B_i $i = 1, \ldots, 2m - 1$ are linear functions Γ_i of the input data:

$$B_i = \Gamma_i \left(A(0), A(1), \dot{A}(0), \dot{A}(1), \ldots, A^{(m)}(0), A^{(m)}(1) \right).$$

59

Step 2 consists of an SVD decomposition weighted by the matrix W as described in Proposition 9 to produce the curve $A(t)$.

4.4.1 Left invariance - independence of inertial frame

We ask if the generated motion is independent of the choice of the reference frame $\{F\}$. The answer is given in the following proposition:

Proposition 11. *The projection method on $SE(3)$ is left invariant, i.e., the generated trajectories are independent of the choice of the inertial frame $\{F\}$.*

Proof. Assume the inertial frame $\{F\}$ is displaced to $\{F'\}$ and the transformation matrix giving the displacement of $\{F\}$ in $\{F'\}$ is $Q \in SE(3)$. As seen from the new frame $\{F'\}$, the boundary conditions are specified as

$$QA(0), \; QA(1), \; Q\dot{A}(0), \; Q\dot{A}(1), \ldots, QA^{(m)}(0), \; QA^{(m)}(1)$$

and the interpolating curve in $GA^+(3)$ satisfying the new boundary conditions becomes

$$\bar{B}(t) = \bar{B}_0 + \bar{B}_1 t + \ldots + \bar{B}_{2m-1} t^{2m-1}$$

where

$$\bar{B}_i = \Gamma_i \left(QA(0), QA(1), Q\dot{A}(0), Q\dot{A}(1), \ldots, \right.$$

$$\left. QA^{(m)}(0), QA^{(m)}(1) \right), \; i = 1, \ldots, 2m - 1$$

Since the functions Γ_i are linear, we conclude that $\bar{B}(t) = QB(t)$. Now using Proposition 10, the projection of $QB(t) \in GA^+(3)$ onto $SE(3)$ is simply $QA(t)$. Thus, the projection

60

method on $SE(3)$ consisting of two steps is left invariant, *i.e.*, the generated trajectories are invariant to displacements of the inertial frame $\{F\}$. □

Remark 12. *Due to the linearity on the boundary conditions of the curve in the ambient manifold, the first step is always bi-invariant, i.e., invariant to arbitrary displacements in both the inertial frame $\{F\}$ and the body frame $\{M\}$. The invariance properties of the overall method are, therefore, dictated by the second step. According to Proposition 10, the procedure is bi-invariant with respect only to rotations of $\{F\}$ in the particular case of $W = \alpha I$. In the most general case, i.e., for arbitrary choices of W, the method is left invariant to arbitrary displacements of the inertial frame.*

4.4.2 Uniqueness and smoothness of the projection

Due to the fact that $SE(3)$ has a product structure $SE(3) = SO(3) \times \mathbf{R}^3$ and the metrics that we use are product metrics, it is sufficient to answer the above questions for $SO(3)$ and the ambient $GL^+(3)$. Also, due to the left invariance of the generated trajectories, without loss of generality, we can restrict our attention to curves passing through identity. Finally, in accordance with the scope of this work, the discussion will be limited to geodesics and minimum acceleration curves.

Uniqueness

Let us first note that even if the singular value decomposition of some matrix from $M \in GL^+(3)$: $M = U\Sigma V^T$ is not unique (it is unique up to permutations of the singular

values), the product $R = UV^T$ giving the projection on $SO(3)$ is unique. Finding the projection on $SO(3)$ in the form UV^T using SVD is equivalent to determining the polar decomposition $M = QS$ (Q orthogonal, S symmetric and positive definite) with $Q = R = UV^T$, $S = V\Sigma V^T$. Also, as noted in [72], using the polar decomposition, one can find the orthogonal part Q by averaging the matrix with its inverse transpose until convergence, which can be proved to be cheaper to compute than the actual SVD of the matrix. We use SVD throughout the work simply because one gets more information through SVD than via polar decomposition. For example, proof of Lemma 2 is much simpler than the proof of a somewhat similar result given in the appendix of [72], which uses the Lagrange multiplier method to solve a constrained optimization problem. Also, the invariance properties of the projection become transparent in the SVD. Moreover, the deviation of the actual singular values of some matrix from 1 is a good measure of how far that matrix is from being orthogonal. In the actual implementation of the method, one can always use polar decomposition if the SVD calculation is deemed to be too expensive.

Also, the uniqueness of the projection as in Proposition 7 is guaranteed if MW is nonsingular [42]. Since W is positive definite, we only need to make sure that the smooth curve $M(t)$ generated in the ambient manifold do not leave $GL^+(3)$ (an element of $GL(3)$ with negative determinant will not project to a rotation but to a reflection).

Consider the following interpolant between I at $t = 0$ and $R(1) = e^{\tilde{\omega}_0} \in SO(3)$ at $t = 1$:

$$M(t) = I + (R(1) - I)f(t), \quad t \in [0, 1] \tag{4.12}$$

62

where $f(t)$ is a smooth function with $f(0) = 0$, $f(1) = 1$. According to (A.1) from Appendix A, the singular values of $M(t)$ are given by $\{1, s(t), s(t)\}$ where

$$s(t) = \sqrt{2(1 - \cos\|\omega_0\|)f(t)^2 - 2(1 - \cos\|\omega_0\|)f(t) + 1} \qquad (4.13)$$

By studying the binomial under the square root, it is easy to see that $s(t) > 0, \forall t \in [0, 1]$ if and only if $\|\omega_0\| \neq (2k + 1)\pi$, k integer. $s(t)$ can become zero if and only if $\|\omega_0\| = (2k + 1)\pi$ and $f = 1/2$. Note that this condition corresponds to singular points of the exponential coordinates for $SO(3)$. Therefore, restricting the magnitude of the rotation $0 \leq \|\omega_0\| < \pi$ (which is the usual assumption when exponential coordinates are used as local parameterization of $SO(3)$ around identity) guarantees that the singular values of $M(t)$ stay positive when $t \in [0, 1]$, i.e., $M(t)$ stays in $GL^+(3)$. As a particular case for $f(t) = t$, the geodesic in $GL^+(3)$, $M(t) = I + (R(1) - I)t$, passing through identity at $t = 0$ does not leave $GL^+(3)$ if the magnitude of the rotation is less than π.

For a minimum acceleration curve, we expect this condition to also depend on the magnitudes of the end velocities. Explicitly, the cubic polynomial interpolating boundary conditions on $SO(3)$ given by $R(0) = I$, $\dot{R}(0)$ at $t = 0$ and $R(1)$, $\dot{R}(1)$ at $t = 1$

$$M(t) = I + \dot{R}(0)t + (-3I + 3R(1) - 2\dot{R}(0) - \dot{R}(1))t^2 +$$

$$+(2I - 2R(1) + \dot{R}(0) + \dot{R}(1))t^3 \qquad (4.14)$$

can be rewritten as $M(t) = M_1(t) + M_2(t)$ where

$$M_1(t) = I + (R(1) - I)f(t), \quad f(t) = 3t^2 - 2t^3$$

$$M_2(t) = (t - 2t^2 + t^3)\dot{R}(0) + (-t^2 + t^3)\dot{R}(1)$$

63

Let $\bar{\sigma}(\cdot)$ and $\underline{\sigma}(\cdot)$ denote the largest and smallest singular values of some matrix. Then

$$M(t) > 0 \Leftrightarrow \underline{\sigma}(M(t)) > 0, \ t \in [0, 1]$$

Using

$$\underline{\sigma}(M(t)) \geq \underline{\sigma}(M_1(t)) - \bar{\sigma}(M_2(t))$$

finding a lower bound for $\underline{\sigma}(M(t))$ reduces to finding a lower bound for $\underline{\sigma}(M_1(t))$ and an

upper bound for $\bar{\sigma}(M_2(t))$.

$M_1(t)$ is of the form (4.12), and, therefore, it has singular values at $\{1, s(t), s(t)\}$,

where $s(t)$ is given by (4.13). It is easy to see that for $f(t) = 3t^2 - 2t^3$, $s(t) < 1$, and,

therefore, $\underline{\sigma}(M_1(t)) = s(t)$.

Now assume that the end velocities are upper bounded by $\delta > 0$ in 2-norm, *i.e.*,

$\bar{\sigma}(\dot{R}(0)).\bar{\sigma}(\dot{R}(1)) < \delta$. We have:

$$\bar{\sigma}(M_2(t)) \leq \bar{\sigma}((t - 2t^2 + t^3)\dot{R}(0)) + \bar{\sigma}((-t^2 + t^3)\dot{R}(1)) <$$

$$< (t - t^2)\delta$$

Then, a sufficient condition for $\underline{\sigma}(M(t)) > 0$ is

$$\delta = g(t, \|\omega_0\|) := s(t)/(t - t^2)$$

A plot of $g(t, \|\omega_0\|)$ is presented in Figure 4.1 (a) for $t \in [0, 1]$ and $\|\omega_0\| \in [0, \pi]$. It

can be seen (even though this can be proved rigorously by taking derivatives of $g(t, \|\omega_0\|)$)

that the minimum value of the function is always attained at $t = 0.5$, for all the values

of $\|\omega_0\| \in [0, \pi]$. We conclude that a sufficient condition for a cubic interpolant of

(a)   (b)
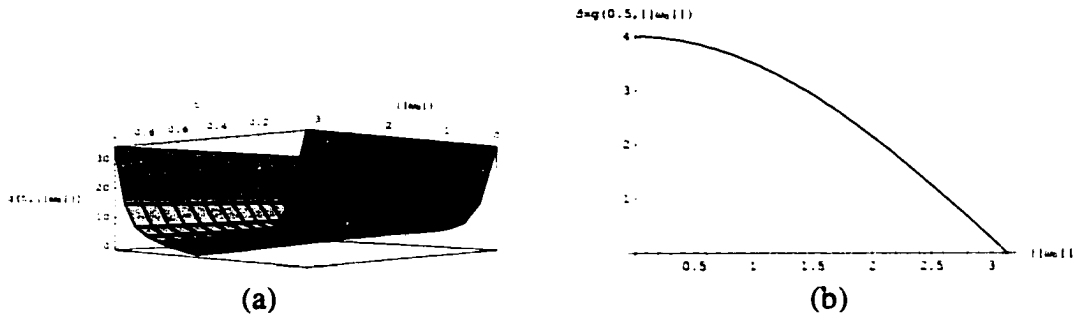
Figure 4.1: Upper bounds on the end velocities on SO(3) are imposed so that the interpolating cubic in the ambient manifold does not leave $GL^+(3)$

the form (4.14) to remain in $GL^+(3)$ for $t \in [0, 1]$ can be expressed in terms of upper bounds on the end velocities as $\delta < g(0.5, \|\omega_0\|)$ To illustrate the magnitudes of the allowed velocities, a plot of $g(0.5, \|\omega_0\|)$ is given in Figure 4.1 (b) for $\|\omega_0\| \in [0, \pi]$. As expected, the upper bound on end velocities becomes more restrictive with the increase on the rotational displacement.

Remark 13. *The bound on the amount of rotation $\theta < \pi$ is not really restrictive since rotations θ larger than π can be always achieved by rotating $2\pi - \theta$ around the same axis but on opposite direction.*

Smoothness

Since the SVD (or polar decomposition) is a smooth operation, and provided that the smooth curve generated in the ambient manifold does not leave $GL^+(3)$ (this guarantees unique projections), the projected curve on $SO(3)$ is smooth.

Singularities might occur due to the projection from $GL^+(3)$ (a 9 dimensional manifold) to $SO(3)$ (a 3-dimensional manifold). Specifically, the projected curve can have a

65

cusp point when the tangent to the curve in the ambient space is also tangent to the fiber of the projection. Also, a curve that meets a fiber in two places will project to a curve with a self intersection. However, provided that the curve in $SO(3)$ is smooth in time, since the goal of this method is motion generation for robots, cusps and self intersection points are allowed. A cusp on a smooth curve on $SO(3)$ will physically correspond to a situation when the angular velocity of the body smoothly decreases to 0 and then starts increasing. This situation mostly occurs in motion generation for nonholonomic robots. A self intersection point corresponds to the body attaining the same pose at two different times.

4.5 Geodesics on $SO(3)$ with Euclidean metric

This section presents some interesting results giving the closeness of the projected curves to the exact geodesics on $SO(3)$ for the particular case when the metric on $SO(3)$ is Euclidean.

The problem to be solved is generating a geodesic $R(t)$ between given end positions $R_1 = R(0)$ and $R_2 = R(1)$ on $SO(3)$. Without loss of generality, it is assumed $R_1 = I$. Indeed, a geodesic between two arbitrary positions R_1 and R_2 is the geodesic between I and $R_1^{-1}R_2$ left translated by R_1. Exponential coordinates $\sigma_1, \sigma_2, \sigma_3$ are considered as local parameterization of $SO(3)$. If $R_2 = e^{\tilde{\omega}_0}$, then the geodesic is the exponential mapping of the uniformly parameterized segment passing through 0 and ω_0 ($\sigma(t) = \omega_0 t$)

66

from the exponential coordinates:

$$R(t) = e^{\hat{\sigma}(t)} = e^{\hat{\omega}_0 t}$$

The geodesic in the ambient manifold $GL(3)$ satisfying the given boundary conditions on $SO(3)$ is

$$M(t) = I + (R_2 - I)t, \quad t \in [0, 1]$$

An analytical expression for the projection of an arbitrarily parameterized line in the ambient $GL(3)$ onto $SO(3)$ is derived, which will answer the following three questions.

- Does the projection of a geodesic from $GL(3)$ follow the same path as the true geodesic on $SO(3)$? If the answer is yes, then the following question makes sense:

- Do the above two curves have the same parameterization? If the answer is no,

- Can one find an appropriate parameterization of the line in the ambient manifold so that the projection is identical to the true geodesic on $SO(3)$?

Proposition 12 is the key result of this section.

Proposition 12. *Let* $M(t) = I + (R_2 - I)f(t)$, $t \in [0,1]$ *be a line in* $GL(3)$ *with* $R_2 = e^{\hat{\omega}_0} \in SO(3)$ *(f continuous, $f(0) = 0$, $f(1) = 1$). Then the projection of this line* $R^{\perp}(t)$ *onto* $SO(3)$ *is the exponential mapping of a segment drawn between the origin and* ω_0 *in exponential coordinates parameterized by* $\theta(t)$:

$$M(t) = U(t)\Sigma(t)V^T(t) \quad \Rightarrow \quad R^{\perp}(t) = U(t)V^T(t) = e^{\hat{\omega}_0\theta(t)} \tag{4.15}$$

$$\theta(t) = \frac{1}{\|\omega_0\|}\text{atan2}(1 - f(t) + f(t)\cos\|\omega_0\|, f(t)\sin\|\omega_0\|) \tag{4.16}$$

67

Proof. The proof is given in Appendix A. □

Note that the obtained parameterization $\theta(t)$ satisfies the boundary conditions $\theta(0) = 0, \theta(1) = 1$

As a particular case of Proposition 12 for $f(t) = t$, the following corollary answers the first two questions at the beginning of this section:

Corollary 4. *The true geodesic on $SO(3)$ and the projected geodesic from $GL(3)$ with ends on $SO(3)$ follow the same path on $SO(3)$ but with different parameterizations. The projected curve is the exponential mapping of the same segment from the exponential coordinates*

$$R^{\perp}(t) = e^{\tilde{\omega}_0\theta(t)}$$

with the following parameterization

$$\theta(t) = \frac{1}{\|\omega_0\|}\mathrm{atan2}(1 - t + t\cos\|\omega_0\|, t\sin\|\omega_0\|)$$

The derivative of the function $\theta(t)$ is given by

$$\frac{d}{dt}\theta(t) = \frac{\sin\|\omega_0\|}{\|\omega_0\|s(t)}$$

where $s(t)$ is given by (A.1). Plots of the function $\theta(t)$ and its derivative are given in Figure 4.2 for $t \in [0, 1]$ and the magnitude of the displacement on the manifold $\|\omega_0\| \in (0, \pi)$.

The conclusion is that even though the line in $GL(3)$ is followed at constant velocity, the projected curve on the manifold has low speed at the beginning, attains its maximum

68

(a)   **(b)**
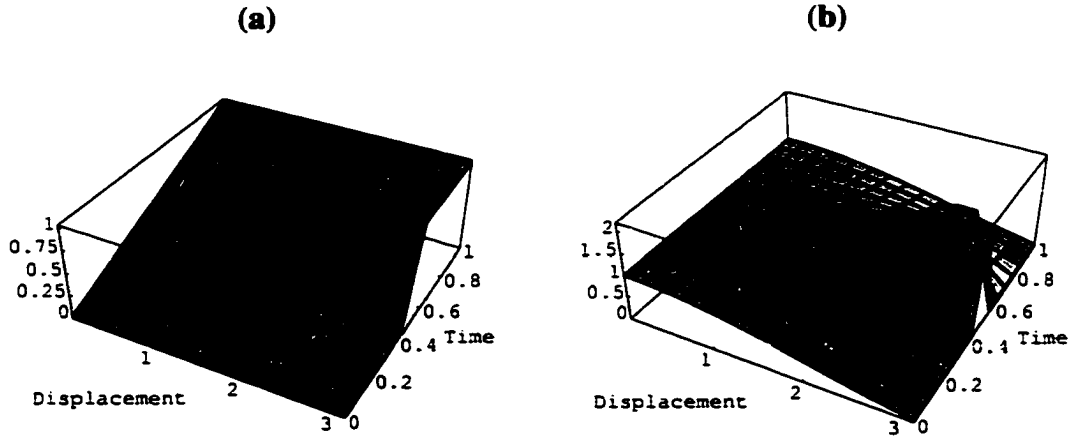
Figure 4.2: (a) The function $\theta(t)$; (b) The derivative $\frac{d}{dt}\theta(t)$

in the middle, and slows down as approaching the end point. The larger the displacement $\|\omega_0\|$, the larger the discrepancy in speeds. Also note that the middle of the line is projected into the middle of the true geodesic because $\theta(0.5) = 0.5$ (i.e the functions t and $\theta(t)$ are equal at $t = 0.5$). This result has been stated in [72] in the context of unit quaternions as local parameters of $SO(3)$ (viewed as the unit sphere S^3 in the projective space RP^3).

To answer the third question, one needs to find a parameterization $f(t)$ ($f(0) = 0$, $f(1) = 1$) of the line in $GL(3)$ with ends on $SO(3)$, which gives uniform parameterization t of the projected curve in exponential coordinates. The solution of the following equation in f

$$\mathrm{atan2}(1 - f(t) + f(t)\cos\|\omega_0\|, f(t)\sin\|\omega_0\|) = t$$

69

(a) **(b)**
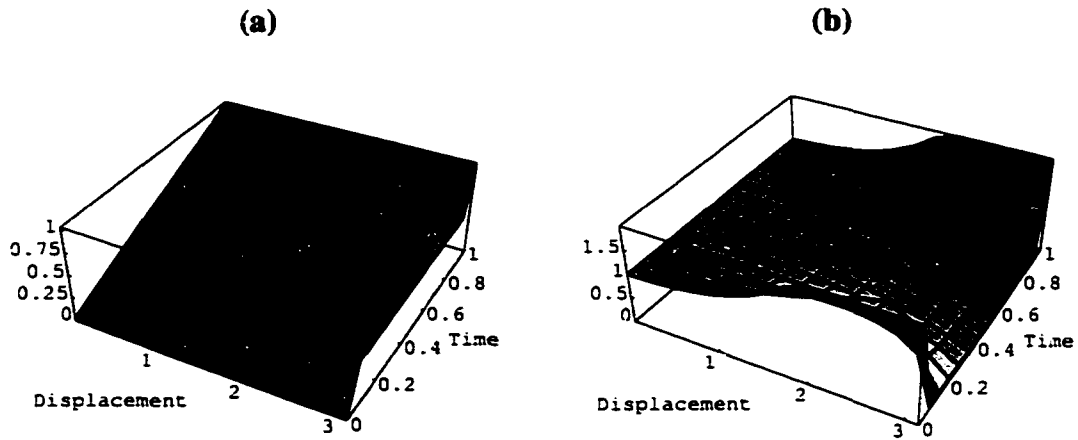
Figure 4.3: (a) The function $f(t)$; (b) The derivative $\frac{d}{dt}f(t)$

is of the form

$$f(t) = \frac{\sin(\|\omega_0\|t)}{\sin(\|\omega_0\|(1-t)) + \sin(\|\omega_0\|t)}$$

The answer to the third question is stated in the following corollary:

Corollary 5. *The true geodesic on $SO(3)$ starting at I and ending at $R_2 = e^{\tilde{\omega}_0}$ is the projection of the following line from the ambient manifold $GL(3)$:*

$$M(t) = I + (R_2 - I)f(t), \quad t \in [0,1], \quad f(t) = \frac{\sin(\|\omega_0\|t)}{\sin(\|\omega_0\|(1-t)) + \sin(\|\omega_0\|t)}$$

Illustrative plots of $f(t)$ and its derivative are given in Figure 4.3 for $t \in [0,1]$ and different values of the displacement $\|\omega_0\| \in (0, \pi)$.

As expected, to get a uniform speed on $SO(3)$, the line in $GL(3)$ should be followed at high speed at the beginning, slow down in the middle, and accelerating again near the end point.

70

Remark 14. *The result in Corollary 5 is similar to the formula for spherical linear interpolation 'Slerp' in terms of quaternions [72]. The curve interpolating q_1 and q_2, with parameter u moving from 0 to 1, is given by:*

$$\text{Slerp}(q_1, q_2; u) = \frac{\sin(1 - u)\theta}{\sin\theta}q_1 + \frac{\sin u\theta}{\sin\theta}q_2$$

where $q_1 \cdot q_2 = \cos\theta$.

4.6 Projection vs. relaxation: comparison and simulation results

This section demonstrates how minimum energy and acceleration motions for a rigid body can be constructed using the projection method. The obtained curves are compared with the ones generated by using the relaxation method to numerically solve the exact equations of the optimal curves, when they are known.

We will first focus on $SO(3)$. Due to the product structure of both $SE(3) = SO(3) \times \mathbb{R}^3$ and the metric $<,>_{SE}$ for $a = 0$, all the results are straightforward to extend to $SE(3)$.

4.6.1 Geodesics and minimum acceleration curves on $SO(3)$ by the relaxation method

The relaxation method [66] is used to generate geodesics when $G \neq \alpha I$ and minimum acceleration curves when $G = \alpha I$. The translational parts (3.14) and (3.21) are easily

71

integrable leading to polynomial solutions. For the rotational part, a local parameterization of $SO(3)$ should be chosen and three first order differential equations relating ω to the derivatives of the parameters should augment the system. We choose exponential coordinates (as described in Section 2.5) as local parameterization of $SO(3)$. Three more differential equations described by (2.19) will augment systems (3.13) and (3.20) to solve for the rotational part. Boundary conditions are imposed at times 0 and 1. In the relaxation method, the ODE's are replaced by finite difference equations on a mesh of points corresponding to the time domain. If we define

$$x_1 = \sigma, \ x_2 = \omega, \ x_3 = \omega, \ x_4 = \ddot{\omega},$$

the geodesic (subscript g) and the minimum acceleration (subscript a) ODE's can be written as

$$\dot{x}_i = f_i(x_i), \ i \in \{g, a\} \tag{4.17}$$

where

$$x_g = [x_1^T \ x_2^T]^T, \ x_a = [x_1^T \ x_2^T \ x_3^T \ x_4^T]^T$$

$$f_g(x_g) = [f_1^T \ f_{g2}^T]^T, \ f_a(x_a) = [f_1^T \ f_{a2}^T \ f_{a3}^T \ f_{a4}^T]^T$$

$$f_1 = \left(I + \frac{1}{2}\hat{x}_1 + (1 - \alpha(\|x_1\|)) \frac{\hat{x}_1^2}{\|x_1\|^2}\right) x_2 \tag{4.18}$$

$$f_{g2} = -G^{-1}(x_2 \times (Gx_2)), \ f_{a2} = x_3, \ f_{a3} = x_4, \ f_{a4} = -x_2 \times x_4$$

Note that the expression of f_1 is in accordance with the time derivative of exponential coordinates on $SO(3)$ as in (2.19) where $\alpha(y) = (y/2)cot(y/2)$. If N is the number of coupled first order differential equations in (4.17) and M is the number of mesh points, a

72

solution consists of values for N dependent functions at each of the M mesh points, i.e. $N \times M$ variables in all. The relaxation method determines the solution by starting with a guess and improving it iteratively. At each step, the method produces a matrix equation whose solution is increments for each entry in the $N \times M$ matrix of interest. When this increments are sufficiently small, we say that the method has converged, or the matrix has relaxed to the true solution. For more details the interested reader is referred to [66].

4.6.2 Geodesics and minimum acceleration curves on $SO(3)$ by the projection method

If the projection method described in Section 4.4 is used, one solves the problem in $GL^+(3)$, while keeping the proper boundary conditions for $SO(3)$.

Geodesics are found in $GL^+(3)$ and eventually projected back onto $SO(3)$. The geodesic in $GL^+(3)$ is

$$M(t) = R_0 + (R_1 - R_0)t, \ t \in [0, 1]$$

The projection onto $SO(3)$ using the metric W is given by:

$$M(t)W = U(t)\Sigma(t)V(t)^T,$$

$$R(t) = U(t)V(t)^T, \ W = \frac{1}{2}Tr(G)I_3 - G \tag{4.19}$$

For minimum acceleration curves, the boundary conditions $R(0)$, $R(1)$, $\dot{R}(0)$, $\dot{R}(1)$ are assumed to be specified. The minimum acceleration curve in $GL^+(3)$ with a constant

73

metric $<, >_{GL^+}$ is a cubic given by

$$M(t) = M_0 + M_1 t + M_2 t^2 + M_3 t^3,$$

where $M_0, M_1, M_2, M_3 \in GL^+(3)$ are

$$M_0 = R(0), \quad M_1 = \dot{R}(0),$$

$$M_2 = -3R(0) + 3R(1) - 2\dot{R}(0) - \dot{R}(1),$$

$$M_3 = 2R(0) - 2R(1) + \dot{R}(0) + \dot{R}(1).$$

Now the curve on $SO(3)$ is obtained by projecting $M(t)$ onto $SO(3)$ using equation (4.19).

4.6.3 Computational efficiency

It is not difficult to see that, from a computational point of view, it is less expensive to generate interpolating motion using the projection method as opposed to the relaxation method. Recall that the complexity of the SVD of a $n \times n$ matrix is of order n^3 [40]. If M is the number of uniformly distributed points in $[0, 1]$, then the number of flops required by the projection method in $GL^+(n)$ is of order $O(n^3 M)$.

The relaxation method for generating solution at M mesh points of a system of N differential equations with two boundary conditions implies solving a $MN \times MN$ linear system in the corrections iteratively until the method relaxes to the solution (corrections converge to zero) [66]. Gaussian elimination, whose complexity is cubic, is used to solve

74

the linear systems. Therefore, the number of flops required in the relaxation method is of order $O(M^3N^3)$.

Consider the problem of generating geodesics on $SO(n)$. Here $N = n(n - 1)$. The projection method involves $O(n^3M)$ flops while the relaxation method has complexity of the order $O(n^6M^3)$. For $M = 100$, as we used in this paper, the generation of geodesics on $SO(3)$ ($n = 3$) requires millions of flops by the relaxation method, while only thousands by the projection method.

4.6.4 Implementation notes

The relaxation method has been programmed in C, using routines from [66]. The produced executable file is called with line command arguments from a MATLAB™ [2] file, so that the C code is transparent for the user. For both the projection and the relaxation method, the MATLAB™ files ask for input data: position and velocity boundary conditions, and mass and moments of inertia of the body. The output is the trajectory on $SE(3)$. The rotational part can be plotted separately in exponential coordinates. Files of type .frames to generate motion in Jack™ are also created.

---

[2] MATLAB™ is a trademark of the MathWorks, Inc.

4.6.5 Simulation results

Geodesics on $SO(3)$

Without loss of generality, we will assume $R_1 = I$. Indeed, a geodesic between two arbitrary points R_1 and R_2 is the geodesic between I and $R_1^{-1}R_2$ left translated by R_1 [57, 91].

Illustrative examples are shown in Figures 4.4 and 4.5, where end positions on $SO(3)$ are given in exponential coordinates. In all the examples, the initial condition is $\sigma(0) = [0, \ 0, \ 0]^T$, which corresponds to the body frame $\{M\}$ being parallel with the inertial frame $\{F\}$ at $t = 0$. In both Figures 4.4 and 4.5, Case (a) corresponds to final condition $\sigma(1) = [\pi/10, \ \pi/10, \ \pi/10]^T$ (*i.e.*, a rotation of $\pi\sqrt{3}/10$ about the unit vector $[1/\sqrt{3}, \ 1/\sqrt{3}, \ 1/\sqrt{3}]^T$), while Case (b) describes the final condition $\sigma(1) = [\pi/6, \ \pi/3, \ \pi/2]^T$ (*i.e.*, a rotation of $\pi\sqrt{14}/6$ about the unit vector $[1/\sqrt{14}, \ 2/\sqrt{14}, \ 3/\sqrt{14}]^T$). In other words, Case (a) represents a small (compared with π) rotation, while Case (b) is a rotation approximately four times that in (a).

In Figure 4.4, $G = \alpha I$ and the geodesic passing through identity on $SO(3)$ is a uniformly parameterized line through the origin in exponential coordinates. Also, as proved in [4], the projected geodesic follows the same path but with a different parameterization. When the displacement is small (Case (a)), the parameterizations of the curves obtained by relaxation and projection are almost the same. The difference in parameterization is more pronounced in case (b), when the excursion is large.

In Figure 4.5, $G \neq \alpha I$ and the geodesics in exponential coordinates are not straight

76

(a)   (b)
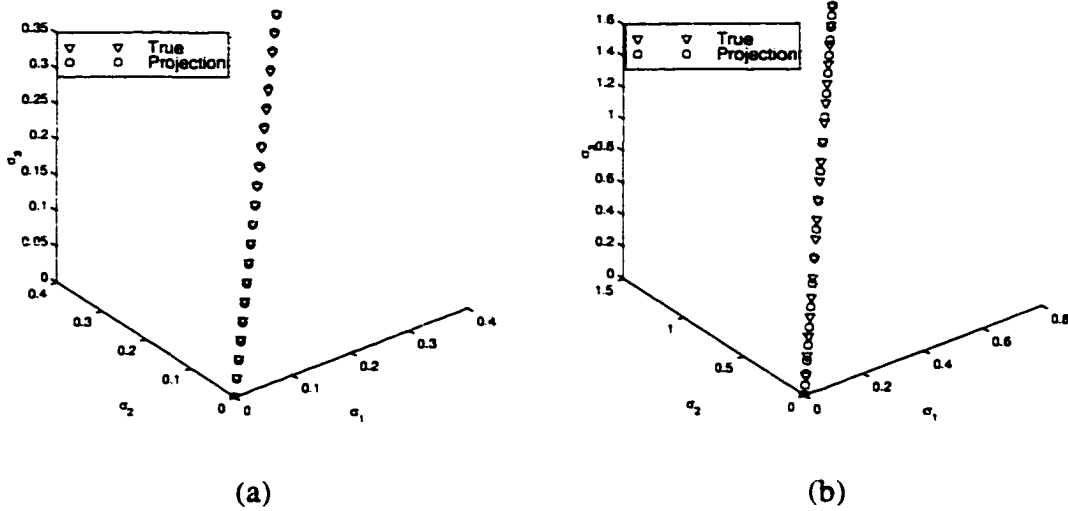
Figure 4.4: Geodesics on $SO(3)$ for an isotropic metric $G = \text{diag}\{3, 3, 3\}$ drawn in exponential coordinates: (a) $\sigma(1) = [\pi/10, \pi/10, \pi/10]^T$; (b) $\sigma(1) = [\pi/6, \pi/3, \pi/2]^T$

(a)   (b)
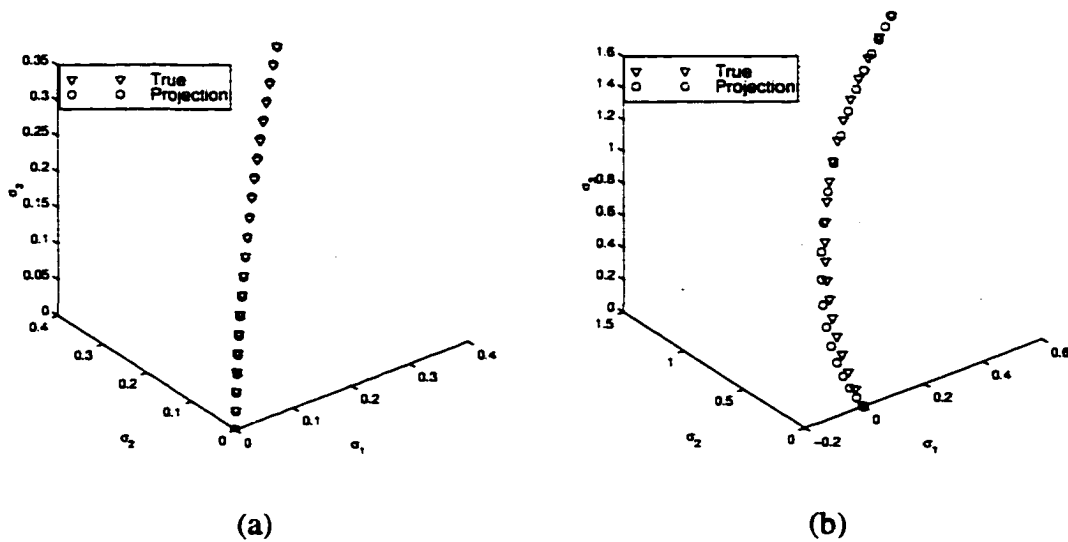
Figure 4.5: Geodesics on $SO(3)$ for metric $G = \text{diag}\{10, 10, 3\}$ drawn in exponential coordinates: (a) $\sigma(1) = [\pi/10, \pi/10, \pi/10]^T$; (b) $\sigma(1) = [\pi/6, \pi/3, \pi/2]^T$.

77

(a) **(b)** **(c)**
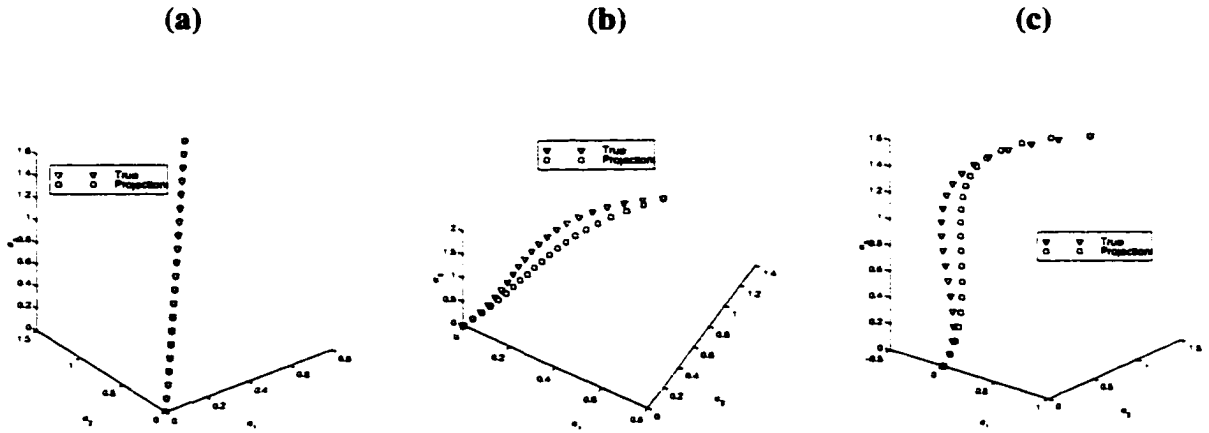
Figure 4.6: Minimum acceleration curves on $SO(3)$ with canonical metric: (a) Velocity boundary conditions along the geodesic; (b) End velocity perturbed by e_1; and (c) End velocity perturbed by $5e_1$.

lines anymore. Also, the geodesic and the projected curve follow different paths. Again, the difference between the geodesic obtained by relaxation and the projected curve is more noticeable for larger displacements (Case (b)).

Minimum acceleration curves on $SO(3)$

The following examples present comparisons between the minimum acceleration curves generated using the projection method and the curves obtained directly on $SO(3)$ by integrating equations (3.20) using the relaxation method. All the generated curves are drawn in exponential local coordinates.

In Figure 4.6.5, the following position boundary conditions were used:

$$\sigma(0) = \begin{bmatrix} 0 & 0 & 0 \end{bmatrix}^T, \ \sigma(1) = \begin{bmatrix} \frac{\pi}{6} & \frac{\pi}{3} & \frac{\pi}{2} \end{bmatrix}^T \qquad (4.20)$$

78

The initial velocity is the one corresponding to the geodesic passing through the two positions:

$$\omega_0 = \left[\begin{array}{ccc} \frac{\pi}{6} & \frac{\pi}{3} & \frac{\pi}{2} \end{array} \right]^T$$

Cases (a), (b) and (c) differ by the velocity at the end point. Figure 4 (a) corresponds to a final velocity $\omega_1 = \omega_0$, therefore one gets a minimum acceleration curve for which the end velocities are along the velocity of the corresponding geodesic, leading to a geodesic parameterized by a cubic of time [91]. The final velocity is $\omega_1 = \omega_0 + e_1$ in case (b) and $\omega_1 = \omega_0 + 5e_1$ in case (c), where $e_1 = [1 \ 0 \ 0]^T$.

As seen in Figure 4 (a), the paths of the projected and the optimal curves are the same, the parameterizations are slightly different though, as expected. In cases (b) and (c), although the deviation of the final velocity from being homogeneous is large, the curves are close. Note that the boundary conditions are rigorously satisfied.

Geodesics on $SE(3)$

Since we know how to generate near optimal curves in $SO(3)$, the extension to $SE(3)$ is simply adding the well known optimal curves from $\mathbf{R}^3$. A homogeneous parallelepipedic rigid body is assumed to move (rotate and translate) in free space. We assume that the body frame $\{M\}$ is placed at the center of mass and aligned with the principal axes of the body. Let a, b and c be the lengths of the body along its x, y and z axes respectively, and m the mass of the body.

For visualization, a small square is drawn on one of its faces and the center of the

79

parallelepiped is shown starred.

The matrix G of metric $<, >_{SO}$ is given by

$$G = \begin{bmatrix} \frac{m}{24}(b^2 + c^2) & 0 & 0 \\ 0 & \frac{m}{24}(a^2 + c^2) & 0 \\ 0 & 0 & \frac{m}{24}(a^2 + b^2) \end{bmatrix}$$
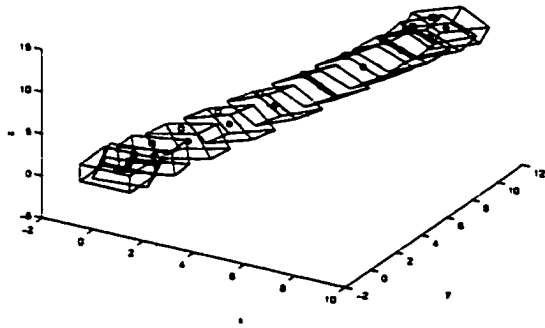
(a)   (b)
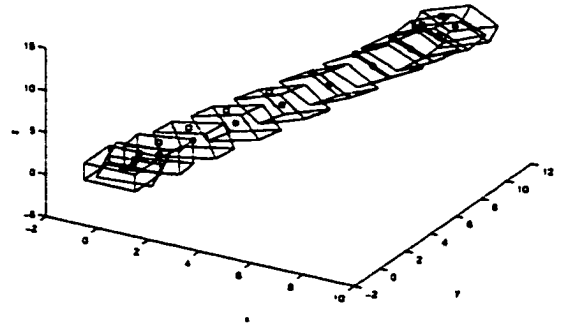
Figure 4.7: Minimum acceleration motion for a cube in free space: (a) relaxation method; (b) projection method.

The following boundary conditions were considered:

$$\sigma(0) = \begin{bmatrix} 0 & 0 & 0 \end{bmatrix}^T, \ \sigma(1) = \begin{bmatrix} \frac{\pi}{6} & \frac{\pi}{3} & \frac{\pi}{2} \end{bmatrix}^T$$

$$\omega(0) = \begin{bmatrix} 1 & 2 & 3 \end{bmatrix}^T, \ \omega(1) = \begin{bmatrix} 2 & 1 & 1 \end{bmatrix}^T$$

$$d(0) = \begin{bmatrix} 0 & 0 & 0 \end{bmatrix}^T, \ d(1) = \begin{bmatrix} 8 & 10 & 12 \end{bmatrix}^T$$

$$\dot{d}(0) = \begin{bmatrix} 1 & 1 & 1 \end{bmatrix}^T, \ \dot{d}(1) = \begin{bmatrix} 1 & 5 & 3 \end{bmatrix}^T$$

80
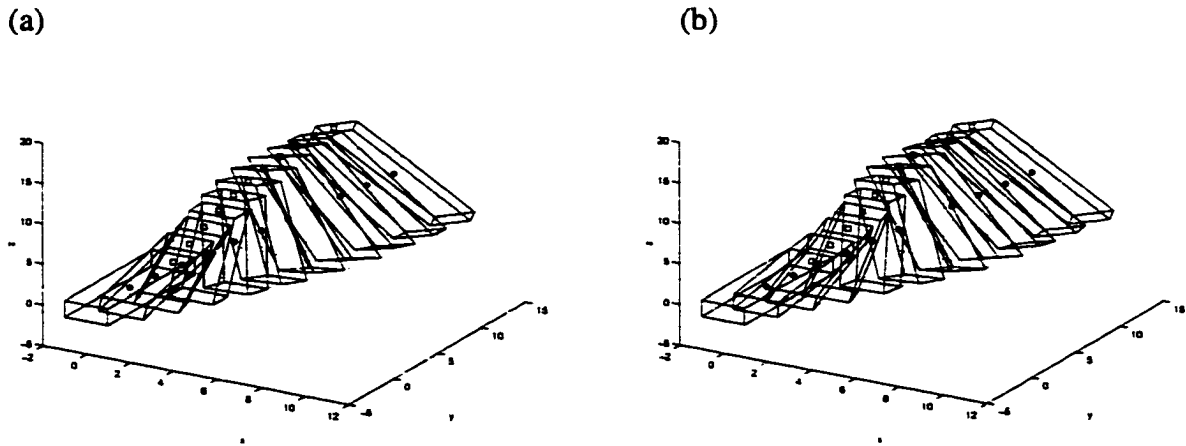
Figure 4.8: Geodesics for a parallelepipedic body: (a) relaxation method; (b) projection method.

True and projected minimum acceleration motions for a cubic rigid body with $a = b = c = 2$ and $m = 12$ are given in Figure 4.7 for comparison. Note that for this case $G = \alpha I$ with $\alpha = 4$.

Geodesics for the same boundary conditions and a parallelepipedic body with $a = c = 2, b = 10$ and $m = 12$ are given in Figure 4.8. For this case,

$$G = \begin{bmatrix} 52 & 0 & 0 \\ 0 & 4 & 0 \\ 0 & 0 & 52 \end{bmatrix}$$

As seen in Figures 4.7 and 4.8, even though the total displacement between the initial and final positions on $SO(3)$ is large (rotation angle of $\pi\sqrt{14}/6$), there is no noticeable difference between the true and the projected motions.

Three frames from the geodesic motion of the same parallelepiped generated using the relaxation method and Jack™ [3] are shown for illustration in Figure 4.9. Jack™ is a

[3]Jack™ is a trademark of the University of Pennsylvania

81

program which facilitates constructing geometric objects, positioning figures in a scene, and describing motion of the figures. It also has facilities for specifying lighting and surface property information.

Figure 4.9: Frames from a movie produced with Jack™

4.7 Discussion

This chapter develops a method for generating smooth trajectories for a moving rigid body with specified conditions at end points. The method involves two key steps: (1) the generation of optimal trajectories in $GA^+(n)$; and (2) the projection of the trajectories from $GA^+(n)$ to $SE(n)$. The overall procedure is invariant with respect to both the local coordinates on the manifold and the choice of the inertial frame. The benefits of the method are three-fold. First, it is possible to apply any of the variety of well-known, efficient techniques to generate optimal curves on $GA^+(n)$ [33, 35]. Second, the method yields nearly optimal solutions for general choices of Riemannian metrics on $SE(3)$. For example, we can incorporate the dynamics of arbitrarily shaped rigid bodies. Third, from a computational point of view, the method we propose is less expensive than traditional methods. We presented the application of the basic ideas to a motion generation problem

82

with specified boundary conditions.

Chapter 5

Optimal motion generation for groups

of robots

This chapter develops a method for generating smooth trajectories for a set of mobile robots satisfying constraints on relative positions. It is shown that, given two end configurations of the set of robots, by tuning one parameter, the user can choose an interpolating trajectory from a continuum of curves varying from the trajectory corresponding to maintaining a rigid formation to trajectories that allow the formation to change and the robots to reconfigure while moving.

The fundamental idea is based on the definition of a kinetic energy metric in the configuration space. It is well known from classical mechanics that any energy metric can be used to derive geodesics which represent the trajectory of the unforced system. We decompose the kinetic energy into the energy of the motion of a rigid structure and

84

the energy corresponding to motions that violate the rigidity constraint. The first set of motions can be associated to velocity vectors that are tangential to orbits of the Euclidean group, $SE(3)$ or $SE(2)$. The second set of motions corresponds to velocity vectors which are orthogonal to the first. The kinetic energy metric is "shaped" by assigning different weights to each contribution[1]. The geodesic flow for this modified metric is derived, and trajectories of the individual robots are generated. When the weights are biased toward the rigid body motion, the obtained trajectories correspond to optimal rigid body motions in 3-D space $(SE(3))$ or in the plane $(SE(2))$. Other choices of weights lead to the special cases of the robots moving toward each other or each individual robot traversing its own optimal path.

This chapter is organized as follows. The problem is formulated and the notation is introduced in Section 5.1. Section 5.2 gives a mathematical description of the rigidity constraint. The configuration space is endowed with a metric in Section 5.3, which is used for infinitesimal decomposition of motion into rigid and non-rigid. An example of optimal motion planning for a rigid formation is given in Section 5.4. The rigidity constrained is relaxed and the kinetic energy metric is "shaped" in Section 5.5. The chapter ends with examples and discussions.

---

[1]This idea of a "decomposition" and a subsequent "modification" is related to the methodology of controlled Lagrangians described in [20, 87].

5.1 Problem statement and notation

Consider N robots moving (rotating and translating) in 3-D space with respect to an inertial frame $\{F\}$. We choose a reference point on each robot at its center of mass O_i. A moving frame $\{M_i\}$ is attached to each robot at O_i (see Figure 5.1).
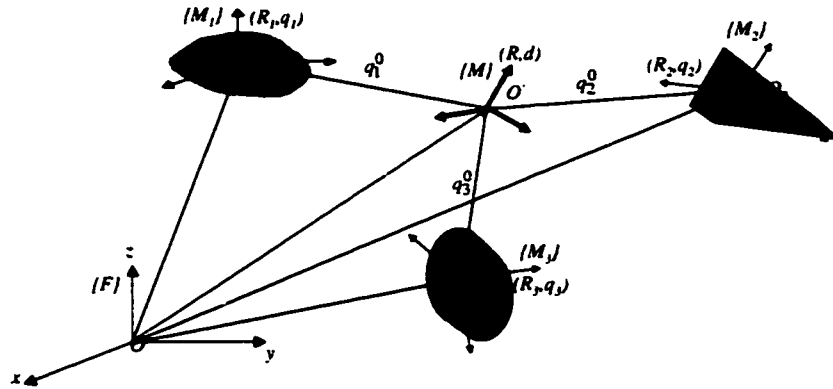
Figure 5.1: A set of $N = 3$ robots.

Robot i has mass m_i and matrix of inertia H_i with respect to frame $\{M_i\}$. Let $R_i \in SO(3)$ denote the rotation of $\{M_i\}$ in $\{F\}$ and $q_i \in \mathbb{R}^3$ the position vector of O_i in $\{F\}$. Let ω_i denote the expression in $\{M_i\}$ of the angular velocity of $\{M_i\}$ with respect to $\{F\}$. The *formation* is defined by the reference points O_i. The moving formation is called *rigid* if the relative distance between any of the points O_i is maintained constant. Sometimes it is also useful to define a *formation frame* $\{M\}$, attached at some virtual point O' and with pose $(R, d) \in SE(3)$ in $\{F\}$. Let q_i^0 denote the position vectors of O_i in $\{M\}$.

The configuration space is the $6N$-dimensional manifold, $SE(3) \times SE(3) \times \ldots SE(3)$,

86

given by the poses of each robot. Given two configurations at times $t = 0$ and $t = 1$ respectively, the goal is to generate smooth interpolating motion for each robot so that the total kinetic energy is minimized.

The kinetic energy T of the system of robots is the sum of the individual energies. Since the frames $\{M_i\}$ were placed at the centroids O_i of the robots, T can be written as the sum of the total rotational energy T_r and the total translational energy T_t in the form:

$$T = T_r + T_t, \quad T_r = \frac{1}{2}\sum_{i=1}^{N}(\omega_i^T H_i \omega_i), \quad T_t = \frac{1}{2}\sum_{i=1}^{N}(m_i \dot{q}_i^T \dot{q}_i) \tag{5.1}$$

Since our definition of a formation only involves the reference points O_i, a formation requirement will only constrain the q_i's from the above equation. Therefore, due to the decomposition in equation (5.1), minimizing the total energy is equivalent to solving $N+1$ independent optimization subproblems:

$$\min_{\sigma_i} \int_0^1 \omega_i^T H_i \omega_i dt, \quad i = 1, \ldots, N, \tag{5.2}$$

$$\min_{q_i=1,\ldots,N} \int_0^1 T_t dt \tag{5.3}$$

where σ_i is some parameterization of the rotation of $\{M_i\}$ in $\{F\}$, i.e., some local coordinates on $SO(3)$. The solutions to equations (5.2) are given by N geodesics on $SO(3)$ with left invariant metrics with matrices H_i. Two different methods to obtain the solution are given in Chapter 4 and a short example is given in Section 5.4.

The main focus in this chapter is solving problem (5.3) while satisfying constraints on the positions of the reference points O_i that may be imposed by the requirements on the task. Thus the configuration space we are interested in is just the $3N$ dimensional

87

$Q = \{q | q = (q_1, \ldots, q_N)\}$, which collects all the position vectors of the chosen reference points. Maintaining a rigid formation (a virtual structure) imposes constraints on the configuration space, Q, and these constraints may be relaxed as necessary.

5.2 The rigidity constraint - virtual structures

The group of N robots is said to form a *virtual structure* if the relative distances among the reference points O_i are maintained constant. Let $q = [q_1^T, \ldots, q_N^T]^T$ denote an arbitrary point in Q. For an arbitrary pair of reference points with position vectors q_i and q_j, $i, j = 1, \ldots, N$, $i < j$, the constraints can be written as:

$$(q_i - q_j)^T(q_i - q_j) = constant \tag{5.4}$$

or, by differentiation:

$$(q_i - q_j)^T \dot{q}_i - (q_i - q_j)^T \dot{q}_j = 0$$

By lifting this constraint to the configuration manifold Q, the coordinates of the corresponding differential one form can be written as a $1 \times 3N$ row vector:

$$\omega_{ij} = \begin{bmatrix} 0 & \cdots & 0 & (q_i - q_j)^T & 0 & \cdots & 0 & -(q_i - q_j)^T & 0 & \cdots & 0 \end{bmatrix}$$

The non-zero 1×3 blocks in the above matrix are in positions i and j, respectively. If we consider all $(N-1)N/2$ possible constraints, we can construct the codistribution ω_R as the span of all the corresponding covectors:

$$\omega_R = \text{span} \{\omega_{ij}, \; i, j = 1, \ldots, N, \; i < n\}$$

88

It is obvious that not all the $(N-1)N/2$ covectors (constraints) are independent. To insure rigidity, it is necessary and sufficient to impose $2N - 3$ constraints of the type (5.4) in plane, while in 3D, the number is $3N - 6$. This is closely related to the idea of *minimally rigid graphs* [61, 31], or, equivalently, *isostatic graphs* [32, 31]. By simple inspection, it is easy to prove that the annihilating distribution of ω_R ($\omega_R(\Delta_R) = 0$) is:

$$\Delta_R = \text{Range}(A(q)), \quad A(q) = \begin{bmatrix} -\hat{q}_1 & I_3 \\ \cdots & \cdots \\ -\hat{q}_N & I_3 \end{bmatrix} \tag{5.5}$$

Therefore, by lifting each constraint to the configuration manifold Q, the virtual structure (rigidity) constraint can be written as

$$\dot{q} \in \Delta_R(q) \tag{5.6}$$

A *generic* situation is defined as being a configuration in which q_i are not all contained in any proper hyperplane of $\mathbb{R}^d$ ($d = 2, 3$). Of course Δ_R is integrable, therefore regular and involutive. It is interesting to note though that, in a generic situation, the distribution Δ_R is regular and involutive, therefore integrable. The proof of regularity can be found, in a slightly different context in [69]. It is proved that, under the generic situation assumption, a matrix similar to ω_R, called the rigidity matrix, is of rank $3N - 6$ in 3D and of rank $2N - 3$ in plane, which is equivalent to the regularity of the annihilating distribution Δ_R (of rank 3 in plan and 6 in 3D). For involutivity, let $a_1, \ldots, a_6$ (the columns of $A(q)$) denote the basis of Δ_R at q. Then, it is easy to see that

$$a_i = \text{block diag}\{L_i^o, \ldots, L_i^o\}q, \quad i = 1, 2, 3$$

89

Therefore, the involutivity of a_i, $i = 1, \ldots, 6$ is reduced to the involutivity of the standard basis L_i, $i = 1, \ldots, 6$ for $se(3)$, which is assumed known.

The following theorem gives an explicit construction of a foliation of $\mathbb{R}^{3N}$ using the distribution Δ_R. It follows that motion planning (control) problems for a set of N robots in 3D required to maintain a rigid formation can be reduced to motion planning (control) problems for a left invariant control system on $SE(3)$.

Theorem 3. *Assume $q(0) = q^0$ and $\dot{q}(0) \in \Delta_R(q^0)$. Then, the formation constraint (5.6) is satisfied for all $t \geq 0$ if and only if*

$$q_i(t) = d(t) + R(t)q_i^0 \tag{5.7}$$

where $(R(t), d(t))$ is a trajectory of the left invariant control system

$$\dot{g}(t) = gS \tag{5.8}$$

starting from $R(0) = I_3$, $d(0) = 0$.

Proof. To prove sufficiency, if $s = [\omega^T \ v^T]^T \in \mathbf{R}^6$ are the coordinates of $S \in se(3)$ in the standard basis $L_1, \ldots, L_6$, then for each $i = 1, \ldots, N$, we have:

$$\dot{q}_i = \dot{d} + \dot{R}q_i^0 = Rv + R\hat{\omega}q_i^0 = Rv + R\hat{\omega}R^T(q_i - d) =$$

$$= Rv + \widehat{R\omega}(q_i - d) = \begin{bmatrix} -\hat{q}_i & I \end{bmatrix} \begin{bmatrix} R\omega \\ dR\omega + Rv \end{bmatrix} = \begin{bmatrix} -\hat{q}_i & I \end{bmatrix} Ad_g s$$

from which it follows that $\dot{q} = [\dot{q}_1^T, \ldots, \dot{q}_N^T]^T \in \Delta_R(q)$.

For necessity, let $r \in \mathbf{R}^6$ give the coordinates of $\dot{q}$ in the chosen basis of $\Delta_R(q)$:

$$\dot{q} = A(q)r \tag{5.9}$$

90

Then, we will show that the system (5.8) starting at $R(0) = I$, $d(0) = 0$ with

$$s = \begin{bmatrix} R^T & 0 \\ -R^T \dot{d} & R^T \end{bmatrix} r = Ad_{g^{-1}} r \tag{5.10}$$

gives $q_i(t) = d(t) + R(t)q_i^0$. Let $s = [\omega^T \, v^T]^T$. Then, the control system can be written as

$$\dot{R} = R\hat{\omega}, \quad \dot{d} = Rv \tag{5.11}$$

Using (5.9), (5.10), and (5.11), we have, for any $i = 1, \ldots, N$:

$$\dot{q}_i = -\hat{q}_i(R\omega) + \dot{d}R\omega + Rv = \widehat{R\omega}q_i - \widehat{R\omega}d + Rv$$

$$= R\hat{\omega}R^T q_i - R\hat{\omega}R^T d + Rv = \dot{R}R^T q_i - \dot{R}R^T d + \dot{d}$$

or,

$$\frac{d}{dt}(q_i - d) = \dot{R}R^T(q_i - d)$$

Using

$$RR^T = I \implies \dot{R}R^T = -R\dot{R}^T$$

we end up with

$$\frac{d}{dt}\left(R^T(q_i - d)\right) = 0$$

Using the initial conditions $R(0) = I$, $d(0) = 0$, $q_i(0) = q_i^0$, the above equation can be integrated to (5.7). $\square$

Remark 15. • *The coordinates r of the expansion of $\dot{q} \in \Delta_R(q)$ along the columns of $A(q)$ are exactly the components of the left invariant twist of a virtual structure formed by $(q_1, \ldots, q_N)$ and $\{F\}$ at that instant.*

91

- s is the left invariant twist of a moving rigid structure formed by $(q_1^0, \ldots, q_N^0)$ and $\{M\}$ and for which the mobile frame $\{M\}$ was coincident with $\{F\}$ at $t = 0$.

- $g = (R, d)$ is the pose of the moving frame $\{M\}$ in $\{F\}$.

Corollary 6. *The distribution $\Delta_R(q)$ determines a foliation of Q with leaves given by orbits of $SE(3)$.*

5.3 Motion decomposition: rigid vs. non-rigid

We first define a metric $<, >$ in the position configuration space, which is the same at all points $q \in Q$:

$$< V_q^1, V_q^2 > = V_q^{1^T} M V_q^2, \tag{5.12}$$

$$V_q = \dot{q} \in T_q Q, \quad M = \frac{1}{2} \text{diag}\{m_1 I_3, \ldots, m_N I_3\} \tag{5.13}$$

Metric (5.12) is called the *kinetic energy metric* because its induced norm ($V_q^1 = V_q^2 = \dot{q}$) assumes the familiar expression of the kinetic energy of the system $1/2 \sum_{i=1}^N m_i \dot{q}_i^T \dot{q}_i$.

If no restrictions are imposed on Q, the geodesic between $q(0) = q^0$ and $q(1) = q^1$ for metric (5.12) is obviously a straight line uniformly parameterized in time interpolating between q^0 and q^1 in Q.

At each point q in the configuration space Q, $\Delta_R(q)$ locally describes the set of all rigid body motion directions. The orthogonal complement to $\Delta_R(q)$, $\Delta_{NR}(q)$ will be the set of all directions violating the rigid body constraints [2]. For an arbitrary tangent vector

---

[2] In [20, 87], the tangent space at q to the orbit of $SE(3)$ is called the vertical space at q, Ver_q, and its orthogonal complement is the horizontal space at $q \in Q$, Hor_q.

$V_q \in T_qQ$, let $\mathbf{R}V_q$ denote the projection onto Δ_R and $\mathbf{NR}V_q$ denote the projection onto Δ_{NR}.

Using metric (5.12), the orthogonal complement of the "rigid" distribution $\Delta_R(q)$ is the "non-rigid" distribution

$$\Delta_{NR}(q) = \text{Null}(A(q)^T M) \tag{5.14}$$

Let $B(q)$ denote a matrix whose columns are a basis of $\Delta_{NR}(q)$.

Let ψ denote the components of the projection in this basis: $\mathbf{NR}V_q = B(q)\psi$. Therefore, the velocity at point q can be written as:

$$V_q = \mathbf{R}V_q + \mathbf{NR}V_q = A(q)r + B(q)\psi \tag{5.15}$$

Then, for any V_q^1, $V_q^2 \in T_qQ$, we have:

$$< V_q^1, V_q^2 > = V_q^{1^T} M V_q^2 = r^{1^T} A^T M A r^2 +$$

$$+ r^{1^T} A^T M B \psi^2 + \psi^{1^T} B^T M A r^2 + \psi^{1^T} B^T M B \psi^2 =$$

$$= r^{1^T} A^T M A r^2 + \psi^{1^T} B^T M B \psi^2 =$$

$$= < B\psi^1, B\psi^2 > + < Ar^1, Ar^2 > =$$

$$= < \mathbf{NR}V_q^1, \mathbf{NR}V_q^2 > + < \mathbf{R}V_q^1, \mathbf{R}V_q^2 >$$

because both $A^T M B$ and $B^T M A$ are zero from (5.14). Also, note that

$$r = (A^T M A)^{-1} A^T M V, \tag{5.16}$$

$$\psi = (B^T M B)^{-1} B^T M V$$

93

where the explicit dependence of A and B on q was omitted for simplicity. Therefore, the translational kinetic energy (which is the square of the norm induced by metric (5.12)) becomes:

$$T_t(q, \dot{q}) = \dot{q}^T M \dot{q} = r^T A^T M A r + v^T B^T M B v \qquad (5.17)$$

In (5.17), $r^T A^T M A r$ captures the energy of the motion of the system of particles as a rigid body, while the remaining part $v^T B^T M B v$ is the energy of the motion that violates the rigid body restrictions. For example, in the obvious case of a system of $N = 2$ particles, the first part corresponds to the motion of the two particles connected by a rigid mass-less rod, while the second part would correspond to motion along the line connecting the two bodies.

5.4 Motion generation for rigid formations

In this section, we will assume that the robots are required to move in *rigid formation*, *i.e.*, the distances between any two reference points O_i are preserved, or, equivalently, the reference points form a rigid polyhedron.

In our geometric framework, the rigid body requirement means restricting the trajectory $q(t) \in Q$ to be a $SE(3)$ - orbit, or equivalently, $\mathbf{N}\mathbf{R}\dot{q} = 0$ or $\dot{q} \in \Delta_R(q)$, for all q.

In this case, one can imagine a body frame $\{M\}$ moving with the virtual structure determined by the O_i's. Initially $(t = 0)$, the frame $\{M\}$ is coincident with $\{F\}$ and $q(0) = q^0$. The position vector of O_i in $\{M\}$ is constant during this motion and equal to

94

q_i^0.

From Theorem 3, $\dot{q}_i = [-\hat{q}_i^0 \; I]s$, and therefore, the kinetic energy T_t becomes:

$$T_t = s^T \mathcal{M} s, \quad \mathcal{M} = A(q^0)^T M A(q^0) \tag{5.18}$$

where $s \in se(3)$ is the instantaneous twist of the virtual structure.

Therefore, if the set of robots is required to move while maintaining a constant shape q^0, the optimization problem is reduced from dimension $6N$ to dimension $3N + 6$, and consists of solving for N geodesics on $SO(3)$ with metrics H_i (individual rotations) and one geodesic on the $SE(3)$ of the virtual structure with left invariant metric $\mathcal{M}$ as in (5.18).

5.4.1 Example: Five identical robots in 3D space

For illustration, we consider five identical parallelepipedic robots $m_i = m$, $i = 1, \ldots, 5$ required to move in formation while minimizing energy. The initial and final poses together with the geometrical properties of the robots are given in Figure 5.2. The body frames and the formation frame placed at the center of mass and aligned with the principal axis are drawn. The inertial frame is coincident with the formation frame at $t = 0$. As seen from the inertial frame, the formation frame is translated by $(X, 0, Z)$ and rotated by -90 degrees around the y-axis.

As outlined in the previous section, generating optimal motion for this group of robots

95
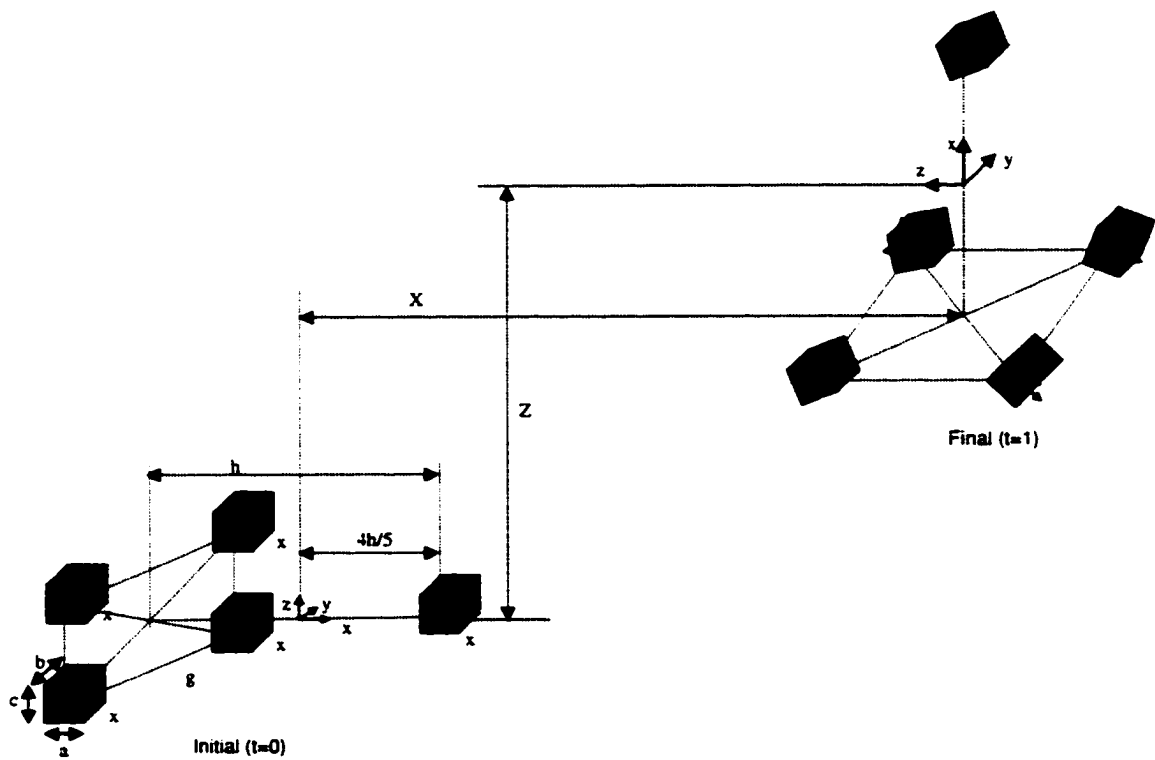
Figure 5.2: Geometry of the robots and of the virtual structure showing the initial and the final configurations. The relevant dimensions are chosen to be: a=c=2, b=10, h=20, l=10, X=20, Z=20, m=12.

reduces to generating five geodesics on the $SO(3)$ of each robot with left invariant metric

$$H_i = \frac{m}{24} \begin{bmatrix} b^2 + c^2 & 0 & 0 \\ \\ 0 & a^2 + c^2 & 0 \\ \\ 0 & 0 & a^2 + b^2 \end{bmatrix}, \ i = 1, \dots, 5$$

and one geodesic on the $SE(3)$ of the virtual structure endowed with a left invariant metric with matrix

$$G = \frac{m}{2} \begin{bmatrix} 2l^2 & 0 & 0 & 0 \\ \\ 0 & l^2 + \frac{4h^2}{3} & 0 & 0 \\ \\ 0 & 0 & l^2 + \frac{4h^2}{3} & 0 \\ \\ 0 & 0 & 0 & 3I_3 \end{bmatrix}$$

The resulting motion is presented in Figure 5.3.

We used exponential coordinates σ_i, $i = 1, 2, 3$ as local parameterization of $SO(3)$ [4].

5.5 Motion generation by kinetic energy shaping

By shaping the kinetic energy, we mean smoothly changing the corresponding metric (5.12) at T_qQ so that motion along some specific directions is allowed while motion along some other directions is penalized. The new metric will no longer be constant - the Christoffel symbols of the corresponding symmetric connection will be non-zero. The associated geodesic flow gives optimal motion.

97
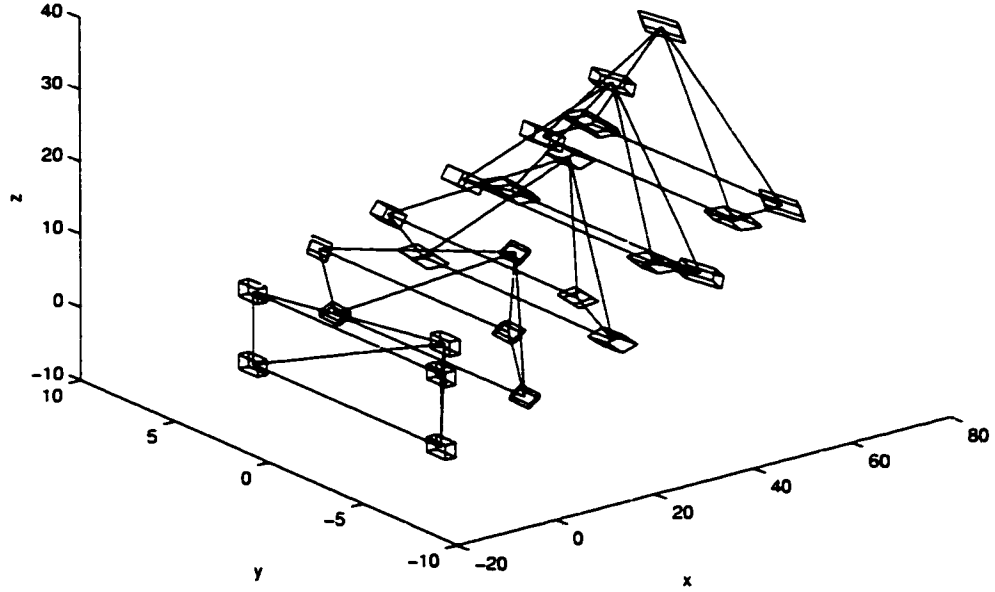
Figure 5.3: Optimal motion for five identical robots required to maintain a rigid formation

In this work, the original metric (5.12) is shaped by putting different weights on the terms corresponding to the rigid and non-rigid motions:

$$< V_q^{-1}, V_q^{-2} >_\alpha = \alpha < \mathbf{NR}V_q^{-1}, \mathbf{NR}V_q^{-2} > +(1 - \alpha) < \mathbf{R}V_q^{-1}, \mathbf{R}V_q^{-2} > \qquad (5.19)$$

Using (5.16) to go back to the original coordinates, we get the modified metric in the form:

$$< V_q^{-1}, V_q^{-2} >_\alpha = V_q^{-1^T} M_\alpha(q) V_q^{-2}, \qquad (5.20)$$

where the new matrix of the metric is now dependent on the artificially introduced parameter α and the point on the manifold $q \in Q$:

$$M_\alpha(q) = \alpha M A (A^T M A)^{-T} A^T M + (1 - \alpha) M B (B^T M B)^{-T} B^T M \qquad (5.21)$$

98

The influence of the parameter α can be best seen by examining the significance of α taking on the values of 0, 0.5 and 1. As α tends to 0, the preferred motions will be ones where robots cluster together through much of the duration of the trajectory, thus minimizing the *rigid body energy* consumption. As α approaches 0.5, the motions degenerate toward uncoordinated, independent motions. As α tends to 1, the preferred motions are ones where the robots stay in rigid formation through most of the trajectory, thus minimizing the energy associated with *deforming* the formation.

We use the geodesic flow of metric (5.20) to produce smooth interpolating motion between two given configurations:

$$q^0 = q(0), \quad q^1 = q(1) \in \mathbf{R}^{3N} \tag{5.22}$$

To simplify the notation, let x_i, $i = 1, \ldots, 3N$ denote the coordinates $q_i \in \mathbf{R}^3$, $i = 1, \ldots, N$ on the configuration manifold Q. In this coordinates, the geodesic flow is described by the following differential equations [29]:

$$\ddot{x}_i + \sum_{j,k} \Gamma^i_{jk} \dot{x}_j \dot{x}_k = 0, \quad i = 1, \ldots, 3N \tag{5.23}$$

where Γ^k_{ij} are the Christoffel symbols of the unique symmetric connection associated to metric (5.20):

$$\Gamma^k_{ij} = \frac{1}{2} \sum_h \left(\frac{\partial m_{hj}}{\partial x^i} + \frac{\partial m_{ih}}{\partial x^j} - \frac{\partial m_{ij}}{\partial x^h} \right) m^{hk} \tag{5.24}$$

m_{ij} and m^{ij} are elements of M_α and M_α^{-1}, respectively.

Because $\alpha = 0$ and $\alpha = 1$ make the metric singular, (5.24) can only be used for $0 < \alpha < 1$.

99

5.5.1 Example: two bodies in the plane

Consider two bodies of masses m_1 and m_2 moving in the $x - y$ plane. The configuration space is $Q = R^4$ with coordinates $q = [x_1, y_1, x_2, y_2]^T$. The A and B matrices describing $\Delta_R(q)$ and $\Delta_{NR}(q)$ as in (5.5) and (5.14) are:

$$A = \begin{bmatrix} -y_1 & 1 & 0 \\ x_1 & 0 & 1 \\ -y_2 & 1 & 0 \\ x_2 & 0 & 1 \end{bmatrix}, \quad B = \begin{bmatrix} \frac{m_2(x_2-x_1)}{m_1(y_1-y_2)} \\ -\frac{m_2}{m_1} \\ \frac{x_1-x_2}{y_1-y_2} \\ 1 \end{bmatrix}$$

The 64 Christoffel symbols $\Gamma^k = (\Gamma^k_{ij})_{ij}$ of the connection associated with the modified metric at $q \in Q$ become:

$$\Gamma^1 = \frac{2(1-2\alpha)}{\alpha} \frac{m_2}{m_1 + m_2} \frac{d_x}{(d_x^2 + d_y^2)^2} \Gamma$$

$$\Gamma^2 = \frac{2(1-2\alpha)}{\alpha} \frac{m_2}{m_1 + m_2} \frac{d_y}{(d_x^2 + d_y^2)^2} \Gamma$$

$$\Gamma^3 = -\frac{2(1-2\alpha)}{\alpha} \frac{m_1}{m_1 + m_2} \frac{d_x}{(d_x^2 + d_y^2)^2} \Gamma$$

$$\Gamma^4 = -\frac{2(1-2\alpha)}{\alpha} \frac{m_1}{m_1 + m_2} \frac{d_y}{(d_x^2 + d_y^2)^2} \Gamma$$

where

$$\Gamma = \begin{bmatrix} -d_y^2 & d_x d_y & d_y^2 & -d_x d_y \\ d_x d_y & -d_x^2 & -d_x d_y & d_x^2 \\ d_y^2 & -d_x d_y & -d_y^2 & d_x d_y \\ -d_x d_y & d_x^2 & d_x d_y & -d_x^2 \end{bmatrix}$$

100

and $d_x = x_1 - x_2$, $dy = y_i - y_2$. It can be easily seen that, as expected, all Christoffel symbols are zero if $\alpha = 0.5$. Also, the actual masses of the robots are not relevant, it's only the ratio m_1/m_2 which is important.

In this example, we assume $m_2 = 2m_1$ and the boundary conditions:

$$q^0 = \begin{bmatrix} 1 \\ 0 \\ -0.5 \\ 0 \end{bmatrix}, \quad q^1 = \begin{bmatrix} 3 - \frac{\sqrt{2}}{2} \\ -\frac{\sqrt{2}}{2} \\ 3 + \frac{\sqrt{2}}{4} \\ \frac{\sqrt{2}}{4} \end{bmatrix}$$

which correspond to a rigid body displacement so that we can compare our results to the optimal motion corresponding to a rigid body.

If the structure was assumed rigid, then the optimal motion is described by uniform rectilinear translation of the center of mass between $(0,0)$ and $(3,0)$ and uniform rotation between 0 and $3\pi/4$ around $-z$ placed at the center of mass. The corresponding trajectories of the robots are drawn in solid line in all the pictures in Figure 5.4. It can be easily seen that there is no difference between the optimal motion of the virtual structure solved on $SE(2)$ and the geodesic flow of the modified metric with $\alpha = 0.99$ (Figure 5.4, bottom). If $\alpha = 0.5$, all bodies move in straight line as expected (Figure 5.4, middle). For $\alpha = 0.2$, the bodies go toward each other first, and then split apart to attain the final positions (Figure 5.4, top).
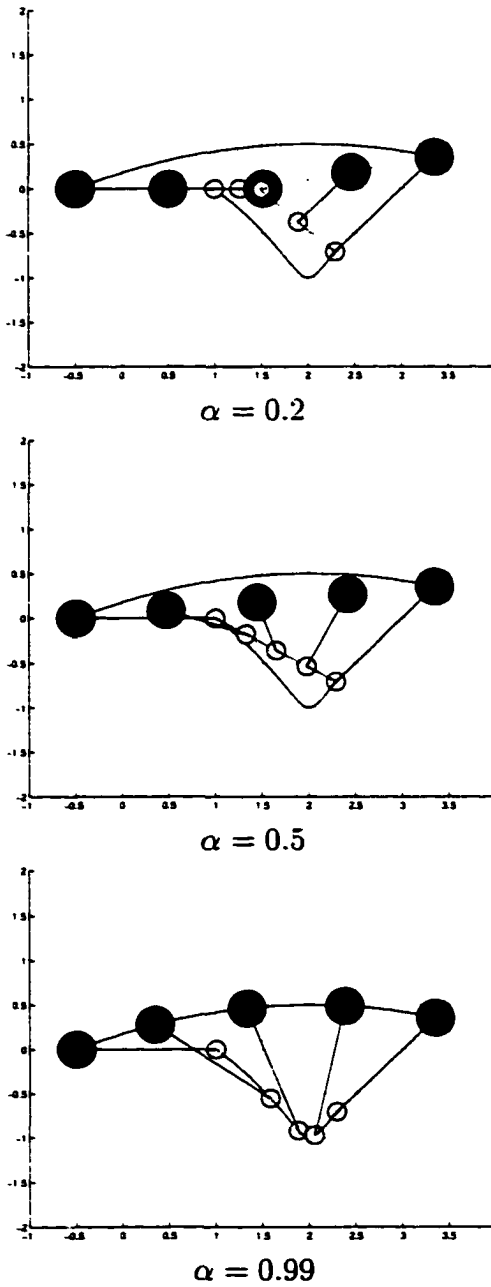
Figure 5.4: Three interpolating motions for a set of two planar robots as geodesics of a modified metric defined in the configuration space.

102

$$\alpha = 0.2$$

$$\alpha = 0.5$$

$$\alpha = 0.99$$
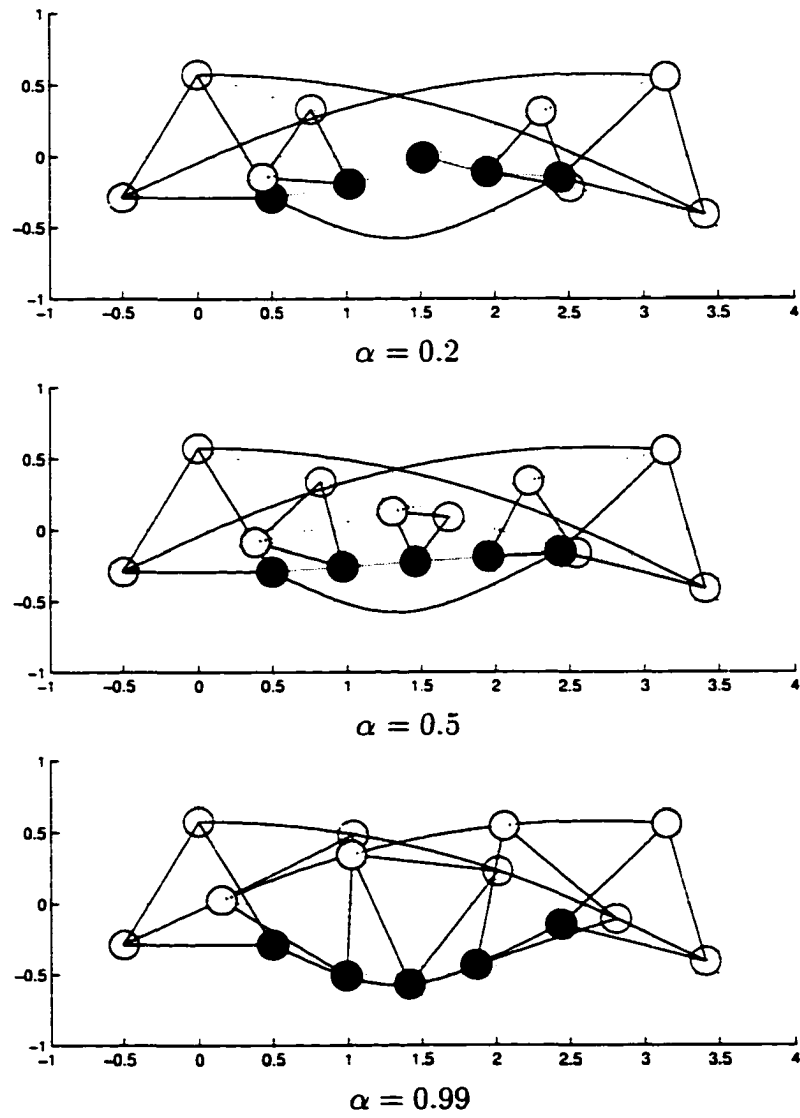
Figure 5.5: Three interpolating motions for a set of three planar robots as geodesics of a modified metric defined in the configuration space.

103

5.5.2 Example: three bodies in the plane

The calculation of the trajectories for three bodies moving in the plane is simplified by assuming that the robots are identical, and, without loss of generality, we assume $m_1 = m_2 = m_3 = 1$. The rigid and the non-rigid spaces at a generic configuration

$$q = [x_1, y_1, x_2, y_2, x_3, y_3]^T \in Q = \mathbf{R}^6$$

are given by

$$\Delta_R = \text{Range}(A), \quad A = \begin{bmatrix} -y_1 & 1 & 0 \\ x_1 & 0 & 1 \\ -y_2 & 1 & 0 \\ x_2 & 0 & 1 \\ -y_3 & 1 & 0 \\ x_3 & 0 & 1 \end{bmatrix},$$

$$\Delta_{NR} = \text{Range}(B), \quad B = \begin{bmatrix} \frac{x_3-x_1}{y_1-y_2} & \frac{y_2-y_3}{y_1-y_2} & \frac{x_2-x_1}{y_1-y_2} \\ -1 & 0 & -1 \\ \frac{x_1-x_3}{y_1-y_2} & \frac{y_3-y_1}{y_1-y_2} & \frac{x_1-x_2}{y_1-y_2} \\ 0 & 0 & 1 \\ 0 & 1 & 0 \\ 1 & 0 & 0 \end{bmatrix}$$

For simplicity, we omit the expressions of the modified metric and of the Christoffel symbols. The simulation scenario resembles the one in Section 5.5.1: the end poses correspond to a rigid structure consisting of a equilateral triangle with side equal to 1.

104

The optimal trajectory solved on $SE(2)$ corresponds to rectilinear uniform motion of the center of mass (line between (0,0) and (3,0) in Figure 5.5) and uniform rotation from angle 0 to $3\pi/4$ around axis $-z$. The resulting motion of each robot is shown solid, while the actual trajectory for the corresponding value of α is shown dashed. First note for $\alpha = 0.99$ the trajectories are basically identical with the optimal traces produced by the virtual structure, as expected. In the case $\alpha = 0.5$ the bodies move in straight line (corresponding to the unmodified metric). The tendency to cluster as α decreases is seen for $\alpha = 0.2$. Note also that due to our choice $m_1 = m_2 = m_3$, the geometry of the equilateral triangle is preserved for all values of α, it only scales down when α decreases from 1.

5.6 Discussion

This chapter presented a strategy for generating a family of smooth interpolating trajectories for a team of mobile robots. The family is parameterized by a scalar α. As α becomes closer to zero, the robots are pulled together as they move between the initial and final positions. The case $\alpha = 0.5$ corresponds to a totally uncoordinated strategy: each robot will move from its initial to its final position while minimizing its own energy. Finally, as α tends to 1, the robots try to preserve the distances between them and minimize the overall energy of the motion.

While the chapter provides a useful conceptual framework for motion planning and generation of trajectories, there is a practical limitation to this work. As the number of

105

robots, N, increases, the generation of the Christoffel symbols and the solution of the two-point boundary value problem becomes more complicated.

Chapter 6

Abstraction and control for groups of fully-actuated planar robots

In this chapter, we consider the problem of controlling a large number of robots required to accomplish a task as a group. For example, consider the problem of moving hundreds of planar robots with arbitrary initial positions through a tunnel while staying grouped so that the distance between each pair does not exceed a certain value. The simplest solution, generating reference trajectories and control laws for each robot to stay on the designed trajectory, is obviously not feasible from a computational viewpoint. It is desired to have a certain level of abstraction: the motion generation/control problem should be solved in a lower dimensional space which captures the behavior of the group and the nature of the task. For example, the robots can be required to form a *virtual structure*. In this case, as shown in Chapter 5, the motion planning problem is reduced to a left invariant control

107

system on $SE(3)$ (or $SE(2)$ in the planar case). However, the virtual structure constraint might be too much, or simply not appropriate in many applications, including obstacle avoidance, tunnel passing, etc.

We propose an abstraction based on the definition of a map from the configuration space of the robots to a lower dimensional abstract manifold, whose dimension does not scale with the number of robots. The task to be accomplished by the team suggests a natural feedback control system on the small dimensional manifold. In this chapter we focus on planar fully actuated robots and require the abstract manifold to have a product structure of a Lie *group*, which captures the dependence of the ensemble on the chosen world coordinate frame, and a *shape manifold*, which is an intrinsic description of the team. We design decoupled controls for group and shape. We also show that the individual control laws which are mapped to the desired behavior of the formation can be realized by feedback depending only on the current state of the robot and the state on the formation manifold, so that the robots have to broadcast their states and only have to listen to some coordinating agent with small bandwidth.

This chapter is organized as follows. The problem is formulated in Section 6.1 and our geometric approach to solving it is outlined in Section 6.2. Sections 6.3, 6.4, and 6.5 define an abstraction, discuss its significance and show that the requirements of the problem formulated in Section 6.1 are satisfied. Interesting simulation results are included in Section 6.6. The chapter concludes with statement of contributions and future work in Section 6.7.

108

6.1 Definitions and problem formulation

Consider N kinematically controlled robots with states q_i belonging to manifold Q_i and control spaces U_i. For planar fully actuated agents, the states are position vectors $q_i \in Q_i = \mathbf{R}^2$, $i = 1, \ldots, N$ with respect to some world frame $\{W\}$, and the controls $u_i \in U_i = \mathbf{R}^2$:

$$\dot{q}_i = u_i \tag{6.1}$$

Collecting all the robot states together, we get a $2N$-dimensional control system

$$\dot{q} = u \tag{6.2}$$

where $q \in Q = \prod_{i=1}^{N} Q_i = \mathbf{R}^{2N}$, $u \in U = \prod_{i=1}^{N} U_i = \mathbf{R}^{2N}$ and the canonical projections:

$$\pi_i(q) = q_i, \quad d\pi_i(u) = u_i \tag{6.3}$$

The motion (behavior) of the ensemble of robots is determined if the corresponding velocities are specified:

Definition 4 (Behavior). *Any vector field $X_Q \in TQ$ is called a behavior.*

Individual behaviors are obtained by projecting the collective behavior X_Q using (6.3).

Given a large number of robots evolving on the configuration space Q, we want to be able to solve motion generation / control problems on a smaller dimensional space, which captures the essential features of the group, according to the class of tasks to be accomplished. We want the dimension of the control problem to be independent of the

109

number of agents and also independent of the possible ordering of the robots. These requirements will provide control laws which are robust to individual failures and also good scaling properties.

We also need to make sure that, after solving the task on the small dimensional space, we can go back and generate control laws for the individual agents. All these ideas lead to the following definitions:

Definition 5 (Abstraction). *Any surjective submersion*

$$\phi : Q \to A, \quad \phi(q) = a \tag{6.4}$$

is called an abstraction if it is invariant to permutations of the robots and the dimension n of A is not dependent on the number of robots N. A and a are called abstract manifold and abstract state, respectively.

It is assumed that the abstract state a is physically significant in accordance to the task to be accomplished.

In addition, if possible, it is desired that A have a product structure

$$A = G \times S, \quad a = (g, s), \quad \phi = (\phi_g, \phi_s) \tag{6.5}$$

where G is a Lie group. An arbitrary $g \in G$ defines the gross position and orientation of the team in the world frame $\{W\}$ and it is called the *group* variable. $s \in S$ is called the *shape* variable. The main idea is to have a control suited description of the team of robots a in terms of the pose g of a virtual structure, which captures the dependence of the team on the world frame $\{W\}$, plus a shape s, which is decoupled from g, and therefore, an

110

intrinsic property of the formation. In other words, if $\bar{g}$ is an arbitrary element of G, we require the map ϕ to satisfy

$$\phi(q) = (g,\ s) \Rightarrow \phi(\bar{g}q) = (\bar{g}g,\ s) \tag{6.6}$$

where $\bar{g}q$ represents the action of the group element $\bar{g}$ on the configuration $q \in Q$ and $\bar{g}g$ represents the left translation of g by $\bar{g}$ using the composition rule on the group G. Since we only approach planar robots in this paper, G is a subset of $SE(2)$. $\bar{g}q$ represents a rigid displacement of all the robots by $\bar{g}$. (6.6) shows that the map ϕ is left invariant, which gives invariance of our to be designed control laws to the pose of the world frame $\{W\}$. Indeed, if the world frame $\{W\}$ is displaced by $\bar{g}$, the shape s is not affected while the pose g is left translated by $\bar{g}$.

Instead of designing high dimensional behaviors X_Q, we want to be able to describe collective behaviors in terms of time-parameterized curves on the lower dimensional abstract manifold A.

Definition 6 (Abstract behavior). *Any vector field $X_A \in TA$ is called an abstract behavior.*

Let $d\phi$ denote the differential (tangent) of the map ϕ. Note that the submersion condition in Definition 5 guarantees the surjectivity of the differential $d\phi$ at any $q \in Q$, which will guarantee the existence of vector fields X_Q pushed forward to any abstract behavior X_A.

The abstraction ϕ gives a decomposition of the space of behaviors on Q into behaviors which can be "seen" in the abstract manifold A and behaviors which cannot be seen in A.

111

Definition 7 (Detectable behaviors). *A behavior* $X_Q \in TQ$ *which is mapped to a non-zero abstract behavior* $X_A \in TA$ *is called a detectable behavior. A behavior which is not detectable is called non-detectable.*

Our goal in this paper is to generate individual control laws which are mapped to desired abstract (collective) behaviors, *i.e.*, wisely chosen low-dimension descriptions. Therefore, we will not allow individual motions which cannot be captured in A, because this would be a waste of energy. However, non-detectable behaviors can be useful to accommodate specifications which are not captured by A.

We are now able to formulate the main problem:

Problem 1 (Control of fully actuated robots). *Determine physically meaningful formation abstractions* ϕ, *abstract behaviors* X_A, *and corresponding individual robot control laws* u_i *satisfying the following requirements:*

(i) *The abstract state* a *is stationary if and only if all the robots* q_i *are stationary.*

(ii) *The abstract manifold* A *has a product structure (6.5) and* ϕ *satisfies the left invariance property (6.6).*

(iii) *The control systems on the group* G *and shape* S *are decoupled.*

(iv) *If the state* a *of the abstract manifold is bounded, then the state of each robot* q_i *is bounded.*

Requirement (i) from Problem 1 guarantees that each individual motion on Q_i can be "seen" in the small dimensional manifold A and, therefore, can be "penalized" by

112

control. This is equivalent to the detectability of the corresponding behavior X_Q. If requirements (ii) and (iii) are satisfied, then one can design control laws for the interest variables on a separately, e.g. change the pose of the formation g while preserving the shape s. Requirement (iv) is self-explanatory.

In addition to the requirements explicitly formulated in Problem 1, it is desired that the energy spent by the individual robots to produce a desired abstract behavior be kept to a minimum. Also, the amount of inter-robot communication in the overall control architecture should be limited.

6.2 Approach

In this section we characterize the solution to Problem 1. First, note that the map φ gives a foliation of the configuration space Q. We assume that the abstract manifold has the desired product structure $A = G \times S$. Let Ω_g be the codistribution spanned by the differential one forms obtained by differentiating each component of ϕ_g. Similarly, Ω_s is the codistribution determined by ϕ_s. Let Δ_g and Δ_s denote the corresponding annihilating distributions, i.e.,

$$\Omega_g(\Delta_g) = 0, \ \Omega_s(\Delta_s) = 0 \tag{6.7}$$

Let $\bar{\Delta}_g$ be any distribution so that $\bar{\Delta}_g + \Delta_y = TQ$ and $\dim\bar{\Delta}_g + \dim\Delta_g = \dim Q$. Similarly, denote by $\bar{\Delta}_s$ any distribution so that $\bar{\Delta}_s + \Delta_s = TQ$ and $\dim\bar{\Delta}_s + \dim\Delta_s = \dim Q$. Then,

$$X_Q \in \bar{\Delta}_g \tag{6.8}$$

113

guarantees that, on the abstract manifold, at $a = (g, s)$, g changes in time whenever q does. Similarly,

$$X_Q \in \bar{\Delta}_s \tag{6.9}$$

corresponds to a change in the shape variable s. The set of detectable behaviors is given by $\bar{\Delta}_g + \bar{\Delta}_s$. Requirement (i) from Problem 1 can therefore be written as:

$$X_Q \in \bar{\Delta}_g + \bar{\Delta}_s \tag{6.10}$$

In other words, system (6.2) is forbidden to move on a leaf $\phi = const.$ (motion which could not be "observed" on the abstract manifold A) if and only if (6.10) is satisfied.

To formulate the decoupling condition between the control of the group G and the shape S of A (item (iii) of Problem 1), we first require that the distributions $\bar{\Delta}_g$ and $\bar{\Delta}_s$ be independent, $i.e.$, $\bar{\Delta}_g \cap \bar{\Delta}_s = 0$, where 0 denotes the zero vector field. Then the decoupling condition is satisfied if the codistribution corresponding to g annihilates the visible motion corresponding to s and the other way around. Explicitly,

$$\Omega_g(\bar{\Delta}_s) = 0, \ \Omega_s(\bar{\Delta}_g) = 0 \tag{6.11}$$

This is easy to see if we differentiate $g = \phi_g(q)$ in coordinates to obtain $\dot{g} = d\phi_g \dot{q}$. If $\dot{q}$ is detectable (satisfies (6.10)), then we can write $\dot{q} = A_g u_g + A_s u_s$, where A_g and A_s are some matrices whose columns span $\bar{\Delta}_g$ and $\bar{\Delta}_s$. u_s does not affect $\dot{q}$ if and only if $d\phi_g A_s = 0$, which, if we go back to the coordinate free representation, means $\Omega_g(\bar{\Delta}_s)$. Similar reasoning can be made for the shape s. u_g and u_s separately control g and s. They will be the actual controls for group and shape, after some convenient rescaling.

114
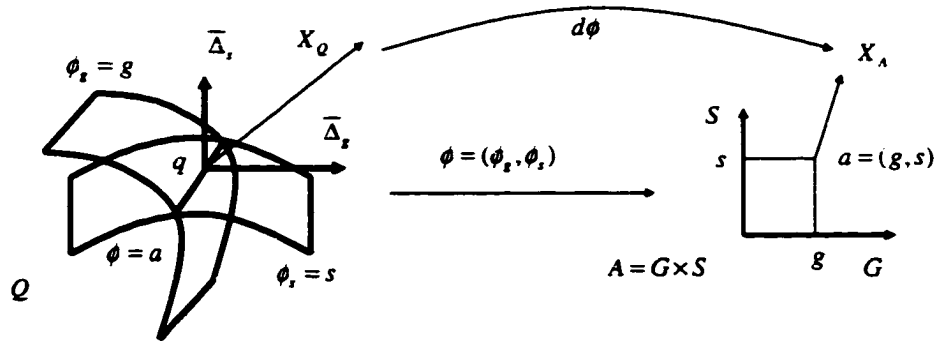
Figure 6.1: The map $\phi = (\phi_g, \phi_s)$ gives a foliation of the configuration space Q. The leaf $\phi(q) = a$ is the intersection of the leaves $\phi_g(q) = g$ and $\phi_s(q) = s$. The set of detectable behaviors at q is $\bar{\Delta}_g + \bar{\Delta}_s$. Decoupled control systems on G and S are obtained if the distributions $\bar{\Delta}_g$ and $\bar{\Delta}_s$ are orthogonal.

For (iv), note that Problem 1 can actually be seen as an input - output linearization problem [45] for the control system (6.2) with output $a = \phi(q)$. The total relative degree is $\dim(Q) - n$ since each robot is kinematically controlled. The vector field X_A guarantees some desired behavior of the output (which we call abstract state) a, which will, of course, guarantee its boundness. Now the hardest problem, as usual in input - output linearization, is calculating and stabilizing the internal dynamics. This would imply, in general, finding the appropriate coordinate transformation separating the internal dynamics from output dynamics, calculating the corresponding zero dynamics and studying its stability. To avoid this, we try to define the output map so that bounds on output would easily imply bounds on the state, so it will not be necessary to explicitly calculate the internal dynamics.

Given a vector field $X_A \in TA$, the set of all vector fields $X_Q \in TQ$ which maps to X_A is underdetermined. For simplicity, let $\dot{q}$ and $\dot{a}$ denote the coordinates of X_Q and X_A,

115

respectively. Then,

$$d\phi\dot{q} = \dot{a} \tag{6.12}$$

The usual way of solving the undetermined linear problem (6.12) is to find the minimum norm vector $\dot{q}$ satisfying it. Assume the metric in Q is described (at each point) by a symmetric positive definite matrix $M \in \mathbb{R}^{2N \times 2N}$. Then the solution to the minimization problem

$$\min_{\dot{q}} \dot{q}^T M \dot{q} \tag{6.13}$$

under the constraint (6.12) is given by

$$\dot{q} = M^{-1}d\phi^T(d\phi M^{-1}d\phi^T)^{-1}\dot{a} \tag{6.14}$$

Note that, since φ is a submersion, $\varphi_1, \ldots, \varphi_n$ are functionally independent, or, equivalently, $d\phi$ is full row rank, which implies that $d\phi M^{-1}d\phi^T$ is invertible. By writing $d\phi^T = (d\phi_g^T, d\phi_s^T)$, $a^T = (g^T, s^T)$, (6.14) becomes

$$\dot{q} = M^{-1}d\phi_g^T(d\phi_q M^{-1}d\phi_g^T)^{-1}\dot{g} + M^{-1}d\phi_s^T(d\phi_s M^{-1}d\phi_s^T)^{-1}\dot{s} \tag{6.15}$$

if

$$d\phi_g M^{-1}d\phi_s^T = 0 \tag{6.16}$$

Note that $\dot{q}$ from (6.15) satisfies the detectability and decoupling conditions formulated in terms of distributions (6.10) and (6.11) if, in coordinates, $\bar{\Delta}_g$ and $\bar{\Delta}_s$ are spanned by $M^{-1}d\phi_g^T$ and $M^{-1}d\phi_s^T$, respectively. Indeed, the linear independence of $d\phi_g$ and $d\phi_s$ implies the independence of $\bar{\Delta}_g$ and $\bar{\Delta}_s$ and (6.11) is implied by (6.16). Moreover, (6.7) implies that $\bar{\Delta}_g$ and Δ_g are orthogonal in metric M. The same is true for $\bar{\Delta}_s$ and Δ_s.

116

The metric M can be anything that makes sense from an application point of view. If no other constraints are imposed, we suggest that the kinetic energy metric (5.13) be used. Even though all the results in this chapter are valid for general choices of kinetic energy metrics, we restrict our attention to $M = I_{2N}$, which can be seen as the kinetic energy for identical robots of mass 1.

Finally, to limit the amount of inter - robot communication in the overall control architecture, we propose *partial state feedback*. Ideally, we want to achieve an architecture where the control law of a robot only depends on its own state and the low dimensional state of the team from the group manifold:

$$u_i = u_i(q_i, a) \tag{6.17}$$

Pictorially, the desired control architecture combining abstraction and partial state feedback features is given in Figure 6.2.

6.3 Abstraction

In this section we define a physically significant abstraction (6.4) and show that it satisfies requirements (iii), (iv), and (vi) from Problem 1. Then we construct individual control laws in accordance with requirements (i) and (ii). Satisfaction of requirement (v) is proved in Section 6.4.

For an arbitrary configuration $q \in Q$, the group part g of the abstract state a is defined

117
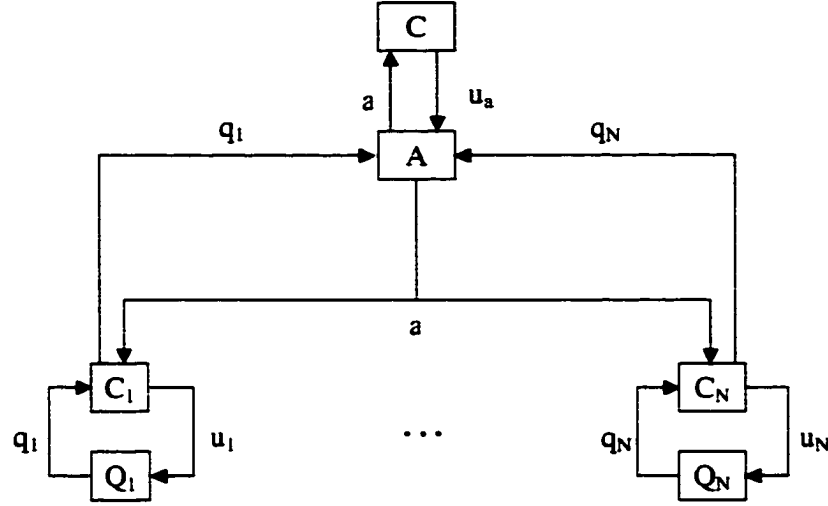
Figure 6.2: A control architecture combining abstraction and partial state feedback features: the formation is controlled on the "abstract", small dimensional formation manifold A; the control law of each robot is only dependent on its own state q_i and the abstract state a.

by $g = (R, \mu) \in G = SE(2)$. Let

$$\mu = \frac{1}{N} \sum_{i=1}^{N} q_i \in \mathbf{R}^2 \qquad (6.18)$$

Define

$$r_i = [x_i, y_i]^T = R^T(q_i - \mu), \quad i = 1, \ldots, N \qquad (6.19)$$

The rotation part $R \in SO(2)$ is defined by the following equation

$$\sum_{i=1}^{N} x_i y_i = 0 \qquad (6.20)$$

In this paper we restrict our attention to a 2 - dimensional shape $s = [s_1, s_2]$ defined by

$$s_1 = \frac{1}{N-1} \sum_{i=1}^{N} x_i^2, \quad s_2 = \frac{1}{N-1} \sum_{i=1}^{N} y_i^2 \qquad (6.21)$$

Since $SO(2)$ is 1-dimensional, the dimension of the abstract manifold A is $n = 5$, independent of the number of robots N. Also it is obvious that our definitions (6.18), (6.20),

118

(6.21) of group and shape are invariant to permutations of robots, as required by Definition 5. The submerssion condition will be studied later in this section.

Before we show that the abstraction ϕ defined above solves Problem 1, we study its physical significance.

6.3.1 Significance

There are two slightly different interpretations of the abstraction defined by (6.18), (6.19), (6.20), and (6.21). Let

$$\Sigma = \frac{1}{N-1} \sum_{i=1}^{N} (q_i - \mu)(q_i - \mu)^T \tag{6.22}$$

and

$$\Gamma = -(N-1)E_3 \Sigma E_3 \tag{6.23}$$

where E_3 is defined by (6.31). Equation (6.23) simply states that Γ is obtained from $(N-1)\Sigma$ by interchanging the diagonal elements and multiplying the extra - diagonal elements by -1. Therefore, Γ and $(N-1)\Sigma$ have the same eigenstructure.

Spanning rectangle

μ and Γ in (6.18) and (6.23) can be seen as the centroid and inertia tensor of the system of particles q_i with respect to the centroid and orientation $\{W\}$. Let $\{M\}$ define a virtual frame with pose $g = (R, \mu)$ in $\{W\}$. Then r_i is the expression of $q_i - \mu$ in the virtual frame $\{M\}$. The rotation equation (6.20) defines the orientation of the virtual frame so that the inertia tensor of the system of points r_i in $\{M\}$ is diagonal. $(N-1)s_1$ and

119

$(N-1)s_2$ are the eigenvalues of the tensor and are therefore measures of the spatial distribution of the robots along the axis of the virtual frame $\{M\}$.

It is interesting to note that the shape variables provide a bound for the region occupied by the robots. From (6.21), it immediately follows that, for any $i = 1, \ldots, N$,

$$|x_i| \leq \sqrt{(N-1)s_1}, \quad |y_i| \leq \sqrt{(N-1)s_2} \tag{6.24}$$

The conclusion can be stated as follows: *An ensemble of N robots described by a 5 - dimensional abstract variable $a = (g, s) = (R, \mu, s_1, s_2)$ is enclosed in a rectangle centered at μ and rotated by $R \in SO(2)$ in the world frame $\{W\}$. The sides of the rectangle are given by $2\sqrt{(N-1)s_1}$ and $2\sqrt{(N-1)s_2}$.*

We call the rectangle described by (R, μ, s_1, s_2) the *spanning rectangle*.

Concentration ellipsoid

μ and Σ given by (6.18) and (6.22) can be interpreted as sample mean and covariance of a random variable with realizations q_i. If the random variable is known to be normally distributed, then, for a sufficiently large N, μ and Σ converge to the real parameters of the normal distribution. R in (6.20) is the rotation that diagonalizes the covariance and s_1, s_2 are the eigenvalues of the covariance matrix. This means that, for a large number of normally distributed robots, μ, R, s_1 and s_2 give the pose and semiaxes of a concentration ellipsoid.

120

Specifically, it is known that contours of constant probability p for normally distributed points in plane with mean μ and covariance Σ are ellipses described by

$$(x - \mu)^T \Sigma^{-1}(x - \mu) = c, \quad c = -2\ln(1 - p) \qquad (6.25)$$

The ellipse in (6.25), called *equipotential* or *concentration ellipse*, has the property that p percent of the points are inside it, and can be therefore used as a spanning region for our robots, under the assumption that they are normally distributed. Therefore we can make the following statement: *p percent of a large number N of normally distributed robots described by a 5 - dimensional abstract variable $a = (g, s) = (R, \mu, s_1, s_2)$ is enclosed in an ellipse centered at μ, rotated by $R \in SO(2)$ in the world frame $\{W\}$ and with semiaxes $\sqrt{cs_1}$ and $\sqrt{cs_2}$, where c is given by (6.25).*

Even though the normal distribution assumption might seem very restrictive, we show in Section 6.3.4 that it is enough that the robots be normally distributed in the initial configuration. Our controls laws will preserve the normal distribution.

Spanning rectangle vs. concentration ellipsoid

The abstraction based on the spanning rectangle as defined in Section 6.3.1 has the advantage that it provides a rigorous bound for the region occupied by the robots and does not rely on any assumption on the distribution of the robots. The main disadvantage is that this estimate becomes too conservative when the number of robots is large. Indeed, the lengths of the sides of the rectangle scale with $\sqrt{N - 1}$, so for a large N the spanning rectangle might become very large, even though the robots might be grouped around the

121

centroid μ.

On the other hand, the size of a concentration ellipsoid as defined in Section 6.3.1 does not scale with the number of robots, which makes this approach very attractive for very large N. However, it has the disadvantage of assuming a normally distributed initial configuration of the team and does not provide a rigorous bound for the region occupied by the robots. Roughly speaking, $(1 - p)N$ are left out of the p-ellipse. Increasing p will decrease the number of the robots which be outside but will also increase the size of the ellipsoid.

To have an idea of what is a "large" number N for which the second approach is more feasible, note that the spanning rectangle and the rectangle in which the concentration ellipsoid is inscribed are similar and the ratio is $\sqrt{(N-1)/c}$. The ratio of their areas is therefore $(N-1)/c$ For example, if $p = 0.99$, we have $c = 9.2103$, and the spanning rectangle becomes larger for $N \geq 11$. If $N = 100$, the area of the spanning rectangle is 10.7488 larger than the area of the rectangle circumscribing the ellipse, and only one robot might be left out of the ellipse.

6.3.2 Left invariance

In this section we show that that requirement (iii) of Problem 1 is satisfied. We have:

Proposition 13. *The abstraction ϕ defined by (6.18),(6.20), and (6.21) satisfies the left invariance property (6.6).*

Proof: It is easy to see that R, s_1, and s_2 are defined by

$$\text{diag}(s_1, s_2) = \frac{1}{N-1} \sum_{i=1}^{N} r_i r_i^T = R^T \Sigma R \tag{6.26}$$

To prove the left invariance property (6.6), let $\bar{g} = (\bar{R}, \bar{d}) \in SE(2)$ denote a displacement of the world frame $\{W\} \to \{W'\}$. Then, in the new world frame $\{W'\}$, the positions of the robots are given by $q_i' = \bar{R}q_i + \bar{d}$. The new formation variables are primed. It is easy to see that

$$\mu' = \bar{R}\mu + \bar{d} \tag{6.27}$$

and $r_i' = R'^T \bar{R}(q_i - \mu)$. Also

$$\text{diag}(\rho_1', \rho_2') = \frac{1}{N} \sum_{i=1}^{N} r_i' r_i'^T = R'^T \bar{R} \Sigma \bar{R}^T R' \tag{6.28}$$

From (6.27) and (6.28) it follows that

$$\rho_1' = \rho_1, \ \rho_2' = \rho_2 \tag{6.29}$$

each of the pairs being the spectrum of Σ which is invariant to orthogonal transformations. Moreover, R and $\bar{R}^T R'$ are both orthogonal matrices diagonalizing Σ. We conclude that

$$R' = \bar{R}R \tag{6.30}$$

Collecting (6.27) and (6.30), we get $g' = \bar{g}g$, which, together with (6.29), proves the claim

$\square$

123

6.3.3 Detectable behaviors and decoupling of group and shape

In this section, under the assumption that the configuration space Q is equipped with an Euclidean metric, we construct detectable behaviors and decoupled control systems for group and shape, in accordance with requirements (i) and (iv) from Problem 1.

To this end, we need to bring our definitions of formation variables (6.18), (6.20), (6.21) to more convenient forms. Let

$$E_1 = \begin{bmatrix} 0 & 1 \\ 1 & 0 \end{bmatrix}, \quad E_2 = \begin{bmatrix} 1 & 0 \\ 0 & -1 \end{bmatrix},$$

$$E_3 = \begin{bmatrix} 0 & -1 \\ 1 & 0 \end{bmatrix}$$

(6.31)

and

$$H_1 = I_2 + R^2 E_2, \quad H_2 = I_2 - R^2 E_2,$$

$$H_3 = R^2 E_1$$

(6.32)

where I_2 is the 2×2 identity matrix. Using a parameterization

$R = [\cos(\theta) \ -\sin(\theta); \sin(\theta) \ \cos(\theta)]$, it is easy to see that the matrices H_i are symmetric and

$$H_1^2 = 2H_1, \quad H_2^2 = 2H_2, \quad H_3^2 = I_2$$

(6.33)

$$H_1 H_2 = 0, \quad H_1 H_3 = H_3 - E_3,$$

$$H_2 H_3 = H_3 + E_3$$

(6.34)

Then, some simple calculations and the observation that E_3 is skew-symmetric show that equation (6.20) defining the rotational part becomes

$$\sum_{i=1}^{N} (q_i - \mu)^T H_3 (q_i - \mu) = 0$$

(6.35)

124

while the description of the shape (6.21) takes the form

$$s_1 = \frac{1}{2(N-1)} \sum_{i=1}^{N} (q_i - \mu)^T H_1 (q_i - \mu),$$

$$s_2 = \frac{1}{2(N-1)} \sum_{i=1}^{N} (q_i - \mu)^T H_2 (q_i - \mu) \tag{6.36}$$

Let the rotation $R \in SO(2)$ be parameterized by θ. If the amount of rotation is restricted to $\theta \in (-\pi/2, \pi/2)$, a unique solution of equation (6.35) is given by

$$\theta = \frac{1}{2} \text{atan2} \left(\sum_{i=1}^{N} (q_i - \mu)^T E_1 (q_i - \mu), \right.$$

$$\left. \sum_{i=1}^{N} (q_i - \mu)^T E_2 (q_i - \mu) \right) \tag{6.37}$$

We now characterize the set of detectable behaviors (6.10) for the map ϕ given by equations (6.18), (6.37), (6.36) together with definitions (6.31) and (6.32).

First note that

$$dH_1 = 2H_3 d\theta, \quad dH_2 = -2H_3 d\theta \tag{6.38}$$

Using (6.18), (6.38), (6.35), it follows that

$$ds_1 = \frac{1}{N-1} \sum_{i=1}^{N} (q_i - \mu)^T H_1 dq_i \tag{6.39}$$

and

$$ds_2 = \frac{1}{N-1} \sum_{i=1}^{N} (q_i - \mu)^T H_2 dq_i \tag{6.40}$$

By differentiating (6.35) and using (6.18), (6.36), we have

$$d\theta = \frac{1}{(N-1)(s_1 - s_2)} \sum_{i=1}^{N} (q_i - \mu)^T H_3 dq_i \tag{6.41}$$

Then, the codistributions Ω_g and Ω_s as defined in Section (6.2) are given by

$$\Omega_g = \text{span}\{d\mu, d\theta\}, \quad \Omega_\rho = \text{span}\{ds_1, ds_2\} \tag{6.42}$$

125

and the control distributions corresponding to group $\bar{\Delta}_g$ and shape $\bar{\Delta}_s$ by

$$\bar{\Delta}_g = \text{span}\{X_q^\mu, X_q^\theta\} \tag{6.43}$$

and

$$\bar{\Delta}_s = \text{span}\{X_q^{s_1}, X_q^{s_2}\} \tag{6.44}$$

where

$$X_q^\mu = \begin{bmatrix} I_2 \\ \vdots \\ I_2 \end{bmatrix}, \; X_q^\theta = \begin{bmatrix} H_3(q_1 - \mu) \\ \vdots \\ H_3(q_N - \mu) \end{bmatrix} \tag{6.45}$$

and

$$X_q^{s_1} = \begin{bmatrix} H_1(q_1 - \mu) \\ \vdots \\ H_1(q_N - \mu) \end{bmatrix}, \; X_q^{s_2} = \begin{bmatrix} H_2(q_1 - \mu) \\ \vdots \\ H_2(q_N - \mu) \end{bmatrix} \tag{6.46}$$

I_2 is the identity matrix.

Therefore, in accordance with (6.10), requirement (i) of Problem 1 is satisfied if we restrict the behaviors to the set $\bar{\Delta}_g + \bar{\Delta}_s$ given by (6.43), (6.44), (6.45), and (6.46).

We now show that the control distributions $\bar{\Delta}_g$ and $\bar{\Delta}_s$ are orthogonal, so decoupled control systems can be designed for group and shape, in accordance with requirement (iii) of Problem 1. Indeed, the two columns of X_q^μ are obviously orthogonal. It is easy to see that X_q^θ, $X_q^{s_1}$ and $X_q^{s_2}$ are orthogonal to X_q^μ by the definition of μ (6.18). Since $H_1 H_2 = 0$, $X_q^{s_1}$ and $X_q^{s_2}$ are also perpendicular. Finally, X_q^θ is orthogonal to both $X_q^{s_1}$ and $X_q^{s_2}$ by (6.34), (6.35), and by noting that E_3 is a skew symmetric matrix. We conclude that the two control distributions $\bar{\Delta}_g$ and $\bar{\Delta}_s$ are orthogonal so requirement (iii) of Problem 1) is

126

verified. Moreover since orthogonal control directions are chosen as basis for $\bar{\Delta}_g$ and $\bar{\Delta}_s$, each of the formation variables can be individually controlled.

6.3.4 The individual control laws

The differential map $d\phi_q : T_qQ \to T_a\mathcal{A}$ is given by:

$$
d\phi = \frac{1}{N-1} \begin{bmatrix} \frac{N-1}{N} I_2 & \cdots & \frac{N-1}{N} I_2 \\ \frac{1}{s_1-s_2}(q_1 - \mu)^T H_3 & \cdots & \frac{1}{s_1-s_2}(q_N - \mu)^T H_3 \\ (q_1 - \mu)^T H_1 & \cdots & (q_N - \mu)^T H_1 \\ (q_1 - \mu)^T H_2 & \cdots & (q_N - \mu)^T H_2 \end{bmatrix} \tag{6.47}
$$

The minimum norm vector $\dot{q}$ on TQ which is mapped to a vector field $\dot{a}$ in $T\mathcal{A}$ is given by $\dot{q} = d\phi^T(d\phi d\phi^T)^{-1}\dot{a}$. Some simple calculations show that

$$
\dot{q} = X_q^\mu \dot{\mu} + \frac{s_1 - s_2}{s_1 + s_2} \dot{\theta} X_q^\theta + \frac{\dot{s}_1}{4s_1} X_q^{s_1} + \frac{\dot{s}_2}{4s_2} X_q^{s_2} \tag{6.48}
$$

Note that the controls $\dot{\mu}$, $\dot{\theta}$, $\dot{s}_1$, $\dot{s}_2$ act on orthogonal directions so one can explicitly control each of the formation variables without affecting the others.

We define the individual controls as projections $d\pi_i$ of the minimum norm vector (6.48):

$$
\begin{aligned}
u_i = \dot{q}_i &= \dot{\mu} + \frac{s_1-s_2}{s_1+s_2} H_3(q_i - \mu)\dot{\theta} \\
&+ \frac{1}{4s_1} H_1(q_i - \mu)\dot{s}_1 + \frac{1}{4s_2} H_2(q_i - \mu)\dot{s}_2
\end{aligned} \tag{6.49}
$$

Remark 16. *Note that the overall control architecture implementing (6.49) fits the structure in Figure 6.2. Each robot i needs to implement controller C_i, which is only dependent*

127

on its own state q_i and the small dimensional abstract state a. Also, each robot has to send its own state to the abstract control system, which calculates and then broadcasts the updated abstract state. Therefore, robot i only has to broadcast its 2-dimensional state q_i and listen to a the 5-dimensional abstract state a, independent on the number of robots N.

Remark 17. *$d\phi d\phi^T$ is invertible if and only if $s_1 \neq 0$ and $s_2 \neq 0$, which is also equivalent to the submersion condition in Definition 5. Also, the control law (6.49) is not defined at $s_1 = 0$ and $s_2 = 0$. The abstract behavior on A should be designed so that $s_1 > 0$ and $s_2 > 0$, for all t. A simple inspection of (6.21) shows that the cases $s_1 = 0$ and $s_2 = 0$ physically correspond to degenerate situations when all the robots are on the Oy and Ox axis of the formation frame $\{M\}$, respectively.*

Remark 18. *If $s_1 = s_2$, the derivative of the orientation θ is not defined, as seen from (6.41). Indeed, in this case, the robots are equally distributed along the axes of the formation frame, and there is no orientation information. When orientation is not important for a certain application, a simpler abstraction might be defined as in Section 6.5*

Remark 19. *Note that if control law (6.49) is applied to all the robots, then the team undergoes an affine transformation. Indeed, the orbits of the affine group $GA(2)$ in Q are described by $q_i = d + Aq_i^0$, $d \in \mathbf{R}^2$, $A \in GL(2)$, which, by differentiation, gives $\dot{q}_i = \dot{d} + \dot{A}A^{-1}(q_i - d)$, which is the same as (6.49) with $\mu = d$ and $\dot{A}A^{-1} = (s_1 - s_2)/(s_1 + s_2)H_3\dot{\theta} + 1/(4s_1)H_1\dot{s}_1 + 1/(4s_2)H_2\dot{s}_2$. Any affine transformation is known to preserve collinearity, ratios of distances on lines, and parallelism. Therefore, control law*

128

(6.49) can be used for formations in which preserving properties like the ones mentioned above is important. Even more interesting, it is known that affine transformations preserve the normal distribution. This means that if the robots are initially normally distributed, by applying the control laws (6.49), they remain normally distributed. The 5 - dimensional abstract state, interpreted as sample mean μ and sample covariance Σ, gives us control over the pose, aspect ratio and size of the concentration ellipsoid as defined in Section 6.3.1.

Remark 20. *All the results derived in this chapter remain valid if the Euclidean metric $M = I_{2N}$ is replaced by a general kinetic energy metric (5.13) and the abstract variables are obviously redefined as:*

$$\mu = \frac{\sum_{i=1}^{N} m_i q_i}{m}, \tag{6.50}$$

$$s_1 = \frac{1}{2m} \sum_{i=1}^{N} m_i (q_i - \mu)^T H_1 (q_i - \mu), \tag{6.51}$$

$$s_2 = \frac{1}{2m} \sum_{i=1}^{N} m_i (q_i - \mu)^T H_2 (q_i - \mu), \tag{6.52}$$

$$\theta = \frac{1}{2} \text{atan2} \left(\sum_{i=1}^{N} m_i (q_i - \mu)^T E_1 (q_i - \mu), \right. \tag{6.53}$$

$$\left. \sum_{i=1}^{N} m_i (q_i - \mu)^T E_2 (q_i - \mu) \right) \tag{6.54}$$

where $m = \sum_{i=1}^{N} m_i$ is the total mass of the system of robots. The control law (6.49) remains unchanged.

129

6.4 Abstract behavior

Equation (6.49) gives the control law which should be implemented by controller C_i as shown in Figure 6.2 if the output function ϕ is defined as in Section 6.3. At each time instant t, the control system on A acquires all the states q_i, updates its own state a in accordance to (6.18), (6.37), (6.36), (6.31), and (6.32), flows along its designed control vector field $\dot{a}$ and disseminates its state a to all the robots.

Assume the goal is to move the robots from arbitrary initial positions $q_i(0)$ to final rest positions of desired mean μ^d, orientation θ^d, and shape s_1^d, s_2^d.

An obvious choice of the control vector field $\dot{a} = [\dot{\mu}, \dot{\theta}, \dot{s}_1, \dot{s}_2]$ on the abstract manifold A is

$$\dot{\mu} = K_\mu(\mu^d - \mu)$$

$$\dot{\theta} = k_\theta(\theta^d - \theta)$$

$$\dot{s}_1 = k_{s_1}(s_1^d - s_1)$$
(6.55)

$$\dot{s}_2 = k_{s_2}(s_2^d - s_2)$$

where $K_\mu \in \mathbf{R}^{2\times2}$ is a positive definite matrix and $k_\theta, k_{s_{1,2}} > 0$.

More generally, the task might require the robots to follow a desired trajectory $a^d(t) = [\mu^d(t), \theta^d(t), s_1^d(t), s_2^d(t)]$ on A. A control vector field on F can be of the form:

$$\dot{\mu} = K_\mu(\mu^d(t) - \mu(t)) + \dot{\mu}^d(t)$$

$$\dot{\theta} = k_\theta(\theta^d(t) - \theta(t)) + \dot{\theta}^d(t)$$

$$\dot{s}_1 = k_{s_1}(s_1^d(t) - s_1(t)) + \dot{s}_1{}^d(t)$$
(6.56)

$$\dot{s}_2 = k_{s_2}(s_2^d(t) - s_2(t)) + \dot{s}_2{}^d(t)$$

130

Note that (6.55) (or (6.56)) only guarantees the desired behavior on the abstract manifold A. If the imposed trajectory $a^d(t)$ is bounded at all times, it is easy to see that $a(t)$ is bounded. For the problem to be well defined, we still need to make sure that the internal states are bounded (requirement (v) of Problem 1). We have:

Proposition 14. *If a is bounded, then so are q_i, $i = 1, \ldots, N$.*

Proof: It is enough to assume boundedness of μ, s_1, and s_2 to prove boundedness of q_i. Assume

$$\| \mu - \mu^d \| \leq M_\mu, \tag{6.57}$$

$$|s_1 - s_1^d| \leq M_{s_1}, \tag{6.58}$$

$$|s_2 - s_2^d| \leq M_{s_2} \tag{6.59}$$

First note that from (6.36) it follows that

$$s_1 + s_2 = \frac{1}{N-1} \sum_{i=1}^{N} (q_i - \mu)^T (q_i - \mu) \tag{6.60}$$

from which, by using (6.58) and (6.59), we have

$$\| q_i - \mu \| \leq \sqrt{N(s_1 + s_2)} \leq$$

$$\sqrt{(N-1)(M_{s_1} + M_{s_2} + s_1^d + s_2^d)}, \quad i = 1, \ldots, N$$

Finally, using (6.57), we have

$$\| q_i - \mu^d \| = \| q_i - \mu + \mu - \mu^d \| \leq \| q_i - \mu \| + \| \mu - \mu^d \|$$

$$\leq \sqrt{(N-1)(M_{s_1} + M_{s_2} + s_1^d + s_2^d)} + M_\mu$$

which concludes the proof.

131

In the stabilization to a point case, the boundness and globally asymptotic convergence to the desired values of the abstract variables are guaranteed by (6.55). Proposition 14 proves the boundness of the internal dynamics. We still need to study the equilibria and regions of convergence for each robot. We have the following Proposition:

Proposition 15. *For any μ^d, θ^d, s_1^d, s_2^d, the closed loop system (6.49), (6.55),(6.18), (6.37), (6.36) globally asymptotically converges to the equilibrium manifold $\mu = \mu^d$, $\theta = \theta^d$, $s_1 = s_1^d$, $s_2 = s_2^d$.*

Proof: First, from (6.49), (6.18), (6.41), (6.39) and (6.40) it is easy to see that the abstract state is in equilibrium ($\dot{a} = 0$) if and only if each robot is in equilibrium ($\dot{q}_i = 0$, $i = 1, \ldots, N$). Therefore, the equilibria of the closed loop system are sets described by $\mu = \mu^d$, $\theta = \theta^d$, $s_1 = s_1^d$, $s_2 = s_2^d$.

For the second part, consider the following Lyapunov function defined on Q:

$$V(q) = \tfrac{1}{2}\|\mu^d - \mu\|^2 + \tfrac{1}{2}(\theta^d - \theta)^2$$
$$+\tfrac{1}{2}(s_1^d - s_1)^2 + \tfrac{1}{2}(s_2^d - s_2)^2 \tag{6.61}$$

and consider the derivative of V along the vector field on Q:

$$\dot{V}(q) = -K_\mu\|\mu^d - \mu\|^2 - k_\theta(\theta^d - \theta)^2$$
$$-k_{s_1}(s_1^d - s_1)^2 - k_{s_2}(s_2^d - s_2)^2 \tag{6.62}$$

Therefore, $\dot{V}(q) \leq 0$, $\forall q \in \mathbf{R}^{2N}$ and $\dot{V} = 0$ if and only if $\mu = \mu^d$, $\theta = \theta^d$, $s_1 = s_1^d$, and $s_2 = s_2^d$, which is also an invariant set for the closed loop system. According to the

132

Global Invariant Set Theorem (LaSalle), to prove the proposition we only have to prove that $V(q) \to \infty$ as $\|q\| \to \infty$. We prove this by contradiction. Suppose $\|q\| \to \infty$ and there exists some $L > 0$ so that $V(q) < L$. This implies

$$\|\mu - \mu^d\| \leq \sqrt{2L}, \quad |s_1 - s_1^d| \leq \sqrt{2L}, \quad |s_2 - s_2^d| \leq \sqrt{2L}$$

By an argument similar to the one used in the proof of Proposition 14, we can conclude that

$$\|q_i - \mu^d\| \leq \sqrt{(N-1)(s_1^d + s_2^d + 2\sqrt{2L})} + \sqrt{2L},$$

which means that all q_i are bounded, $i = 1, \ldots, N$. But $\|q\| \to \infty$ implies that, for at least one $i = 1, \ldots, N$, $\|q_i\| \to \infty$. Therefore, we reached a contradiction and the theorem is proved.

□

6.5 Contractions and expansions

When orientation is not relevant for a certain application, we can define a simpler 3 - dimensional abstraction as follows. The group g is restricted to the position of the centroid μ. Let $s = s_1 + s_2$ be the new shape variable. Since $H_1 + H_2 = 2I_2$, we have

$$s = \frac{1}{N-1} \sum_{i=1}^{N} (q_i - \mu)^T (q_i - \mu), \tag{6.63}$$

For the new abstraction (μ, s), it is easy to see that the left invariance property (6.6) is satisfied. Concerning the bound of the region occupied by the robots, note that (6.63)

133

implies

$$\|q_i - \mu\| \leq \sqrt{(N-1)s} \tag{6.64}$$

from which we conclude that the N robots described by a 3 - dimensional abstract variable $a = (\mu, s)$ are enclosed in a circle centered at μ and with radius $\sqrt{(N-1)s}$. The new control directions become

$$X_q^\mu = \begin{bmatrix} I_2 \\ \vdots \\ I_2 \end{bmatrix}, \; X_q^s = \begin{bmatrix} (q_1 - \mu) \\ \vdots \\ (q_N - \mu) \end{bmatrix} \tag{6.65}$$

The decoupling is obvious by the definition of μ. Concerning the internal dynamics, it is easy to check, following the proof of Proposition 14, that q_i is bounded if $a = (\mu, s)$ is bounded. The individual control laws (6.49) become:

$$\dot{q}_i = u_i = \dot{\mu} + \frac{q_i - \mu}{2s} \dot{s}, \; i = 1, \ldots, N \tag{6.66}$$

It is interesting to note that control laws (6.66) preserve the shape and orientation of the structure formed by the position vectors q_i in the given inertial frame. Indeed, let $l_{ij} = \|q_i - q_j\|$, $i \neq j$. Using $l_{ij}^2 = (q_i - q_j)^T (q_i - q_j)$, it is easy to see by integration that

$$l_{ij}(t) = l_{ij}(0) \sqrt{\frac{s(t)}{s(0)}}, \; \forall t > 0$$

and therefore

$$\frac{l_{ij}(t)}{l_{kl}(t)} = \frac{l_{ij}(0)}{l_{kl}(0)}, \; \forall i, j, k, l = 1, \ldots, N, \; \forall t > 0$$

from which we conclude that the geometric shape is preserved and the scale factor is

134

proportional to $\sqrt{s(t)}$. Also, straightforward calculations show that

$$\frac{d}{dt}\left(\frac{q_i - q_j}{\|q_i - q_j\|}\right) = 0, \; i \neq j$$

proving that the orientation of the structure is also preserved during the motion.

Remark 21. *In this case, the abstraction is reduced to the position of the centroid and the scale factor of a geometric figure of given shape and orientation determined by the initial positions of the robots.*

6.6 Simulation results

This section presents simulations illustrating the theoretical results proved in this paper. First, we show how a team of robots can be driven through a tunnel by designing controls on a 5 - dimensional space. For a very large number of initially normally distributed robots, we control a equiprobability ellipsoid. For tens of robots, we control the spanning rectangle. Finally, an expansion example is included.

6.6.1 Tunnel passing

Consider the task of driving a team of robots from arbitrary initial positions through a tunnel of given geometry, and spread out at the end of tunnel. Independent of the number of robots, the problem can be reduced to a 5 - dimensional control problem using one of the abstractions proposed in this paper. If the number of robots is of the order of tens, the spanning rectangle as defined in Section 6.3.1 can be used. For hundreds and thousands

135

of robots, the spanning rectangle becomes too conservative. In this case, if it is allowed to lose a very small percentage of them and if their initial distribution is assumed normal, we propose the control of a concentration ellipsoid, as described in Section 6.3.1.

In both cases, we divide the task into three subtasks:

(1) Gather the robots in front of the tunnel in such a shape that they can pass through it.

(2) Drive the robots through the tunnel.

(3) Spread out at the end of the tunnel.

Control using the concentration ellipsoid

Assume $N = 100$ and it is desired that "almost all" of the robots accomplish the task. Assuming that the robots are normally distributed in the initial configuration, they remain normally distributed by applying the control laws (6.49), according to **Remark 19**. If 99 percent is an acceptable quantization of "almost all", according to Section 6.3.1, the problem can be reduced to a 5-dimensional control problem for a concentration ellipsoid of probability $p = 0.99$.

For the subtask of regrouping in front of the tunnel (1), we use the globally stabilizing controllers (6.49), (6.55). Considering the geometry, position, and orientation of the tunnel, we chose $\mu^d = [3\ 23]$, $\theta^d = 0$, $s_1^d = 10.8574$, $s_2^d = 0.3518$. The chosen shape corresponds to semiaxes of $\sqrt{cs_1^d} = 10$ and $\sqrt{cs_2^d} = 1.8$ along x and y, respectively. The abstract controller parameters were $K_\mu = 2I_2$, $k_\theta = 2$, $k_{s_1} = k_{s_2} = 2$. Note that in

136

this first subtask both shape and pose are controlled. Four snapshots from the produced motion are shown in the first row of Figure (6.3).

Since the ellipse from step (1) is small enough and oriented to fit the tunnel, no shape and orientation control is necessary to accomplish subtask (2). We use trajectory following controllers of type (6.56) on A to move the ellipse through the tunnel. If we want to uniformly move the ellipse at $[50\ 23]$ in 1 second while keeping shape and orientation constant, we only have to control μ_x, therefore $\dot{\mu}_y = \dot{\theta} = \dot{s}_1 = \dot{s}_2 = 0$. We use $\mu_x^d(t) = (1-t)3 + t50$ (therefore $\dot{\mu}_x^d(t) = 47$). The second row of Figure (6.3) shows four instants of the generated trajectories. As expected, shape and orientation is preserved, therefore illustrating the control decoupling proved in Section 6.3.3.

For the third subtask, we illustrate control of shape decoupled from pose, which is maintained constant. We again use the globally stabilizing controllers (6.49), (6.55) with $\dot{\mu} = 0$, $\dot{\theta} = 0$, $s_1^d = s_2^d = 20$, $k_{s_1} = k_{s_2} = 2$. The obtained expansion is shown in the last row of Figure (6.3).

Control using the spanning rectangle

If it is now required that all the robots accomplish the task, we need to use the spanning rectangle as an abstraction. The advantage is that no assumption is being made on the initial distribution of the robots. On the other hand, as stated in Section 6.3.1, the spanning rectangle becomes too conservative an estimation of the region occupied by the robots, as the number of robots increases.

137

Figure 6.3: 99 of $N = 100$ normally distributed planar robots are driven through a tunnel by designing 5 - dimensional controls for the corresponding equiprobability ellipse. First row: the robots gather in front of the tunnel inside an ellipse whose shape and orientation allows passing through the tunnel. Second row: the robots pass through the tunnel, the shape and orientation of the ellipse are kept constant. Third row: the robots spread out by keeping the pose of the ellipse fixed and changing the shape.

We consider $N = 10$. The control procedure follows exactly the one described in 6.6.1. The control parameters are also the same. The only exception is that, for the first subtask, we used $s_1^d = 11.1111$ and $s_2^d = 0.36$, which correspond to a spanning rectangle of sides $2\sqrt{(N-1)s_1^d} = 20$ and $\sqrt{(N-1)s_2^d} = 3.6$, which is thin enough to fit through the tunnel. The simulation results are shown in Figure 6.4.

6.6.2 Expansions

Consider $N = 30$ robots, distributed on three concentric circles. We apply the geometric shape preserving control laws (6.66) to illustrate contractions and expansions. We use global convergence to a point for the abstract state $a = (\mu, s)$. Figure 6.5 shows a pure expansion obtained with $\mu = 0$ and $\dot{s} = k_s(s^d - s)$ with $k_s = 2$ and $s^d = 400$.

138
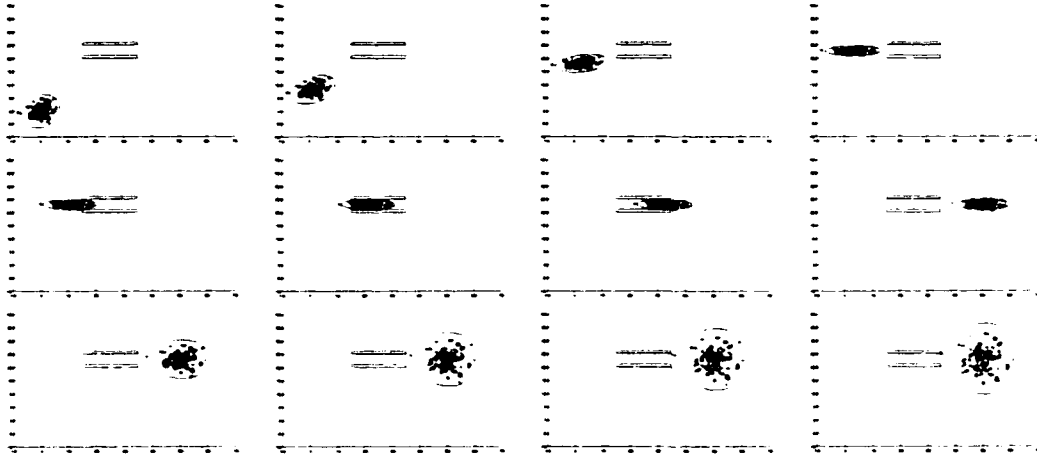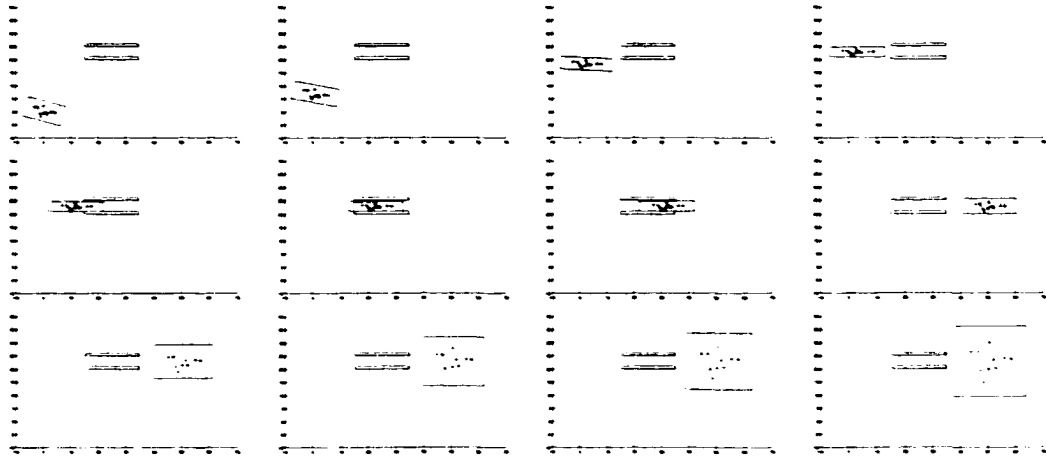
Figure 6.4: $N = 10$ planar robots are driven through a tunnel by designing 5 - dimensional controls for the corresponding spanning rectangle. First row: the robots gather in front of the tunnel inside a rectangle whose sides and orientation allow passing through the tunnel. Second row: the robots pass through the tunnel, the sides and orientation of the rectangle are kept constant. Third row: the robots spread out by keeping the pose of the rectangle fixed and increasing the lengths of the sides.

6.7 Discussion

In this paper we propose a control method for a large number of robots based on an abstraction of the team to a small dimensional manifold invariant to permutations of the robots and whose dimension does not scale with the number of robots. The task to be accomplished by the team suggests a natural feedback control system on the formation manifold. We focus on planar fully actuated robots and show that it is possible to provide the abstract manifold with a product structure of a *group* and a *shape*. We also prove that completely decoupled control systems can be designed for group and shape. The individual control laws which are mapped to the desired behavior of the formation can be realized by feedback depending only on the robots' current state and the small dimensional state

139
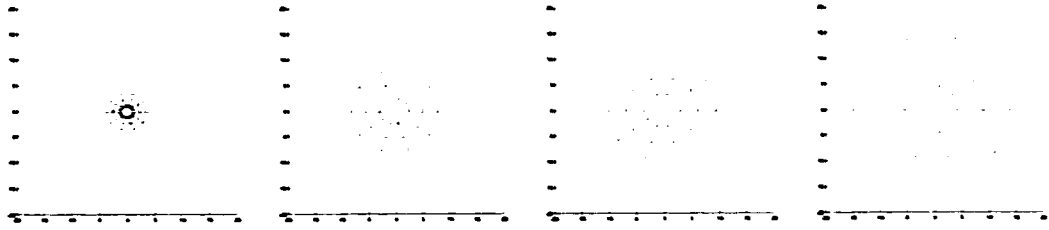
Figure 6.5: $N = 30$ robots experiencing an expansion using control laws (6.66). The centroid is kept fixed. Orientation, paraleliem, angles, and ratios of lengths are preserved.

on the formation manifold.

140

Chapter 7

Control of a team of car-like robots

using abstractions

In this chapter, we show how the abstraction method developed in Chapter 6 can be applied to control a team of car-like robots. The robots are modeled as under-actuated kinematic drift - free control systems. We define outputs as Cartesian coordinates of some reference points on the robots, which are used in the formulation of the collective tasks, *i.e.,*, in a cooperative mission, the robots are represented by their reference points. Using input - output feedback linearization for each robot, the controls are related to the velocities of the output (reference points) through a linear nonsingular map. We then use the abstraction defined in Chapter 6 to map the set of all reference points to a lower dimensional *abstraction manifold*. Controls are designed for the small dimensional abstraction manifold in accordance to the cooperative task to be accomplished. They correspond to

141
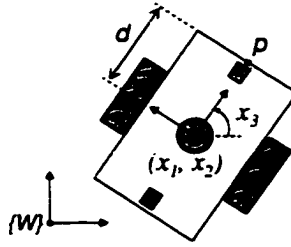
Figure 7.1: Kinematic model of a car-like robot

certain velocities of the reference points, which are then translated back to controls for the under-actuated robots.

This chapter is organized as follows. In Section 7.1, we formulate the problem and introduce the notation. The control laws to be applied to each robot so that the team has a desired cooperative behavior specified in terms of the chosen reference points are given in Section 7.2. We describe our experimental platform in Section 7.3, the results of the experiments in Section 7.4, and final remarks in 7.5.

7.1 Problem formulation

Consider N identical car - like planar robots. as the one shown in Figure 7.1. In the world frame $\{W\}$, robot i is described by a 3 - dimensional state vector $x^i = [x_1^i, x_2^i, x_3^i]^T$, $i = 1, \ldots N$, where (x_1^i, x_2^i) give the Cartesian coordinates of the robot center and x_3^i measures the orientation of the robot frame in $\{W\}$ (see Figure 7.1). Each robot is modeled as a kinematic, drift free control system

$$\dot{x}^i = G(x^i)u^i = g_1(x^i)u_1^i + g_2(x^i)u_2^i \tag{7.1}$$

142

where the control vector fields are given by

$$g_1(x) = \begin{bmatrix} \cos x_3 \\ \sin x_3 \\ 0 \end{bmatrix}, \quad g_2(x) = \begin{bmatrix} 0 \\ 0 \\ 1 \end{bmatrix} \tag{7.2}$$

for $x = [x_1, x_2, x_3]^T$. The control $u^i = (u_1^i, u_2^i)$ consists of driving and steering speeds. On each robot we pick a reference point P_i different from the robot center. The Cartesian coordinates $q^i = (q_1^i, q_2^i)$ of the reference points P_i is $\{W\}$ are used to formulate cooperative tasks. In other words, for each robot i, $i = 1, \ldots, N$, we define an output map

$$q^i = h(x^i) \tag{7.3}$$

where h is given by

$$h(x) = \begin{bmatrix} x_1 + d \cos x_3 \\ x_2 + d \sin x_3 \end{bmatrix} \tag{7.4}$$

Problem 2 (Control of car-like robots). *Design control laws* u^i, $i = 1, \ldots, N$ *so that the team of N car - like robots accomplishes a cooperative task formulated in terms of the chosen reference points q^i.*

As in Chapter 6, examples of tasks include stabilization inside a given region of the space, tunnel passing, expansions and contractions, etc.

143

7.2 Robot control laws

Note that the choice of the output function h together with the linearity of dynamics (7.1) in u^i leads to a linear nonsingular relationship between the derivative of the output $\dot{q}^i$ and the control variables $\dot{q}^i = dh(x^i)G(x^i)u^i$, unless $d = 0$. dh denotes the differential of h. Therefore, we can define new inputs

$$\dot{q}^i = v^i \tag{7.5}$$

which are related to the original ones by

$$u^i = A(x^i)v^i \tag{7.6}$$

where

$$A(x) = (dh(x)G(x))^{-1} = \begin{bmatrix} \cos x_3 & \sin x_3 \\ -\frac{\sin x_3}{d} & \frac{\cos x_3}{d} \end{bmatrix} \tag{7.7}$$

Equations (7.1), (7.3), (7.5) and (7.6) represent an input output feedback linearization problem [45]. The next natural step would be to set $v^i = \dot{q}^{id} + k(q^{id} - q^i)$, $k > 0$ so that q^i exponentially tracks a given desired trajectory $q^{id}(t)$. Alternatively, in the next section we show how the redefined inputs v^i can be designed so that the robots described by the reference points q^i, $i = 1, \dots, N$ have a desired collective behavior, using the abstraction procedure developed in Chapter 6.

Collect all the robot outputs q^i and redefined inputs v^i together into a $2N$-dimensional control system

$$\dot{q} = v, \ q \in Q, \ v \in V \tag{7.8}$$

144

where

$$Q = \{q| = (q^1, \ldots, q^N) \in \mathbb{R}^{2N}\}$$
$$V = \{v| = (v^1, \ldots, v^N) \in \mathbb{R}^{2N}\}$$

(7.9)

and allow to recover the individual states and controls by using the canonical projection

$$\pi_i(q) = q^i, \ \pi_i(v) = v^i, \ i = 1, \ldots, N$$

(7.10)

Given a large number of robots represented by the Cartesian coordinates q_i of the chosen reference points P_i, or, equivalently, a $q \in Q$, we want to solve motion generation / control problems on a smaller dimensional space, which captures the essential features of the group, according to the class of tasks to be accomplished. For this, we use the abstraction map $\phi : Q \rightarrow A$ defined in Chapter 6 to formulate an input - output linearization problem for the system described by (7.8) and (6.4). Let the new inputs be denoted by $w \in \mathbb{R}^n$, where n is the dimension of the abstraction manifold A. Then

$$\dot{a} = w$$

(7.11)

and, since $w = d\phi(q)v$, we have

$$v = d\phi^T (d\phi d\phi^T)^{-1} w$$

(7.12)

Everything else follows exactly the same lines as the abstraction defined in Chapter 6. For convenience, we give below all the equations necessary to implement the individual controllers.

Given the position of the reference points q_i, $i = 1, \ldots, N$, the abstract state can be

145

calculated as $a = (g, s)$, where the group part $g = (\mu, \theta)$ is given by

$$\mu = \frac{1}{N} \sum_{i=1}^{N} q_i$$

$$\theta = \frac{1}{2} \text{atan2} \left(\sum_{i=1}^{N} (q_i - \mu)^T E_1 (q_i - \mu), \sum_{i=1}^{N} (q_i - \mu)^T E_2 (q_i - \mu) \right)$$

(7.13)

and the shape is described by

$$s_1 = \frac{1}{2(N-1)} \sum_{i=1}^{N} (q_i - \mu)^T H_1 (q_i - \mu),$$

$$s_2 = \frac{1}{2(N-1)} \sum_{i=1}^{N} (q_i - \mu)^T H_2 (q_i - \mu)$$

(7.14)

where

$$E_1 = \begin{bmatrix} 0 & 1 \\ 1 & 0 \end{bmatrix}, \quad E_2 = \begin{bmatrix} 1 & 0 \\ 0 & -1 \end{bmatrix}, \quad E_3 = \begin{bmatrix} 0 & -1 \\ 1 & 0 \end{bmatrix}$$

(7.15)

and

$$H_1 = I_2 + R^2 E_2, \quad H_2 = I_2 - R^2 E_2, \quad H_3 = R^2 E_1$$

(7.16)

The abstract variables are controlled by stabilization at a point

$$\dot{\mu} = w_\mu = K_\mu (\mu^d - \mu), \quad \dot{\theta} = w_\theta = k_\theta (\theta^d - \theta)$$

$$\dot{s}_1 = w_{s_1} = k_{s_1} (s_1^d - s_1), \quad \dot{s}_2 = w_{s_2} = k_{s_2} (s_2^d - s_2)$$

(7.17)

or by trajectory tracking

$$\dot{\mu} = w_\mu = K_\mu (\mu^d(t) - \mu(t)) + \dot{\mu}^d(t)$$

$$\dot{\theta} = w_\theta = k_\theta (\theta^d(t) - \theta(t)) + \dot{\theta}^d(t)$$

$$\dot{s}_1 = w_{s_1} = k_{s_1} (s_1^d(t) - s_1(t)) + \dot{s}_1^d(t)$$

$$\dot{s}_2 = w_{s_2} = k_{s_2} (s_2^d(t) - s_2(t)) + \dot{s}_2^d(t)$$

(7.18)

where $K_\mu \in \mathbf{R}^{2 \times 2}$ is a positive definite matrix and k_θ, $k_{s_{1,2}} > 0$. Finally, using (7.6),

146
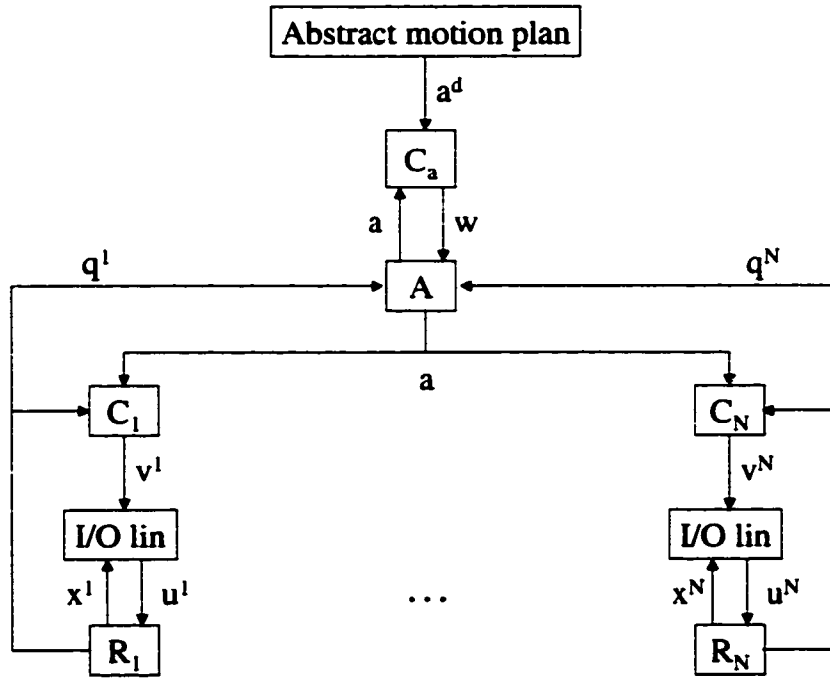
Figure 7.2: Overall control architecture

individual control laws are generated for each robot in the form

$$u^i = A(x^i)\left(w_\mu + \frac{s_1 - s_2}{s_1 + s_2}H_3(q_i - \mu)w_\theta + \frac{1}{4s_1}H_1(q_i - \mu)w_{s_1} + \frac{1}{4s_2}H_2(q_i - \mu)w_{s_2}\right)$$

(7.19)

where $A(x)$ is given by (7.7).

The overall control architecture is given in Figure 7.2.

On the stability of the internal dynamics, we proved in Chapter 6 that the boundness of $a \in A$ together with the definition of ϕ easily imply the boundness of each of q^i, $i = 1, \ldots, N$ The remaining 1 - dimensional internal dynamics of each robot can also be proved to be bounded [28] if each q_i is bounded.

147

7.3 Experimental platform

Our experiments were performed using a team of five car-like robots (see Figure 7.3 (a)). The Clodbuster platform is based upon a 1/10 scale radio controlled model of a monster truck, made by Tamiya Inc. We made significant modifications to the vehicle, to incorporate - an omni-directional camera, additional on-board power, and an improved suspension. The robot has a servo controller on board for steering and a digital proportional speed controller for forward/backward motion. Each robot is equipped with an ultra-portable laptop (PIII 850 Mhz processor, 256MB RAM, built in wireless connectivity, Windows XP operating system). As sensors, they have twelve infra-red position sensitive detectors (PSDs) with three in each corner and a IEEE 1394 firewire based digital camera (manufactured by Point Grey Research) with the Netvision 360 omidirectional lens assembly from Remote Reality Inc. The camera provides a 360 degree angular field of view (see Figure 7.3 (b)). There exists a simple geometric mapping from the image plane to the ground plane or any other plane of interest due to the special parabolic shape of the reflecting surface.

Communication among robots is needed to estimate the individual orientations x_3^i and relies on IEEE 802.11b networking. A calibrated overhead camera is used to localize the Cartesian coordinates of the reference points q^i. A centralized computer calculates the 5 - dimensional team variable $a = (\mu, \theta, s_1, s_2)$ and broadcasts it back to the robots together with q^i from the overhead camera. Each robot has then complete information on its state x^i and the state a and can compute its own control u^i. All this computation is executed

<div align="center">(a)   (b)</div>

Figure 7.3: (a) A team of five GRASP Lab robots (Clodbusters) and (b) a sample image from an omnidirectional camera.

in approximately $15\,Hz$ in the slowest computer. Note that the actual communication architecture that we use in the experiments does not exactly fit the one we claim in Figure 6.2 because in our indoor setup the robots are not able to determine their own position and orientation.

7.4 Experimental results

7.4.1 Group control

In the first experiment we show how the pose of the team can be controlled while shape is preserved, illustrating the decoupling property of controllers (7.6), (6.49). The robots are initially "almost" aligned with the Oy axes of the world frame: $\mu = (2.2020, 1.6817)$, $\theta = -1.499\,rad$, $s_1 = 0.5417$, $s_2 = 1.6798e - 4$. We use controllers (6.55) with $K_\mu = 4I_2$, $k_\theta = 4$, $k_{s_1} = k_{s_2} = 0$ to stabilize the team at $\mu^d = (2.2, 3.7)$, $\theta^d = 0$. The shape, according to our theoretical results, should be preserved. The results are shown in Figure

<div align="center">149</div>
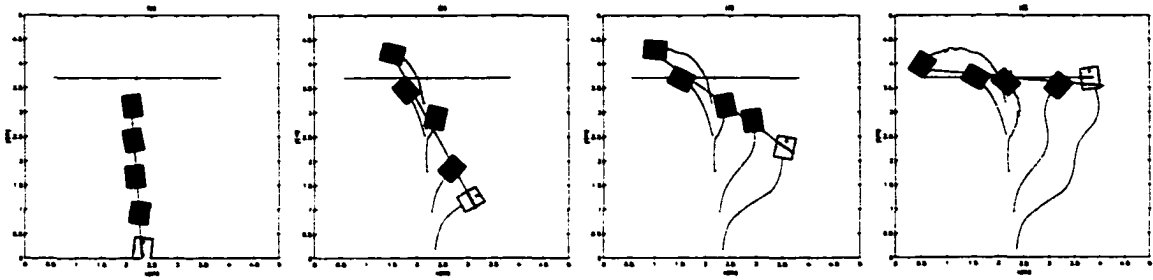
Figure 7.4: The position and orientation of the team is stabilized at desired values while shape is preserved.

Figure 7.5: Sequence of four snapshots in an expansion maneuver - illustrates control of shape while pose in preserved.

7.4.

7.4.2 Shape control

The second experiment illustrates an expansion maneuver. Instead of plotting the experimental data, as in Section 7.4.1, we show four snapshots from the actual experiment in Figure 7.5. The robots were initially grouped in a small circle $s_1 = s_2 = 0.0738$ around $\mu = (2.4607, 2.6185)$. We again used stabilizing controllers (6.55) but this time with $K_\mu = 0$, $k_\theta = 0$, $k_{s_1} = k_{s_2} = 4$ to stabilize the team at $s_1^d = s_2^d = 0.6078$. The pose of the team, as predicted by our theoretical results, was preserved.

150

7.5 Discussion

We used the abstraction method developed in Chapter 6 to control a team of under-actuated car-like robots. First, using a well-known technique, reference points are chosen on the robots so that their velocities are related to the individual controls through linear nonsingular maps. The reference points are used in the formulation of the cooperative tasks. Second, the abstraction defined in Chapter 6 is used to map the reference points to a lower dimensional manifold. Controls are designed for the small dimensional manifold in accordance to the cooperative task to be accomplished. They project to certain velocities of the reference points, which are then translated to controls for the under-actuated robots. We used our Clodbuster robots to illustrate how group and shape can be separately controlled.

151

Chapter 8

Concluding remarks

Multi-agent planning and control gained a lot of interest from the robotics community in the past few years. Applications range from highway workers protection to deep space exploration and laser interferometry. The goal of this work is to provide a better understanding of this problem and to propose a set of mathematical tools which might be useful in developing planning and control algorithms.

8.1 Contributions

As outlined at the beginning of the thesis, our contributions are on three different but related directions.

An efficient method for interpolation on $SE(3)$ The first part of the thesis develops a new method to generate smooth interpolating curves on $SE(3)$. This work was published

152

in [3, 4, 7, 12, 10, 8]. The starting point is [25, 57, 91, 90]. The approach is geometric and the resulting trajectories are invariant with respect to the choice of reference frames and independent of the parameterization of the manifold. It is first shown how a physically significant left or right invariant metric on $SO(n)$ $(SE(n))$ is inherited from the ambient manifold $GL^+(n)$ $(GA^+(n))$ equipped with the appropriate metric. The bi-ivariant metric on $SO(n)$ [26] and the left invariant metric proposed by Park and Brockett [63] are special cases of this general treatment. Next, a projection operator that projects points and curves from the ambient manifold onto $SO(n)$ $(SE(n))$ is defined. The uniqueness and smoothness of the projected trajectory are discussed. Several examples are presented to illustrate how curves generated in the ambient manifold can be projected to get near optimal results on $SO(n)$ and $SE(n)$, especially when the excursion of the trajectories is "small". In certain cases, we are also able to establish quantitative results that measure the closeness of the generated trajectory to the optimal trajectory [4]. The idea of the projection is not completely new [52, 72]. The novelty of this approach mainly relies on invariance of the produced trajectories, the way of defining and inheriting physically significant metrics, and the increased efficiency of the algorithms.

Optimal motion plans for rigid formations The second part of the thesis develops a method of optimal motion planning for groups of robots moving in formation [6, 15, 5, 11, 9]. First, the rigidity of a formation is mathematically formalized by identifying, in the tangent bundle of the configuration space, distributions corresponding to infinitesimal rigid and non-rigid motions. The total kinetic energy is then decomposed into the energy

153

of the motion of a rigid structure and the energy corresponding to motions that violate the rigidity constraint. The corresponding metric is "shaped" by assigning different weights to each contribution. This idea of a "decomposition" and a subsequent "modification" is related to the methodology of controlled Lagrangians described in [20, 87]. When rigidity is required, it is shown how individual motion plans can be constructed so that the overall energy of the formation is minimized. When the rigidity constraint is relaxed. a continuum of trajectories, varying from greedy to cooperative strategies, can be constructed by varying one parameter.

Abstractions for large groups of robots The third part of the thesis proposes a control method for large groups of robots based on the definition of a map from the configuration space of the robots to a lower dimensional abstract manifold, whose dimension does not scale with the number of robots. This work was published in [13, 17, 19, 18, 14, 16]. The task to be accomplished by the team suggests a natural feedback control system on the small dimensional manifold. In this paper we focus on planar fully actuated robots and require the abstract manifold to have a product structure of a Lie *group*, which captures the dependence of the ensemble on the chosen world coordinate frame, and a *shape manifold*, which is an intrinsic description of the team. We design decoupled controls for group and shape. We also show that the individual control laws which are mapped to the desired behavior of the formation can be realized by feedback depending only on the current state of the robot and the state on the formation manifold, so that the robots have to broadcast their states and only have to listen to some coordinating agent with small bandwidth.

154

8.2 Future work

We plan to focus our future work on planning and control for large groups of inexpensive robots using abstractions (output maps) resembling the one defined in Chapter 6.

One first step towards extending the results in this thesis is to consider *more shape variables*. So far, we only considered a two dimensional shape space (6.21) describing the spatial distribution of the robots along the axis of a frame with pose $g \in G$. This was enough to define a bound for the spanning region of the robots, which is essential to approach applications like tunnel passing, obstacle avoidance, etc. If more shape information is necessary, the space S can be easily extended using higher central moments. For example, if the distribution is not normal, then the third moment, called *skewness*, can be used as a measure of how far the distribution is from being symmetric. The fourth central moment, called *kurtosis*, describes the degree of flatness of the distribution curve. Physically this could be used as a measure of the coverage by the robots of the area of the equiprobability ellipse. Indeed, a negative fourth moment (flat distribution) would give a more uniform coverage than a positive one (peaked distribution). This shape variable might be critical in applications where the robots are sensors deployed to uniformly cover a certain area. On the other hand, the calculation of higher moments would increase the complexity of the control algorithm and therefore reduce its robustness.

Another direction of future research is to use non-detectable behaviors (see Definition 7) to accommodate specifications which cannot be captured by the abstract variable. For example, an abstract behavior X_A could specify the time - evolution of the pose (group

155

part g) and semi-axes (shape part s) of an ellipsoid with the guarantee that all the robots are inside it. The behavior X_Q could be the sum of the detectable behavior which produces the desired X_A plus a non-detectable part (not affecting the abstract behavior) which could accomplish the specification that the area inside the ellipsoid is uniformly occupied by the robots.

We are also interested in defining abstractions which can easily accommodate under-actuated robots. Mathematically, the formulation in (6.1), (6.2) and (6.3) can be easily extended to accommodate under-actuated robots, with states q_i belonging to manifolds Q_i equipped with drift free control distributions $\Delta_i : Q_i \times U_i \to TQ_i$ where U_i is the control space and TQ_i is the tangent bundle of Q_i. Then, a similar large control system incorporating all the individual under-actuation constraints can be obtained by collecting all robot states $Q = \prod_{i=1}^{N} Q_i$ and defining a control distribution Δ obtained from the individual control distributions through direct sum $\Delta = \bigoplus_{i=1}^{N} \Delta_i$. The canonical projections are defined by $\pi_i : Q \to Q_i$, $\pi_i(q) = q_i$ and $d\pi_i : TQ \to TQ_i$, $d\pi_i(\Delta) = \Delta_i$. An abstract behavior should incorporate the under-actuation constraints. They naturally arise on A by pushing forward the allowed control directions in Δ through ϕ.

Investigating different types of communication architectures is another possible direction for future research. The one studied in this work falls into the category of *Asymmetric Broadcast Channels (ABC)*, which consists of a supervisor or a leader that broadcasts partial state information about the group, while the individual agents can upload their state information to the supervisor. This up-link can also be implemented by equipping the

156

supervisor with an appropriate sensor (for example, a supervisor UAV with cameras can observe a swarm of UGVs). The ABC architecture is borrowed from models of wireless communication, satellite networks, and users of the world wide web (individual agents require limited upload capability compared to the download volume). In the future, we want to investigate a second architecture, called *Nearest Neighbor Communication Channels (NNCC)*, which allows each agent to communicate only with its neighbors. This is motivated by architectures in parallel computing and MEMS arrays where the interconnections between nodes require this constraint. In multi-agent robot systems, this can be easily implemented without communication by allowing each agent to measure its state and the states of a set of neighbors within a certain neighborhood. For the particular case of abstraction map that we considered in this work, simulations show that if our control laws are applied on circular neighborhoods, and the abstract variables for each neighborhood are controlled so that they converge to the same desired values, then the whole team converges to a configuration described by the same desired abstract values.

Future work will be also be directed towards extending the results to 3-D environments and implementing the obtained control architectures in our blimp - car outdoor experimental platform.

157

Appendix A

Proof of Proposition 12

The SVD decomposition of $M(t) = I + (R_2 - I)f(t) = U(t)\Sigma(t)V(t)^T$ is needed,

where $R_2 = e^{\hat{\omega}_0}$ and $f(t)$ is a continuous function defined on $[0, 1]$ satisfying $f(0) = 0$,

$f(1) = 1$. The first observation is

$$M^T(t)M(t) = I - f(t)(1 - f(t))N, \quad N = 2I - R_2 - R_2^T$$

The eigenstructure of the constant and symmetric matrix N completely determines the

SVD of $M(t)$. Because N is symmetric and real, its eigenvalues will be real and the

corresponding eigenspaces orthogonal. Let λ_i, v_i be an eigenvalue-eigenvector pair of N.

Then,

$$Nv_i = \lambda_i v_i \Rightarrow M^T(t)M(t) = (1 - f(t)(1 - f(t))\lambda_i)v_i$$

So, theoretically, the desired SVD decomposition is determined at this moment:

- The matrix $V(t)$ can be chosen constant of the form $V = [v_1 \ v_2 \ v_3]$ where v_1, v_2, v_3

  are orthonormal eigenvectors of N;

158

- The singular values are given by $s_i^2(t) = 1 - f(t)(1 - f(t))\lambda_i$ (it will be shown shortly that the right hand side of this equality is always positive)

- The time-dependence of the projection will be contained in

$$U(t) = [u_1(t) \ u_2(t) \ u_3(t)], \quad u_i(t) = \frac{M(t)v_i}{s_i}, \quad i = 1, 2, 3$$

Using the Rodrigues formula for $R_2 = e^{\hat{\omega}_0}$, it is easy to see that

$$N = -\frac{1 - \cos \|\omega_0\|}{\|\omega_0\|^2}(\hat{\omega}_0^2 + \hat{\omega}_0^{2T})$$

from which it follows that the eigenvalues of N are given by

$$\lambda(N) = \{0, 2(1 - \cos \|\omega_0\|), 2(1 - \cos \|\omega_0\|)\}$$

and a set of three orthonormal eigenvectors by

$$\left\{ \frac{\omega_0}{\|\omega_0\|}, \ \frac{1}{\sqrt{\omega_3^2 + \omega_1^2}} \begin{bmatrix} -\omega_3 \\ 0 \\ \omega_1 \end{bmatrix}, \ \frac{1}{\sqrt{\omega_2^2\omega_1^2 + (\omega_3^2 + \omega_1^2)^2 + \omega_3^2\omega_2^2}} \begin{bmatrix} -\omega_2\omega_1 \\ \omega_3^2 + \omega_1^2 \\ -\omega_3\omega_2 \end{bmatrix} \right\}$$

where $\omega_0 = [\omega_1 \ \omega_2 \ \omega_3]^T$. With the eigenstructure of N determined, one can write

$$\Sigma(t) = diag\{1, s(t), s(t)\}, \quad s(t) = \sqrt{2(1 - \cos \|\omega_0\|)f^2(t) - 2(1 - \cos \|\omega_0\|)f(t) + 1}$$

(A.1)

where the binomial under the square root is always positive because it is positive at zero and $1 - \cos \|\omega_0\| \in (0, 2)$ gives a negative discriminant. Some straightforward but rather tedious calculation leads to:

$$U(t)V^T = I + \frac{\hat{\omega}_0}{\|\omega_0\|}\gamma_2(t) + (1 - \gamma_1(t)) + \frac{\hat{\omega}_0^2}{\|\omega_0\|^2}$$

159

where

$$\gamma_1(t) = \frac{1 - f(t) + f(t)\cos\|\omega_0\|}{s(t)}, \quad \gamma_2(t) = \frac{f(t)\sin\|\omega_0\|}{s(t)}$$

The discussion is restricted to $\|\omega_0\| \in (0, \pi)$ (in accordance to the exponential coordinates) which will give $\gamma_2(t) > 0$. Note that $\gamma_1^2(t) + \gamma_2^2(t) = 1$, so it is appropriate to define a function $\theta(t) \in (0, 1)$ so that

$$\gamma_1(t) = \cos(\|\omega_0\|\theta(t)), \quad \gamma_2(t) = \sin(\|\omega_0\|\theta(t))$$

By use of the Rodrigues formula again,

$$U(t)V^T = e^{\hat{\omega}_0\theta(t)}$$

so the projected line is the exponential mapping of a segment between the origin and ω_0 in exponential coordinates. The parameterization of the segment is given by

$$\theta(t) = \frac{1}{\|\omega_0\|}\text{atan2}(1 - f(t) + f(t)\cos\|\omega_0\|, f(t)\sin\|\omega_0\|)$$

160

Bibliography

[1] T. Balch and R. Arkin. Behavior-based formation control for multi-robotic teams. *IEEE Transactions on Robotics and Automation*, 14(6):926–934, 1998.

[2] R. W. Beard and F. Y. Hadaegh. Constellation templates: an approach to autonomous formation flying. In *World Automation Congress*, Anchorage, Alaska, 1998.

[3] C. Belta and V. Kumar. An efficient geometric approach to rigid body motion interpolation. In *Proceedings of ASME 2000 Design Engineering Technical Conferences*, Baltimore, MD, 2000.

[4] C. Belta and V. Kumar. New metrics for rigid body motion interpolation. In *Ball 2000 Symposium Commemorating the Legacy, Works, and Life of Sir Robert Stawell Ball*, University of Cambridge, UK, 2000.

[5] C. Belta and V. Kumar. Designing trajectories for formations of fully actuated robots. In *5th SIAM Conference on Control and its Applications*, San Diego, CA, 2001.

161

[6] C. Belta and V. Kumar. Motion generation for formations of robots: a geometric approach. In *IEEE International Conference on Robotics and Automation*, Seoul, Korea, 2001.

[7] C. Belta and V. Kumar. On the computation of rigid body motion. In *2nd Workshop on Computational Kinematics*, Seoul, Korea, 2001.

[8] C. Belta and V. Kumar. Euclidean metrics for motion generation on $se(3)$. *Journal of Mechanical Engineering Science Part C*, 216(C1):47–61, 2002.

[9] C. Belta and V. Kumar. Motion generation for groups of robots: a centralized, geometric approach. In *ASME DETC*, Montreal, Canada, 2002.

[10] C. Belta and V. Kumar. On the computation of rigid body motion. *Electronic Journal of Computational Kinematics*, 1(1), 2002.

[11] C. Belta and V. Kumar. Optimal motion generation for groups of robots: a geometric approach. *Journal of Mechanical Design*, 2002. accepted for publication.

[12] C. Belta and V. Kumar. An svd-based projection method for interpolation on se(3). *IEEE Trans. on Robotics and Automation*, 18(3):334–345, June 2002.

[13] C. Belta and V. Kumar. Towards abstraction and control for large groups of robots. In *2nd International Workshop on Control Problems in Robotics and Automation*, Las Vegas, NV, 2002.

162

[14] C. Belta and V. Kumar. Towards abstraction and control for large groups of robots. In *Control Problems in Robotics*, Springer Tracts in Advanced Robotics, pages 169–182. Springer-Verlag, Berlin, 2002.

[15] C. Belta and V. Kumar. Trajectory design for formations of robots by kinetic energy shaping. In *IEEE International Conference on Robotics and Automation*, Washington, DC, 2002.

[16] C. Belta and V. Kumar. Abstraction and control for groups of fully-actuated planar robots. *IEEE Trans. on Robotics and Automation*, 2003. under review.

[17] C. Belta and V. Kumar. Abstraction and control for groups of fully-actuated planer robots. In *IEEE International Conference on Robotics and Automation*, Taipei, Taiwan, 2003. accepted.

[18] C. Belta. G. Pereira, and V. Kumar. Abstractions and control for swarms of robots. In *11th International Symposium of Robotics Research*, Siena, Italy, 2003. under review.

[19] C. Belta, G. Pereira, and V. Kumar. Control of a team of car-like robots using abstractions. In *42nd IEEE Conference on Decision and Control*, Maui, Hawaii, 2003. under review.

[20] A. Bloch, N. Leonard, and J. Marsden. Controlled lagrangians and the stabilization of mechanical systems i: the first matching theorem. *IEEE Transactions on Automatic Control*, 45(12), 2000.

163

[21] C. M. Breder. Equations descriptive of fish schools and other animal aggregations. *Ecology*, 35(3):361–370, 1954.

[22] F. Bullo and R. Murray. Proportional derivative (pd) control on the Euclidean group. In *1995 European Control Conference*, Rome, Italy, 1995.

[23] W. Burgard, M. Moors, D. Fox, R. Simmons, and S. Thrun. Collaborative multi-robot exploration. In *Proc. IEEE Int. Conf. Robot. Automat.*, pages 476–481, San Francisco, CA, April 2000.

[24] R. Burridge, A. Rizzi, and D. Koditschek. Sequential composition of dynamically dexterous robot behaviors. *Int. J. Robot. Research*, 18(6):534–555, June 1999.

[25] M. Camarinha, F. S. Leite, and P. Crouch. Splines of class c^k on non-Euclidean spaces. *IMA J. Math. Control Inform.*, 12(4):399–410, 1995.

[26] J. Cheeger and D. G. Ebin. *Comparison Theorems in Riemannian Geometry*. North-Holland Publishing Company, Amsterdam, 1975.

[27] P. Crouch and F. S. Leite. The dynamic interpolation problem: on Riemannian manifolds, Lie groups, and symmetric spaces. *J. Dynam. Control Systems*, 1(2):177–202, 1995.

[28] J. Desai, J. P. Ostrowski, and V. Kumar. Controlling formations of multiple mobile robots. In *Proc. IEEE Int. Conf. Robot. Automat.*, pages 2864–2869, Leuven, Belgium, May 1998.

[29] M. P. do Carmo. *Riemannian geometry*. Birkhauser, Boston, 1992.

[30] M. Egerstedt and X. Hu. Formation constrained multi-agent control. In *IEEE Conference on Robotics and Automation*, Seoul, Korea, May 2001.

[31] T. Eren, P. N. Belhumeur, and A. S. Morse. Closing ranks in vehicle formations based rigidity. In *IEEE Conference on Decision and Control*, Las Vegas, NV, December 2002.

[32] T. Eren, P. N. Belhumeur, and B. D. O. A. A. S. Morse. A framework for maintaining formations based on rigidity. In *IFAC World Congress*, Barcelona, Spain, July 2002.

[33] G. E. Farin. *Curves and surfaces for computer aided geometric design : a practical guide*. Academic Press, Boston, 3 edition, 1992.

[34] J. Feddema and D. Schoenwald. Decentralized control of cooperative robotic vehicles. In *Proc. SPIE Vol. 4364, Aerosense*, Orlando, Florida, April 2001.

[35] J. Gallier. *Curves and Surfaces in Geometric Modeling - Theory and Algorithms*. Morgan Kaufmann Publishers, San Francisco, CA, 2000.

[36] V. Gazi and K. M. Passino. Stability analysis of swarms. preprint, 2001.

[37] Q. J. Ge and B. Ravani. Computer aided geometric design of motion interpolants. *ASME Journal of Mechanical Design*, 116:756–762, 1994.

[38] Q. J. Ge and B. Ravani. Geometric construction of Bezier motions. *ASME Journal of Mechanical Design*, 116:749–755, 1994.

[39] F. Gentili and F. Martinelli. Robot group formations: a dynamic programming approach for a shortest path computation. In *Proc. of the IEEE Int. Conference on Robotics and Automation*, San Francisco, CA, 2000.

[40] G. H. Golub and C. F. van Loan. *Matrix computations*. The Johns Hopkins University Press, Baltimore, 1989.

[41] U. Helmke and J. B. Moore. *Optimization and dynamical systems*. Springer, Heidelberg, 1994.

[42] R. A. Horn and C. R. Johnson. *Matrix Analysis*. Cambridge University Press, 1985.

[43] J. Hoschek and D. Lasser. *Fundamentals of Computer Aided Geometric Design*. AK Peters, 1993.

[44] L. Iochhi, K. Konolige, and M. Bayracharya. A framework and architecture for multi-robot coordination. In *Proc. Seventh Int. Symposium on Experimental Robotics (ISER)*, Honolulu, Hawaii, Dec. 2000.

[45] A. Isidori. *Nonlinear Control Systems*. Springer-Verlag, London, 3rd edition, 1995.

[46] B. Jütler. Visualization of moving objects using dual quaternion curves. *Computers and graphics*, 18(3):315–326, 1994.

[47] A. Jadbabaie, J. Lin, and A. S. Morse. Coordination of groups of mobile autonomous agents using nearest neighbor rules. In *41st IEEE Conference on Decision and Control*, Las Vegas, NV, 2002. invited.

166

[48] J. S. Jennings, G. Whelan, and W. F. Evans. Cooperative search and rescue with a team of mobile robots. *Proc. IEEE Int. Conf. on Advanced Robotics*, 1997.

[49] B. Juttler and M. Wagner. Computer aided design with rational b-spline motions. *ASME J. of Mechanical Design*, 118(2):193–201, 1996.

[50] N. E. Leonard and E. Fiorelli. Virtual leaders, artificial potentials, and coordinated control of groups. In *40th IEEE Conference on Decision and Control*, pages 2968 – 2973, Orlando, FL, December 2001.

[51] D. Marthaler. Collective motion algorithms for determining environmental boundaries. SIAM Conference on Applications of Dynamical Systems, 2003.

[52] A. Marthinsen. Interpolation in lie groups and homogeneous spaces. *SIAM J. Numer. Anal.*, 37(1):269–285, 1999.

[53] M. Mataric, M. Nilsson, and K. Simsarian. Cooperative multi-robot box pushing. In *IEEE/RSJ International Conf. on Intelligent Robots and Systems*, pages 556–561, Pittsburgh, PA, Aug 1995.

[54] C. R. McInnes. Autonomous ring formation for a planar constellation of satellites. *AIAA Journal of Guidance Control and Dynamics*, 18(5):1215–1217, 1995.

[55] M. Mesbahi and F. Hadaegh. Formation flying of multiple spacecraft via graphs, matrix inequalities, and switching. *AIAA Journal of Guidance, Control and Dynamics*, 24(2):369–377, March 2001.

167

[56] R. M. Murray, Z. Li, and S. S. Sastry. *A Mathematical Introduction to Robotic Manipulation*. CRC Press, 1994.

[57] L. Noakes, G. Heinzinger, and B. Paden. Cubic splines on curved spaces. *IMA J. of Math. Control & Information*, 6:465–473, 1989.

[58] P. Ogren, M. Egerstedt, and X. Hu. A control lyapunov function approach to multi-agent coordination. In *IEEE Conference on Decision and Control*, Orlando, FL, 2001.

[59] P. Ogren, E. Fiorelli, and N. E. Leonard. Formations with a mission: stable coordination of vehicle group maneuvers. In *Proc. Symp. on Mathematical Theory of Networks and Systems*, Notre Dame, IN, August 2002.

[60] R. Olfati-Saber and R. M. Murray. Distributed cooperative control of multiple vehicle formations using structural potential functions. In *IFAC World Congress*, Barcelona, Spain, July 2002.

[61] R. Olfati-Saber and R. M. Murray. Distributed structural stabilization and tracking for formations of dynamic agents. In *IEEE Conference on Decision and Control*, Las Vegas, NV, December 2002.

[62] R. Olfati-Saber and R. M. Murray. Graph rigidity and distributed formation stabilization of multi-vehicle systems. In *IEEE Conference on Decision and Control*, Las Vegas, NV, December 2002.

168

[63] F. C. Park and R. W. Brockett. Kinematic dexterity of robotic mechanisms. *International Journal of Robotics Research*, 13(1):1–15, 1994.

[64] F. C. Park and I. G. Kang. Cubic interpolation on the rotation group using Cayley parameters. In *Proceedings of the ASME 24th Biennial Mechanisms Conference*, Irvine, CA, 1996.

[65] F. C. Park and B. Ravani. Bezier curves on Riemannian manifolds and Lie groups with kinematics applications. *ASME Journal of Mechanical Design*, 117(1):36–40, 1995.

[66] W. H. Press, S. A. Teukolsky, W. T. Vetterling, and B. P. Flannery. *Numerical Recipes in C.* Cambridge University Press, Cambridge, 1988.

[67] J. H. Reif and H. Wang. Social potential fields: a distributed behavioral control for autonomous robots. *Robotics and Autonomous Systems*, 27:171–194, 1999.

[68] C. Reynolds. Flocks, birds, and schools: a distributed behavioral model. *Computer Graphics*, 21:25–34, 1987.

[69] B. Roth. Rigid and flexible frameworks. *American Mathematical Monthly*, 88:6–21, 1981.

[70] D. Rus, B. Donald, and J. Jennings. Moving furniture with teams of autonomous robots. In *IEEE/RSJ International Conf. on Intelligent Robots and Systems*, pages 235–242, Pittsburgh, PA, Aug 1995.

169

[71] K. Shoemake. Animating rotation with quaternion curves. *ACM Siggraph*, 19(3):245–254, 1985.

[72] K. Shoemake and T. Duff. Matrix animation and polar decomposition. In *Proc. of Graphics Interface '92*, May 1992.

[73] T. R. Smith, H. Hanssmann, and N. E. Leonard. Orientation control of multiple underwater vehicles. In *40th IEEE Conference on Decision and Control*, pages 4598–4603, Orlando, FL, December 2001.

[74] L. Srinivasan and Q. J. Ge. Fine tuning of rational b-spline motions. *ASME Journal of Mechanical Design*, 120(1):46–51, 1998.

[75] D. Stilwell and J. Bay. Toward the development of a material transport system using swarms of ant-like robots. In *IEEE International Conf. on Robotics and Automation*, pages 766–771, Atlanta, GA, May 1993.

[76] T. Sugar and V. Kumar. Control and coordination of multiple mobile robots in manipulation and material handling tasks. In P. Corke and J. Trevelyan, editors, *Experimental Robotics VI: Lecture Notes in Control and Information Sciences*, volume 250, pages 15–24. Springer-Verlag, 2000.

[77] K. Sugihara and I. Suzuki. Distributed motion coordination of multiple mobile robots. In *5th IEEE International Symposium on Intelligent Control*, pages 138–143, Philadelphia, PA, 1990.

170

[78] I. Suzuki and M. Yamashita. Distributed anonymous mobile robots: formation of geometric patterns. *SIAM Journal on Computing*, 28(4):1347–1363, 1999.

[79] D. Swaroop and J. K. Hedrick. String stability of interconnected systems. *IEEE Transactions on Automatic Control*, 41(3):349–357, March 1996.

[80] P. Tabuada, G. J. Pappas, and P. Lima. Feasible formations of multi-agent systems. In *American Control Conference*, Arlington, VA, June 2001.

[81] K. Tan and M. A. Lewis. Virtual structures for high-precision cooperative mobile robot control. *Autonomous robots*, 4(4):387–403, 1997.

[82] C. M. Topaz and A. L. Bertozzi. Dynamics of a two-dimensional continuum model for swarming. SIAM Conference on Applications of Dynamical Systems, 2003.

[83] P. Varaiya. Smart cars on smart roads: problems of control. *IEEE Transactions on Automatic Control*, 38(2):195–207, 1993.

[84] T. Vicsek, A. Czirok, E. B. Jacob, I. Cohen, and O. Schochet. Novel type of phase transitions in a system of self-driven particles. *Physical Review Letters*, 75:1226–1229, 1995.

[85] K. Warburton and J. Lazarus. Tendency-distance models of social cohesion in animal groups. *Journal of Theoretical Biology*, 150:473–488, 1991.

[86] W. Whiteley and T. Tay. Generating isostatic frameworks. *Structural Topology*, 11:21–69, 1985.

171

[87] C. A. Woolsey, A. M. Bloch, N. E. Leonard, and J. E. Marsden. Physical dissipation and the method of controlled lagrangians. In *European Control Conference*, 2001.

[88] D. Yanakiev and I. Kanellakopoulos. A simplified framework for string stability analysis in AHS. In *Proceedings of the 13th IFAC World Congress*, pages 177–182, San Francisco, CA, July 1996.

[89] B. J. Young, R. W. Beard, and J. M. Kelsey. Coordinated control of multiple robots using formation feedback. IEEE Trans on Robotics and Automation (submitted), 2000.

[90] M. Žefran and V. Kumar. Interpolation schemes for rigid body motions. *Computer-Aided Design*, 30(3), 1998.

[91] M. Žefran, V. Kumar, and C. Croke. On the generation of smooth three-dimensional rigid body motions. *IEEE Transactions on Robotics and Automation*, 14(4):579–589, 1995.